Imperial College London

Bio-inspired pH-responsive polymers for intracellular delivery of macromolecules and cell engineering applications

Gabriella Angelique Morrison

Thesis submitted in accordance with the requirements of Imperial College London for the degree of DOCTOR OF PHILOSOPHY

Department of Chemical Engineering Imperial College London

APRIL 2022

Statement of Originality

I can confirm that the research presented within this thesis was the result of my own work. Any results obtained in collaboration have been specifically indicated and acknowledged within the text.

Copyright Declaration

This thesis is submitted for the degree of Doctor of Philosophy at Imperial College London. The research reported herein was carried out under the supervision of Dr Rongjun Chen between October 2017 and October 2021.

I can confirm that the research presented within this thesis was the result of my own work. Any results obtained in collaboration have been specifically indicated and acknowledged within the text.

This thesis does not contain the material that has been previously accepted for the award of any qualification at Imperial College London or any other educational institutions.

This thesis contains 49 figures, 7 tables, and 37,185 words in length excluding the bibliography and appendix.

Parts of this work have been presented at the 11th World Biomaterials Congress (2020).

Parts of this work are to be presented in the following publications:

Morrison G, Kopytynski M, Chen R. “An anionic pH-responsive polymer to potentiate intracellular delivery of different sized biomacromolecules”. In preparation.

Morrison G, Kopytynski M, Chen R. “Polymer-based intracellular delivery platform enhances the cytotoxicity of saporin through multiple death pathways”. To be submitted.

Chen S, **Morrison G,** Kopytynski M, Chen R. “Comb-like pseudopeptidic polymer-mediated pH-triggered rapid intracellular delivery of cargos from a wide size range”. To be submitted.

Gabriella Morrison

April 2022

“For I know the thoughts that I think toward you, saith the LORD, thoughts of peace, and not of evil, to give you an expected end.” **Jeremiah 29:11 KJV**

Acknowledgements

I would like to sincerely thank my supervisor, Dr Rongjun Chen, for giving me the opportunity to join his research group. I am thankful for your continued advice and guidance. I have developed both personally and professionally whilst being in your laboratory research group, and I have you to thank for that.

I want to thank my lab members Nikki Henry, Michal Kopytynski, Apanpreet Bharma, Jie Ren, Yifan Lui, Xinyu Lu, Jiawei Cui and Yuying Tang, for all their help, support, and fun times we have had together throughout the years. To Nikki and Michal, the three amigos, I am thankful for our times spent together in the office and in the lab.

Thank you Xinyu Lu for designing and synthesising the cationic polymers CP1 and CP2 and for allowing me to use them in my research.

I especially would like to give a massive heartfelt thank you to my colleague Michal Kopytynski for your helpful discussions, never-ending encouragement, support, and guidance. In addition, for your contribution to some results in Chapter 3 which was funded by the Department of Chemical Engineering Seed Fund for Translational Research.

I would like to thank the MEng students, Tudor-Octavian Sirbu and Suthinee Phanuvatsuk, who contributed to some of the results in Chapter 4 under my supervision.

To Hannah Tiernan, thank you for being the best emotional support and friend to me over the four years we have spent together at Imperial. This has been an incredible journey, and I am glad we have been able to go through it together.

I wish to express my gratitude to Jess Rowley, Stephen Rothery and Andreas Bruckbauer of Imperial College for their training and never-ending expertise on confocal microscopy and flow cytometry machines. Thank you for always making yourselves available to help, even for the simplest of problems.

To my dearest family and closest friends (whom I consider to be family), thank you for all your love, support and understanding. Thank you for your regular phone calls to check up on me, prayers and words of encouragement. I am especially grateful to my parents, Joyce and Derek, for constantly cheering me on and pushing me to be the best version of myself.

Lastly, I would like to acknowledge the Chemical Engineering Department at Imperial College London and the EPSRC for their financial support over the past years. For helping during COVID to help to the best of your abilities to not delay my research.

Words cannot express how truly grateful I am for every one of you.

Thank you all.

Abstract

Biological macromolecules including peptides, proteins and antibodies can act as therapeutic agents. When delivered intracellularly to their desired target site within the cell, they can modify cell behaviour. However, a long-standing challenge is the efficient delivery of such materials to their intracellular target sites. Although effective in some applications, existing technologies to improve delivery, namely viral vectors, have key limitations in their toxicity and safety. There is thus a need for more effective intracellular delivery tools.

This thesis explores the use of bio-inspired pH-responsive polymers as intracellular delivery platforms for the enhanced uptake of macromolecules. PP50, an anionic polymer comprised of a poly-L-lysine isophthalamide backbone grafted with the hydrophobic amino acid L-phenylalanine at a stoichiometric percentage of 50 mol%, was capable of delivering FITC-dextran, peptides and antibodies into the cell interior when the pH environment was lowered to pH 6.5. Additionally, the ability of PP50 to facilitate the uptake of the ribosome-inactivating protein saporin to induce apoptosis and cell death in 2D monolayer and multicellular spheroids highlights the potential use of PP50 for a wide range of therapeutic applications. PLP-NDA18, another anionic polymer comprised of a poly-L-lysine isophthalamide backbone grafted with decylamine at 18 mol%, also showed enhanced uptake and cytotoxicity of saporin when co-incubated with cells.

For cell engineering applications, two cationic polymers, CP1 and CP2, were investigated for their ability to improve the direct cytoplasmic delivery of the target antigen ovalbumin peptide and induce antigen presentation by DCs. Whilst CP1 displayed superior membrane lytic capabilities at pH 6.5, CP2 showed to be the most promising polymer for the upregulation of MHC I and cytoplasmic delivery of the antigen peptide. In the future, a more comprehensive investigation into the underlying mechanisms of cationic mediated antigen delivery will help to understand the full capabilities of these cationic polymers as intracellular delivery platforms.

Altogether, this work demonstrates that pH-responsive polymers are promising candidates as intracellular delivery platforms for a wide range of applications. Further studies and research are required for each polymer to reach its full potential as a widely adopted intracellular delivery agent.

Table of Contents

List of Figures

List of Tables

List of Abbreviations

A

APC	Antigen presenting cells

C

CIE	Clathrin-independent endocytosis
CME	Clathrin-mediated endocytosis
CPP	Cell-penetrating peptides
Cy5	Cyanine 5

D

DC	Dendritic cell
DCC	*N,N'*-dicyclohexylcarbodiimide
DCU	Dicyclohexylurea
dH_2O	Deionised water
DMAP	4-dimethylaminopyridine
DMEM	Dulbecco's modified Eagle's medium
DMF	*N,N*-dimethylformamide
DMSO	Dimethyl sulfoxide
DNA	Deoxyribonucleic acid

E

EDTA	Ethylenediaminetetraacetic acid
ER	Endoplasmic reticulum

F

FBS	Fetal bovine serum
FITC	Fluorescein isothiocyanate
FITC-dextran	Fluorescein isothiocyanate–dextran

G

GFP	Green Fluorescent Protein

H

HCl	Hydrochloric acid
HSC	Haematopoietic stem cell

I

IC_{50}	The concentration required to decrease the cell viability by half
IT_{50}	The time required to decrease the cell viability by half
IFN-γ	Interferon-gamma

K

kDa	Kilodalton

M

MHC	Major histocompatibility complex
MβCD	Methyl-β-cyclodextrin
MFI	Mean fluorescence intensity
Mw	Molecular weight

N

NMR	Nuclear Magnetic Resonance
NaOH	Sodium hydroxide

P

PAP	Prostatic phosphate antigen
PBS	Dulbecco's phosphate buffered saline
pHe	Extracellular pH
PI	Propidium iodide
PLP	Poly(L-lysine isophthalamide)
PLP-NDA	PLP side chain grafted with decylamine at a stoichiometric ratio of 18%

PP50	PLP side chain grafted with L-phenylalanine at a stoichiometric ratio of 50%
PP75	PLP side chain grafted with L-phenylalanine at a stoichiometric ratio of 75%

R

RBC	Red blood cell
RIP	Ribosome inactivating protein

T

TAT	HIV-1 Trans-activator gene product
TCR	T cell receptor

Chapter 1

Introduction

This chapter introduces the basic concepts, fundamentals, and applications of intracellular delivery, with a particular focus on *in vitro* and *ex vivo* intracellular delivery for cell engineering applications. Intracellular barriers to the successful delivery of therapeutic cargoes are discussed. The limitations of viral and non-viral intracellular delivery methods are summarised with an emphasis on the opportunities of pH-responsive polymers for intracellular delivery. The chapter concludes by outlining the project aims, originality and thesis structure to provide context and understanding to the research presented as a whole.

1.1 The opportunities and challenges of intracellular delivery

1.1.1 Intracellular delivery: fundamentals and applications

Cells are membrane-bound units containing essential biomolecules (including proteins, genes and chemicals) that are required to build and maintain life. Each cell has a designated role in maintaining homeostasis within the body (Björklund, 2019; Nakamura et al., 2019). Consequently, cellular disease can occur when cells dysfunction. For example, cancer can develop due to genetic mutations, an imbalance in the proliferation and death rate of cells, or when cells are unable to evoke an effective immune response (Fouad and Aanei, 2017). Defects in red blood cells can cause sickle cell anaemia (Obeagu et al., 2015). Alzheimer's is a result of neuron cell death (Nelson et al., 2012).

More than 60% of pathways that regulate cell function occur intracellularly (Raman et al., 2021). The introduction of therapeutic molecules and materials into the cell interior, including peptides, proteins, antibodies and nucleic acids is fundamental to understanding the underlying biological processes initiating cell disease. This knowledge can further be used to alter cell function, reprogramme cell behaviour and treat disease (Cerea et al., 2018; Stewart et al., 2018). For example, antibodies or nanoparticles can act as sensors to probe the intracellular environment. DNA and RNA can perform as gene-editing tools to correct or

delete faulty genes or control gene expression (Stewart et al., 2018, 2016). Proteins may alter signalling pathways to activate immune cells for anti-tumour targeting (Fu et al., 2014). The transport of such biopharmaceutics or biomaterials (often referred to as therapeutic cargoes, payloads, or macromolecules) into an intracellular site within the cell can be termed as intracellular delivery. Therapeutic cargoes differ significantly in size, shape and physiochemical properties (Shi et al., 2018). A few examples are highlighted in Table 1-1.

Whilst both immortalised and primary cells are suitable candidates for introducing therapeutic cargoes into their interior, the choice of payload to be delivered intracellularly is primarily dictated by the application of interest, which in turn influences the cell type to be used (Figure 1-1). For example, for cell-based therapies (application), tumour antigen delivery (therapeutic payload) to an antigen-presenting cell (APC), e.g., dendritic cell (DC) or B lymphocyte (cell type) would be most suitable.

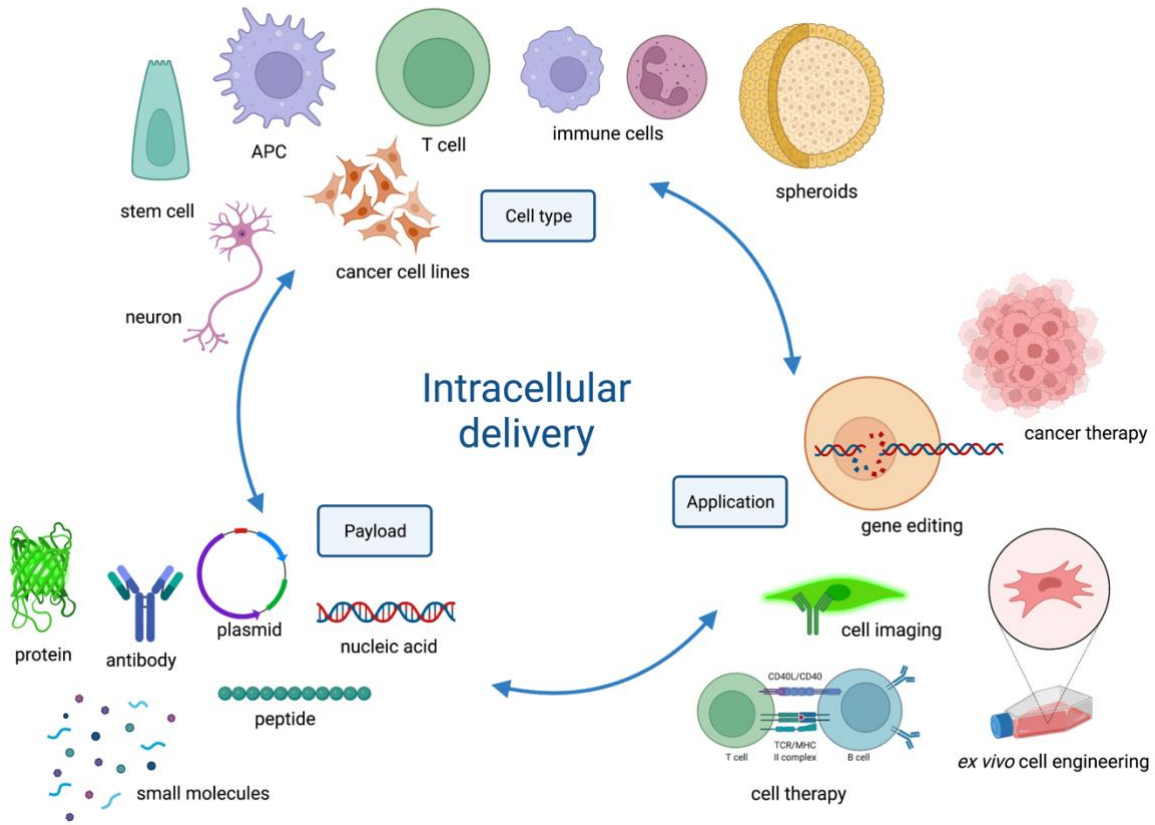

Figure 1-1. Examples of payloads, cell types and applications of interest for intracellular delivery. Abbreviations. APC = antigen-presenting cell.

Table 1-1. Types of cargoes used for intracellular delivery.

Cargo	Size	Example	Delivery method	Cell type	Application	Reference
Small molecules	0.1-1.0 kDa	Bleomycin	Electroporation and sonoporation	CHO	Cancer therapy	(Tamošiūnas et al., 2016)
Cryoprotectants	> 0.1 kDa	Trehalose	pH-responsive polymer	Ovine erythrocytes	Cryopreservation	(Chen et al., 2020)
			Electroporation	Human adipose-derived stem cells		(Dovgan et al., 2017)
Peptides	0.5 – 10 kDa	Bak BH3	pH-responsive polymer	HeLa	Pro-apoptotic cell killing	(Albarran et al., 2011)
		Ovalbumin derived peptides	Streptolysin O	K41	Antigen presentation for cell therapies	(Fu et al., 2008)
			Polymer-peptide conjugate-based nanotransformer	DC2.4		(Gong et al., 2020)

Protein	30-150 kDa	Ovalbumin	Multifunctional micelles	B16-F10	Antigen presentation for cell therapies	(He et al., 2019)
		Cytochrome c	Lipid nanoparticles	H460	Cancer therapy	(Kim et al., 2012)
			Protein nanoparticles	HeLa		(Morales-Cruz et al., 2014)
Antibodies	~150 kDa	Anti α-tubulin monoclonal antibody labelled with Alexa Fluor 488	Light pulses	Primary normal human dermal fibroblasts	Intracellular imaging	(Wu et al., 2015)
		Anti HPV16 E6 oncogene monoclonal antibody	Electroporation	HeLa	Intracellular imaging	(Freund et al., 2013)
Nucleic acids	> 4 kDa	p53 mRNA	Microvesicles	H1229	Cancer therapy	(Q. Wang et al., 2018)
		eGFP-mRNA	Photoporation	HeLa, Jurkat T cells	Cell engineering	(Raes et al., 2020)

1.1.2 Barriers to successful intracellular delivery

Macromolecules must bypass several biological barriers before they reach their target site. For *in vitro* and *ex vivo* intracellular delivery, which will be the primary focus of this thesis, the first immediate barrier is the cell membrane. Translation to *in vivo* settings creates additional barriers. For example, for cancer therapy applications, the mildly acidic pH of the tumour environment, hypoxic core of tumours and abnormal angiogenesis are added obstacles to overcome (Petrova et al., 2018; Subarsky and Hill, 2003).

1.1.2.1 Cellular Barriers

The cell membrane is a highly complex and dynamic but well-ordered structure built up of numerous lipid species and membrane proteins (Edidin, 2003; Yèagle, 1989). In addition to acting as a physical barrier to protect the internal cell environment (cytosol and organelles) from the cells external surroundings, the cell membrane also plays a crucial role in other vital processes: signalling, endocytosis, transport, cell shaping, motility, cell to cell communication and molecule recognition and presentation (Pontes et al., 2013; Zalba and ten Hagen, 2017).

For intracellular delivery to be effective, the desired macromolecule must reach its target site in the cell. Only when this has occurred can the macromolecule transiently or permanently alter the function of the cell for a therapeutically beneficial outcome (Sharei et al., 2015). As the macromolecule possesses the biological activity, if it does not reach its target site, the cell cannot be rendered as therapeutic. Small molecules may passively diffuse across the cell membrane e.g. O_2 or enter via membrane transporters e.g. glucose. However, due to their size, charge and polarity, macromolecules have been rendered impermeable to the cell membrane and therefore direct translocation into the cell interior is mostly inhibited (Sharei et al., 2013; Sun and Duan, 2020; Yang and Hinner, 2015).

Thus, for the macromolecule to bypass the cell membrane, physical disruption is required. Alternatively, the macromolecule must enter the cell via endocytosis and pass through the endosomal pathway initiating endosomal escape before degradation in the lysosomes (Brooks et al., 2020).

1.1.2.2 Endocytosis

The process of endocytosis, first termed in 1963 by de Duve (Mukherjee et al., 1997) is exhibited by all eukaryotic cells (Mellman, 1996) except erythrocytes (Duncan and Richardson, 2012). The function of endocytosis is not only limited to the internalisation of macromolecules but also extends to the uptake of nutrients, cell motility, signalling and antigen presentation (Canton and Battaglia, 2012). There are two broad categories of endocytosis: phagocytosis (involving the uptake of larger particles i.e., cell eating) or pinocytosis (involving the uptake of fluids or solutes i.e., cell drinking) (Mellman, 1996; Sahay et al., 2010).

Phagocytosis is carried out by a specialised subset of cells including macrophages, DCs, monocytes and neutrophils whereby larger particles (> 0.5 μM) are opsonized and engulfed within a plasma-membrane envelope into a phagosome (Duncan and Richardson, 2012; Gordon, 2016; Uribe-Querol and Rosales, 2020). On the other hand, pinocytosis is reserved for the internalisation of smaller particles, solutes and extracellular fluids (Foroozandeh and Aziz, 2018; Lamaze and Schmid, 1995). Pinocytosis can be subcategorised into clathrin-mediated endocytosis (CME) and clathrin-independent endocytosis (CIE). CIE can be further subcategorised into caveolae-mediated endocytosis, micropinocytosis and clathrin and caveolae-independent endocytosis (Figure 1-2) (Sahay et al., 2010). Each morphologically distinct internalisation gateway differs in its regulatory proteins, markers and ligands that facilitate membrane invagination (Duncan and Richardson, 2012). However, all pathways generally comprise of the following fundamental steps: (I) interaction or binding of the particle at the cell surface, (II) plasma membrane budding off into a vesicle and (III) trafficking of vesicle to a subcellular organelle or to the lysosome where its contents in degraded (Canton and Battaglia, 2012; Doherty and McMahon, 2009). Cellular uptake of therapeutic macromolecules and internalisation pathway may be dependent on its surface charge, size, shape and composition.

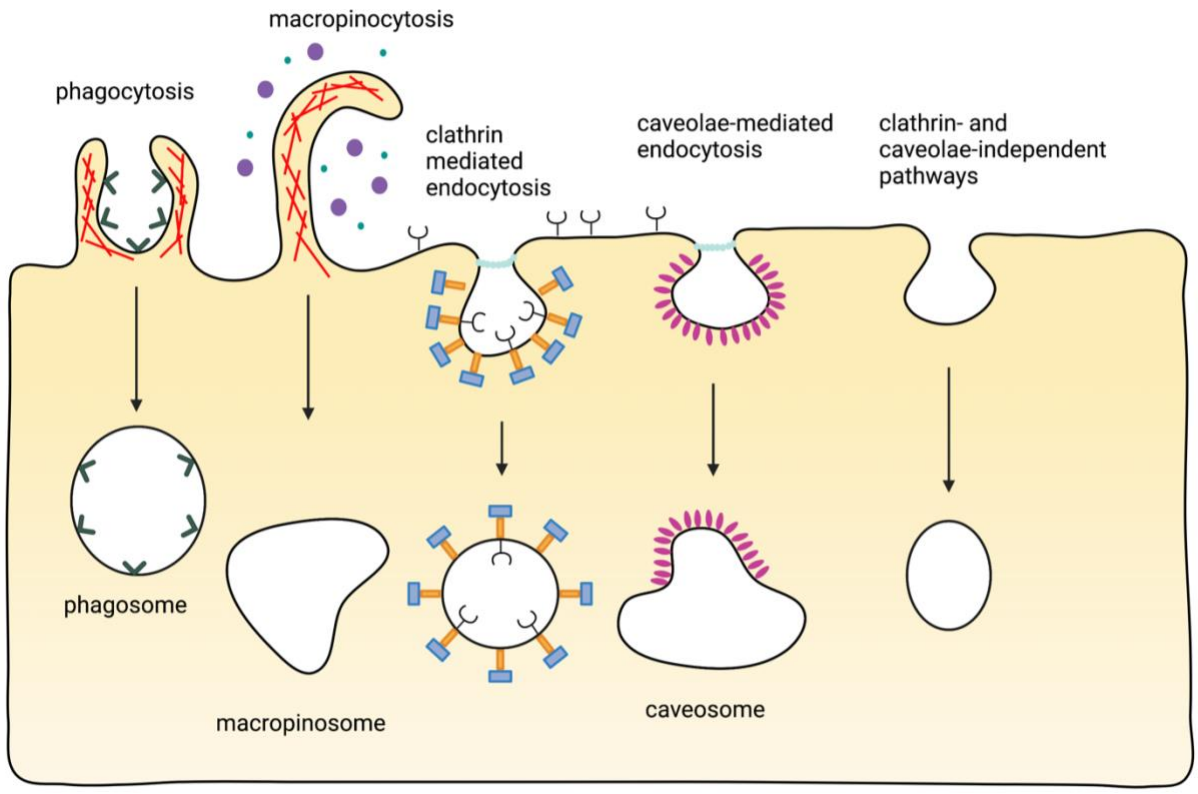

Figure 1-2. Schematic representation of the different endocytic pathways involved in the internalisation of different cargoes. Modified from (Chou et al., 2011) with permission.

1.1.2.3 Endosomal trafficking and escape

The extracellular pH (pHe), often known as physiological pH, of normal cells is approximately 7.4. The cytosolic pH is approximately pH 7.2 to 7.4, and each intracellular compartment has a defined pH which is tightly controlled for it to operate (Casey et al., 2010). Likewise, the pH of each compartment in the endocytic pathway is strictly regulated and controlled by ATP-dependent proton pumps (Shete et al., 2014).

First, the cargo therapeutics arrive at the early endosome, approximately 5-10 minutes after internalisation (Duncan and Richardson, 2012; Dyer et al., 2013; Richardson et al., 2008). The mildly acidic pH of the early endosome is maintained at approximately pH 6.3-6.8. The early endosome is also commonly known as the sorting endosome since its primary function is to sort internalised molecules (Jovic et al., 2010). Here, receptors typically dissociate from their ligands and are recycled back to the plasma membrane. Internalised cargoes can also be directed to the trans-Golgi network or are transported onto later stages of the endocytic pathway (Lam et al., 2007; Poteryaev et al., 2010). Maturation of the early endosome to late

endosome (or multi-vesicular bodies) is characterised by a pH decrease to around pH 4.5–5.5 (Gruenberg et al., 1989; Russell et al., 2006; Shete et al., 2014). Typically, internalised cargoes enter the late endosome after ~30-60 minutes (Duncan and Richardson, 2012). The terminal degradation compartment of the endocytic pathway is the lysosome which has a pH of approximately 4.5. Materials that reach this organelle are degraded by more than 60 acid-dependent hydrolases (Ballabio, 2016; de Duve, 2005; Dell'Angelica et al., 2000; Luzio et al., 2000).

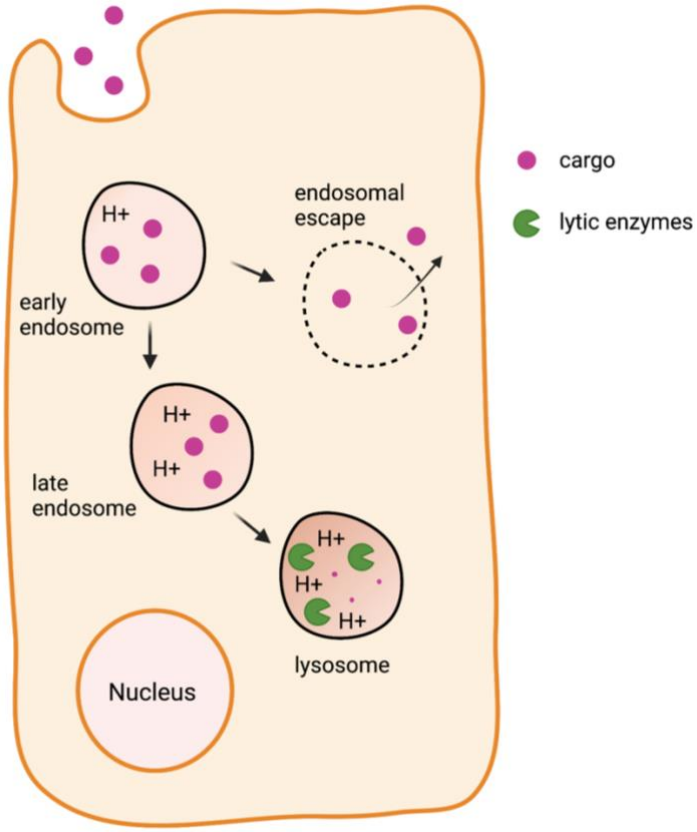

Figure 1-3. Trafficking through endosomolytic pathway. Cargoes internalised via endocytosis traffic through the early to late endosome before reaching the lysosome. Endosomolytic agents may initiate endosomal escape. Cargoes internalised without endosomolytic agents are degraded by lytic enzymes found within the lysosomes. Modified from (Andrian et al., 2021) with permission.

To retain their therapeutic behaviour, it is imperative that therapeutic cargoes that enter the endocytic pathway escape from the degradative environment of the lysosomes (Figure 1-3). Endosomal escape of cargo therapeutics is inefficient, with reportedly less than 1% successfully escaping the endosomes. Accordingly, endosomal release is often the rate-limiting step in the intracellular delivery of therapeutics (Brock et al., 2018; Teo et al., 2021). Opportunistic microorganisms, namely viruses and bacteria, have naturally evolved to initiate endosomal escape and access the cytoplasm for survival and replication. Non-enveloped viruses exploit membrane disruption and pore formation mechanisms. For example, adenoviruses trigger pH-dependent membrane lysis in endosomal compartments. In response to the lowering pH environments in endo-lysosomal compartments, enveloped viruses use membrane fusion mechanisms via fusogenic peptides to promote escape. Examples of fusogenic peptides include hemagglutinin HA-2 N-terminal fusogenic peptide and TAT fusion peptide from HIV-1 (Canton & Battaglia, 2012; Shete et al., 2014; Varkouhi et al., 2011). Their clinical applications and safety as intracellular delivery agents and other intracellular delivery platforms that initiate endosomal escape will be discussed further in section 1.2.3.1.

Alternatively, if a direct cross-membrane transport mechanism is used, the endo-lysosomal pathway can be bypassed, and materials can be delivered directly into the cytoplasm. Examples of such methods are micro/nanoneedles, electroporation, sonoporation, cell squeezing and particle mediated delivery. These membrane disruption modalities have either direct penetration or permeabilising abilities. Direct penetration methods employ a transport mechanism that pierces the cell membrane and simultaneously introduces the macromolecule into the cell, bypassing the cell's natural biological barriers. Permeabilising methods act to transiently disrupt the membrane to create pore like sizes that allow the macromolecules to enter (Sharei et al., 2013; Stewart et al., 2018, 2016). Membrane disruption modalities will also be discussed later in section 1.2.2.

1.1.2.4 Subcellular targeting of organelles

After being delivered safely into the cell cytoplasm, via direct membrane disruption or endocytosis and endosomal escape, the therapeutic cargo must still travel to its desired target site to exert its therapeutic effect (Fu et al., 2014; Torchilin, 2006). Specific membrane-bound

organelles, including the nucleus, mitochondria, endoplasmic reticulum (ER) and Golgi complex can act as key intracellular delivery sites for macromolecules (Figure 1-4) (Azevedo et al., 2018).

For nucleic acids, and some proteins and peptides, the nucleus is ultimately the final target. Due to the huge potential of therapeutic genetic manipulation, crossing the double lipid bilayer of the nuclear envelope is an important step for many biologics (Huang et al., 2011). However, the nuclear pore complex, approximately 9 nm in diameter, selectively only allows small molecules and ions free access to the interior. Larger macromolecules (> 40 kDa) require an active transport mechanism for access. Considering the importance of nuclear targeting, current strategies rely on the conjugation of nuclear localisation signals (which have a high binding affinity to nuclear transport receptors) to the cargo of interest for delivery (Huang et al., 2011; Zhong et al., 2015). For example, Yoshikawa *et al.* (2008) used a nuclear localisation signal peptide and endosome disruptive peptide to enhance the cancer therapeutic Tat-fused p53-derived peptide aptamer entry into the nucleus.

The mitochondria is the key organelle involved in the production of ATP, generation of reactive oxygen species and apoptosis (Torchilin, 2006; Yuan et al., 2019). Mitochondria dysfunction has been related to several diseases, including cancer, Alzheimer's, and Parkinson's. As the mitochondria plays an important role in the intrinsic mediated apoptotic pathway, it has been identified as an important organelle target for cancer therapy. For example, by targeting Bcl-2 proteins e.g. Bim (Kim et al., 2018; Kopytynski et al., 2020; Schnorenberg et al., 2019), which are commonly overexpressed in cancer (Biswas & Torchilin, 2014; Wang et al., 2010).

The ER is the site of post-translational modification of secretory proteins and also serves as an essential target for cancer therapy (Kang et al., 2021). For example, in the delivery of protein toxins (Nowakowska-Gołacka et al., 2019). Direct cross-membrane transport of materials may be achieved by fusing transport vesicles into the surface of the ER (Huang et al., 2011; Tarragó-Trani & Storrie, 2007). The ER also acts as a presentation site for peptide antigens loaded MHC class I (Azevedo et al., 2018).

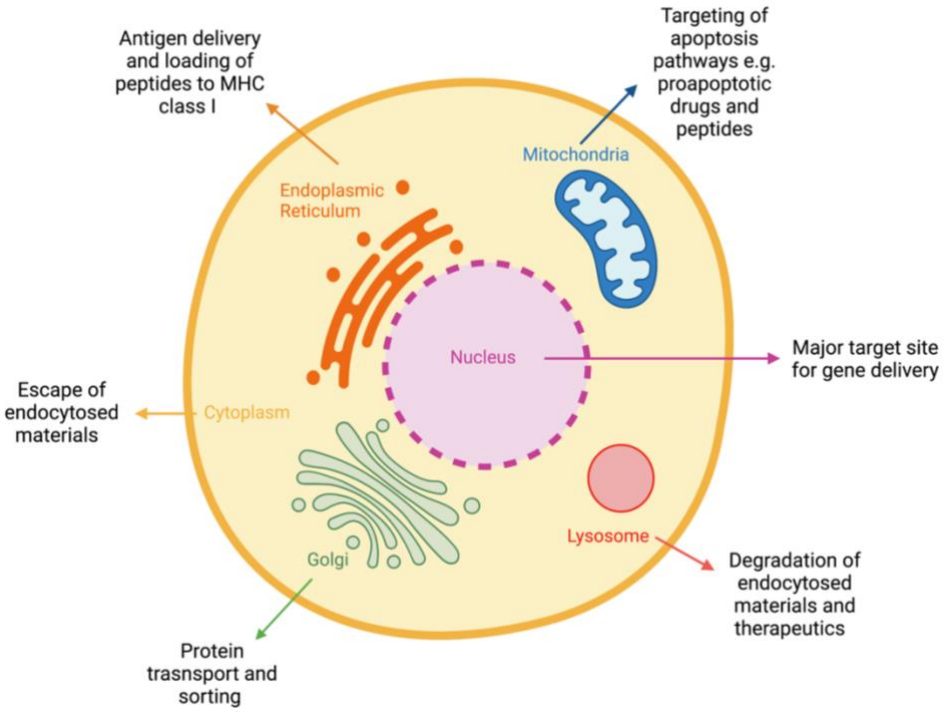

Figure 1-4. Possible target sites for intracellular delivery. The main organelles that cargoes may reach are highlighted. Modified from (Azevedo et al., 2018) with permission.

1.2 *In vitro/ex vivo* intracellular delivery approaches

1.2.1 Ideal features of an intracellular delivery system

An optimum intracellular delivery system should have the following features (Hur and Chung, 2021; Stewart et al., 2016; Sun and Duan, 2020):

- **Maintain cell viability.** Delivery platforms should be biocompatible and should not decrease cell viability during or after the delivery of materials. Complete membrane and cytoplasmic recovery are essential if the cell membrane is disrupted.
- **Minimal cell perturbation.** The delivery platform should not cause off target effects, toxicity, undesirable genotoxicity, or mutagenesis. Undesirable side effects may be avoided by minimising the physical forces or stresses applied to the cell.
- **Deliver a diverse range of materials.** Different therapeutic cargoes have different functions once delivered intracellularly. Although diverse in size and composition, an optimal system should accommodate delivery of all materials.

- **Accommodate delivery across cell types.** An ideal intracellular delivery system should deliver materials to all cells including adherent, suspension and hard to transfect cells.
- **Target intracellular organelles.** Intracellular target sites are distributed throughout the cytoplasm and nucleus. Effective delivery systems should not only be able to facilitate entry into the cytosol (through endosomal escape or membrane disruption) but aid entry to target organelles.
- **Low cost.** Delivery systems should be low in cost to enable large scale manufacturing and ease production costs. Complexity in preparation and operational difficulties may also limit the utility of a delivery platform.
- **Easily scalable.** The number of cells requiring treatment may differ depending on the application. An optimum delivery technology should be high throughput for these occasions.

Whilst many intracellular delivery platforms currently exist, few, if any, meet all the features mentioned above. A broad overview of current delivery technologies will be discussed: physical, biological and chemical.

1.2.2 Physical methods

Membrane disruption techniques use physical methods to provide materials direct access to the cell cytoplasm (Sharei et al., 2014). However, there is a delicate balance between efficiently delivering the therapeutic cargo of interest with high throughput and delivery efficiency whilst not causing irreversible damage to the targeted cell (Wang et al., 2018). Electroporation, optoporation, sonoporation, cell squeezing, nanoneedles and microinjection are a few of the many physical methods used to deliver therapeutic materials. The strengths, challenges and opportunities of membrane disruption as a whole for intracellular delivery are summarised in Table 1-2.

Table 1-2. Strengths, challenges, and opportunities of using membrane disruption modalities for the intracellular delivery of therapeutics. Taken with permission from (Stewart et al., 2016).

	Membrane disruption modalities
Strengths	• Delivery of diverse materials • Capable of addressing many cell types • Optionally vector-free (that is, non-immunogenic) • Transient, defined exposure to membrane disruption • Rapid, almost instantaneous delivery
Challenges	• Loss of cytoplasmic content • Some modalities (such as thermal and electric) can lead to excessive damage to organic molecules, protein denaturation, and internal membrane breakdown • Some approaches (such as microinjection) currently not amenable to high throughput • Some methods can be restricted to adherent-only or suspension-only cells • Less amenable to i*n vivo* translation
Opportunities	• Microfabrication and nanotechnology enable fine control of physical phenomena and makes modalities that were previously intractable more feasible • A better understanding of cell recovery processes may allow mitigation of toxicity and functionality issues • Can be combined with carriers designed for subcellular targeting and controlled release • Engineered switchable valves in plasma membrane to dynamically control permeability • Versatile potential for *in vitro* and *ex vivo* applications

A few of the most successful physical methods will be discussed below.

1.2.2.1 Microfluidic aided cell squeezing

Cell squeezing is a recently developed technique at the forefront of membrane disruption modalities for improving intracellular delivery. This vector free microfluidic device temporarily deforms the cell and disrupts its membrane as it passes through the channel, allowing the target material to enter the cytosol. After 5 minutes, the membrane reseals (Sharei *et al.*, 2015; Szeto *et al.*, 2015; Sharei *et al.*, 2013a).

To date, antibodies, proteins, quantum dots, fluorescein isothiocyanate-dextran (FITC-dextran) and carbon nanotubes have successfully been delivered to a wide array of cells, including fibroblasts, embryonic stem cells, DCs and blood-derived immune cells (Sharei *et al.*, 2013a). However, reduced cell viability was observed in some cells after delivery (Sharei et al., 2013). Most notably, for cell therapy applications and *ex vivo* manipulation of APCs, the system has been used to improve antigen uptake in B cells to express MHC class I molecules. After the intracellular delivery of the model protein antigen ovalbumin, these B cells were subsequently able to prime CD8+ T cells, producing the effector cytokines granzyme B and interferon-gamma (IFN-γ) (Szeto *et al.*, 2015). Moreover, by using the microfluidic device in conjugation with electric fields, DNA was successfully delivered to the nucleus of HeLa cells. Whilst the microfluidic device was able to transport DNA into the cytosol, the electric field was required to disrupt the nuclear envelope to allow the DNA to enter the nucleus (Ding *et al.*, 2017). Key weaknesses of using a microfluidic device include reduced cell viability and clogging due to damaged cells or contaminants. Additionally, it is not known whether the application of external mechanical strength could lead to possible disease development.

1.2.2.2 Electroporation

Electroporation is a widely adopted physical disruption method. Short and intense electric pulses are produced across the cell to permeabilise the membrane and allow the entry of cargo materials (Hui and Li, 2000). Hendel *et al.* (2015) showed that Cas9-sgRNAc complex could be delivered into human primary T cells and CD34+ haematopoietic stem and progenitor cells with high efficiency using electroporation. Vergara *et al.* (2013) used electroporation for the *ex vivo* treatment of retinal cell cultures. GFP-encoding plasmids were successfully delivered with transfection efficiencies around 22-25%. Cultured cells were not affected in their cell survival or differentiation. Further, functional delivery of a PAX6-IRES-GFP plasmid resulted in the upregulation in PAX6 protein levels in treated cultures.

Whilst electroporation is certainly advantageous due to its ability to deliver into hard-to-transfect cells types (Stewart et al., 2018), the method is limited by the need for protocol optimization based on experimental conditions and low cell viabilities after high-voltage exposures (Luo and Saltzman, 2000).

1.2.2.3 Microinjection

Microinjection, the first intracellular delivery method developed, refers to the direct injection of materials into the cell cytosol or nucleus using a glass micropipette (Stewart et al., 2018). In comparison to electroporation, higher precision and efficiency can be achieved using this method (Kaladharan et al., 2021). Microinjection has been used to introduce larger cargoes, proteins, peptides, DNA, dextrans and other biologically active materials into the cell interior (Stewart et al., 2018). For example, for cell therapy and drug delivery applications, Tiefenboeck *et al.* (2017) introduced liposomes and liposomes containing biologically active cargo into HeLa and DCs. Whilst microinjection boasts high cell viabilities and low toxicity to cells, it is a slow and laborious process with low throughout, limiting its applications (Luo and Saltzman, 2000).

1.2.3 Chemical and biological delivery agents

1.2.3.1 Viral vectors

Viral vectors have been attractive candidates for the intracellular delivery of nucleic acids. Examples of extensively researched viruses for gene therapy applications include retroviruses, adenovirus and adeno-associated viruses (Chen et al., 2018; Walther and Stein, 2000). During the viral infection process, membrane-active protein domains are activated during the endosomal acidification pathway, triggering either membrane fusion, pore formation or endosomal membrane disruption which prompts the release of the genomic material into the cytoplasm. For example, the influenza virus enters the cell via receptor-mediated endocytosis. The membrane-active protein domain, HA2, becomes protonated in response to the low pH environment of the endosomes. Subsequently, a conformational change of the fusion protein reveals its fusion peptide domain which enhances its destabilising activity initiating the fusion of the viral membrane with the endosomal membrane (Plank et al., 1998, 1994). Despite the promising outlook, viral vectors have yielded concerns regarding their safety, particularly toxicity and genotoxicity caused by the increased chance of insertional mutagenesis and upregulation of cellular proto-oncogenes (David and Doherty, 2017; Knight et al., 2013).

As a solution, liposomal structures mimicking viral systems have been exploited as intracellular delivery agents (Plank et al., 1998). For example, Chen *et al.* (2016) developed a novel virus-mimicking endosomolytic liposomal system based on the structure and functional traits of the influenza virus. Here, a pH-responsive pseudopeptide was used to mimic the fusogenic peptides in the viral spikes, initiating endosomal release of payloads at low pHs. The viral envelope was mimicked by the liposomal bilayer and the viral genome was mimicked by the drug payload of interest to be delivered.

1.2.3.2 Liposomal based intracellular delivery agents

Liposomes are spherical vesicles composed of one or more phospholipid bilayers with an aqueous core (Bruun and Hille, 2019). Liposomes display several advantageous properties, making them highly desirable intracellular delivery systems. Firstly, due to their structure, liposomes can encapsulate hydrophobic molecules (in the lipid membrane) and hydrophilic molecules (in the aqueous core) (Fan et al., 2021). Also, they are biocompatible and biodegradable (Bruun and Hille, 2019). Liposomes are structurally versatile. Their biological properties can be controlled by modifying lipid composition, vesicle size, lamellarity and surface charge (Trif and Craciunescu, 2015). For example, cationic lipids have been widely used to facilitate the delivery of nucleic acids. The positively charged liposomal surface interacts with the negatively charged plasma membrane to increase internalisation (Chatin et al., 2015). In addition, targeting motives e.g. folate, transferrin or epidermal growth factor can be incorporated into the liposomal surface for active targeting to increase interaction and uptake into cells (Khan et al., 2020).

Further, liposomes can be made stimuli sensitive (Torchilin, 2005). For example, by grafting pH-responsive polymers on the liposomal surface, endosomal release of payloads can be triggered in response to pH (Chen and Chen, 2016). The potential limitations of liposomes, including decreased stability and low circulation time in the body have been overcome by incorporating cholesterol in the liposomal membrane and modification with poly-(ethylene glycol) on the liposomal surface (Fan et al., 2021; Simões et al., 2001). As such, liposomes have shown tremendous advances, comprising a large proportion of clinical-stage trials for the treatment of cancers, solid tumours and other conditions (Beltrán-Gracia et al., 2019; “ClinicalTrials.gov,” 2022; Crommelin et al., 2020) .

1.2.3.3 Cell-penetrating peptides as intracellular delivery agents

Cell-penetrating peptides (CPPs) are a category of small peptides characteristically containing between 5-30 amino acids (Gaston et al., 2019). They typically are amphipathic and have a net positive charge consisting of arginine or lysine rich peptides (Gupta et al., 2005; Yesylevskyy et al., 2009). CPPs are covalently or non-covalently linked to cargoes including proteins, antibodies, DNA or RNA to facilitate intracellular delivery (Gaston et al., 2019).

The precise cellular uptake mechanism of CPPs is not fully known. Endocytosis and direct membrane penetration have been researched as possible mechanisms (Ruseska and Zimmer, 2020). CPPs have shown that they can penetrate cells and bind and insert within membranes, even in the presence of endocytosis inhibitors (Yesylevskyy et al., 2009), but this could be influenced by the cargo to be delivered, concentration of CPP or cell line used (Ruseska and Zimmer, 2020).

One of the most studied and widely employed naturally occurring peptides, TAT, is derived from Human Immunodeficiency Virus transactivator protein (Dinca et al., 2016; Hoffmann et al., 2018). Nevertheless, it has been reported that endosomal release is not initiated by TAT-fused cargo, leaving around 90% trapped in the endosome (Hoffmann et al., 2018). Since the discovery of TAT in the late 1980's, a number of other CPPs have been developed and applied to reach previously inaccessible intracellular targets in the cell. However, poor stability, lack of specificity to cells, and toxicity are some of the drawbacks CPPs face (Gaston et al., 2019; Park et al., 2019; Ruseska and Zimmer, 2020).

1.2.3.4 Polymers

Another promising group of non-viral intracellular delivery agents are polymers. Polymeric carrier systems, including polymeric micelles, polymeric nanoparticles and polymer-therapeutic conjugates are currently being investigated in clinical trials for their ability to enhance the delivery of macromolecules (Table 1-3).

Table 1-3. Clinical trials involving the use of polymers to deliver macromolecules

ClinicalTrials.gov Identifier	Status of development	Intervention/treatment	Condition	Reference
NCT05254665	Phase II	Docetaxel loaded polymeric micelles	Advanced solid tumours	(Jiangsu Simcere Pharmaceutical Co., Ltd., 2022)
NCT03774680	Phase I	Cetuximab loaded polymeric nanoparticles	Colon cancer	(Abdellatif et al., 2020)
NCT05359211	Phase I	Polymer-conjugated receptor agonist NKTR-255	B cell Lymphoma	(Shah et al., 2021)
NCT04751786	Phase I	PLGA nanoparticles loaded with a tumour antigen and an iNKT cell agonist	Advanced solid tumours	(Creemers et al., 2021)
NCT04138342	Phase I	Quantum dot nanoparticles decorated with veldoreotide	Breast cancer	(Abdellatif et al., 2022; Abdellatif, 2019)
NCT03660930	Phase I/II	Nanoparticle bound rapamycin	Soft tissue sarcoma	(University of Washington, 2022)

1.3 Stimuli-responsive polymers

Stimuli-responsive polymers, 'smart polymers', are sensitive to specific triggers and respond after receiving an external signal. Physical or chemical stimuli may include pH, temperature, light, chemicals and magnetic or electrical fields (D. Wang et al., 2016). Once activated, stimuli-response polymers can undergo conformational or chemical changes, which may subsequently vary the physical properties of the polymer (Brighenti et al., 2020; Stuart et al., 2010).

pH-responsive polymers are a subset of stimuli-responsive polymers that have shown great promise as they can exploit the pH differences within the cell to facilitate the intracellular delivery of therapeutic macromolecules. By definition, pH-responsive polymers are systems that contain weak acidic or basic groups in their structure that, in response to increasing or decreasing pH, can accept or release protons (Kocak et al., 2017). This is accompanied by changes in solubility, volume, chain conformation or functionality (Dai et al., 2008; Wei et al., 2016). pH-responsive polymers can be subcategorised into cationic or anionic polymers, depending on whether acidic or basic monomers predominate in their structure (Kocak et al., 2017).

Ideally, an optimal pH-responsive polymer should be non-lytic at pH 7.4. However, they should trigger destabilisation of the cell membrane at mildly acidic pH (5.5-6.5) e.g. at endosomal pH to disrupt the endosomal bilayer and initiate endosomal escape of endocytosed cargoes (Eccleston et al., 2005). Specifically, for *ex vivo* applications where the pHe can be physically altered, pH-responsive polymers may facilitate direct membrane delivery of cargoes into the cytoplasm. As a result, natural or synthetic biodegradable and biocompatible pH-responsive polymers have been designed to enhance the delivery of macromolecules (Chen et al., 2009a; Kopytynski et al., 2020; Takemoto and Nishiyama, 2021).

1.3.1 pH-responsive cationic polymers

Polymeric systems carrying positive charges on the polymer backbone or side groups are termed cationic polymers or polycations (Samal et al., 2012). Most cationic polymers contain basic ionisable functional groups such as amine groups that can be protonated as the pH decreases. Examples of cationic polymers include poly(L-lysine) and poly(ethyleneimine) (Farshbaf et al., 2018; Pack et al., 2005; Zakeri et al., 2018). Therapeutically, cationic polymers have been deemed excellent candidates for non-viral gene therapy and genetic engineering (Kabanov and Kabanov, 2002; Rai et al., 2019). At physiological pH, the polycations can interact with negatively charged nucleic acids through electrostatic interactions to form complexes (polyplexes), protecting the genetic material from enzymatic degradation and mediating cellular entry (Fischer et al., 2003; Meyer et al., 2008; Schmaljohann, 2006; Sonawane et al., 2003). For the transmembrane delivery of other negatively charged payloads

that experience repulsion from the anionic cell membrane, cationic polymers would equally be ideal candidates.

During the endocytosis trafficking pathway, the decrease in pH is accompanied by unprotonated amines absorbing protons as they are pumped into the endosome by ATPase proton pumps. As a result, more protons are pumped into the endosome leading to an influx of water and negatively charged ions. This phenomenon leads to increased osmotic pressure and swelling and subsequent endosomal rupture, which releases entrapped nucleic acids from the endosome into the cytoplasm. This endosomal escape mechanism is referred to as the proton-sponge effect (Benjaminsen et al., 2013; Liechty et al., 2010; Vermeulen et al., 2018).

Despite the promising outlook for cationic polymers, their high toxicity and low transfection efficiency have hampered their clinical progress as intracellular delivery agents (Schmaljohann, 2006).

1.3.2 pH-responsive anionic polymers

Viruses possessing membrane lytic amphiphilic peptides can infect cells by mediating the delivery of nucleic acid to the cytoplasm via membrane disruptive endosome escape (Chen et al., 2005, 2008). Anionic and amphiphilic polymers mimic these membrane lytic properties (Chen et al., 2005), so they can be exploited for their uses as membrane disruptive biomaterials.

Ionisable pendant groups in the polymer backbone or as side groups can accept or donate protons depending on the surrounding pH environment (Bazban-Shotorbani et al., 2017; Roy and De, 2014). For example, weak acids like carboxylic acids are susceptible to changes in their ionisation state in response to pH change (Schmaljohann, 2006). At neutral to high pH, the carboxyl groups become deprotonated, and a linear form of the polymer dominates due to the repulsion between the negative charges. Conversely, at low pHs, the carboxyl groups become protonated, shifting the hydrophobic/hydrophilic balance of the polymer. The hydrophobic regions have decreased water solubility and collapse, resulting in a compact globular structure (Figure 1-5) (Deirram et al., 2019; Ducheyne, 2011). This hydrophobic and

globular polymer has an increased lipophilic nature and, through hydrophobic interactions and hydrogen bonding, associates more strongly with and partition into the cellular membrane (Chen et al., 2005). Thus, the membrane activity of the polymer can be increased or decreased depending on the pH environment (Bratek-Skicki, 2021; Ducheyne, 2011). This advantageous property has prompted the investigation of pH-responsive pseudopeptide polymers, including poly(L-lysine isophthalamide) (PLP) and its derivatives, containing ionisable carboxyl groups for cell membrane disruption to circumvent the intracellular barriers of endosomal entrapment (Chen et al., 2009b; Eccleston et al., 2000).

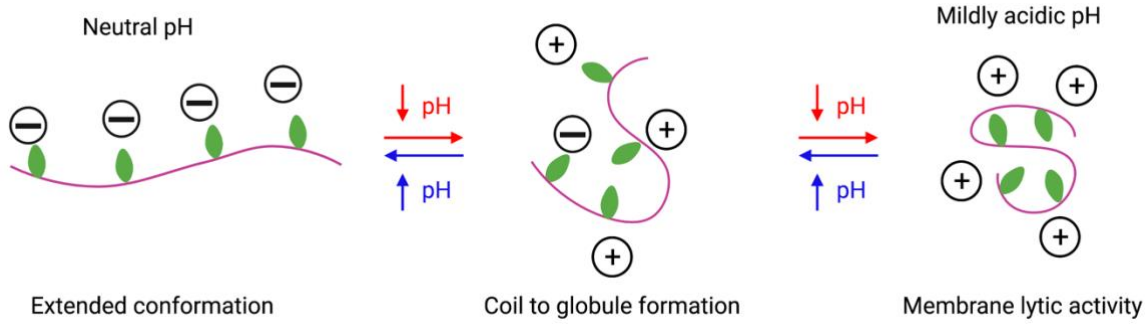

Figure 1-5. Linear to globular conformational change of anionic and amphiphilic polymers. The polymer remains in an extended linear conformation at neutral pH due to the repelling negative charges along the backbone. Upon a decrease in pH and increase in protons, the polymer collapses to a globular form and the hydrophobic regions of the polymer can insert and disrupt the membrane.

1.3.3 PLP and PP family

Poly (L-lysine isophthalamide) (PLP) is an anionic amphiphilic polymer developed by Eccleston *et al.* (1999). PLP is comprised of a hydrophobic backbone and pendant carboxyl groups. Despite exhibiting linear to globular conformation changes, its membrane disruptive capabilities are limited, and membrane disruption is only induced in the narrow pH range of 4.6 to 5 (Chen et al., 2009a). Significant research has been employed to alter PLP's structure to enhance its membrane disruptive biological activity. As the hydrophobicity of the polymer dictates its membrane lytic abilities (Chen et al., 2005), much of this research has been focused on the addition of side groups that increase the hydrophobicity of the polymer.

Furthermore, specific investigation has been made into manipulating PLP to control the pH range at which it is disruptive (Chen et al., 2008).

1.3.3.1 PP75 and PP50

Chen *et al.* (2009b) grafted three hydrophobic amino acids L-valine (PV75), L-leucine (PL75) and L-phenylalanine (PP75, Figure 1-6 and Figure 1-8) at a stoichiometric percentage of 75 mol% onto the carboxylic acids of PLP to determine if their conjugation affected their membrane disruptive behaviour. Red blood cells (RBCs) were used as a model for endosomal membranes and each polymer's haemolytic activity was assessed. The results showed that the increased hydrophobicity of the amino acid (L-valine < L-Leucine < L-phenylalanine) was positively correlated to their polymer haemolytic activity (PLP < PV75 < PL75 < PP75). PP75's (actual degree of grafting is 63% as confirmed by ^{1}H-NMR) optimal membrane disruption was found at pHe 6.0-7.0, but negligible membrane disruption occurred at physiological pHe. To put their haemolytic capabilities into perspective, the membrane disruption of melittin (a toxin in bee venom that possesses strong haemolytic activity) was compared to PL75 and PP75. PP75 was found to be 11 times more disruptive than PL75 and 35 times more disruptive than melittin. Increasing cytotoxic effects were however observed at increasing concentrations of polymer.

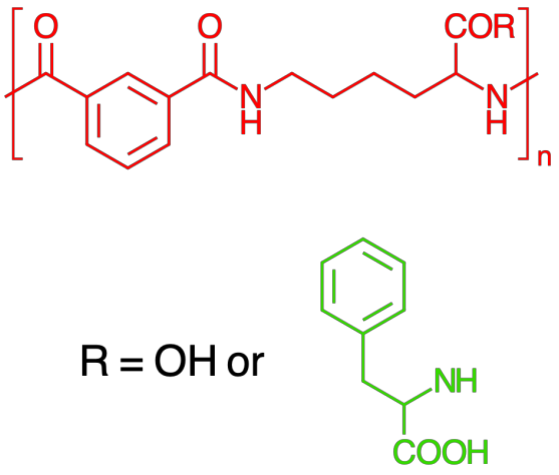

Figure 1-6. Structure of PP50 and PP75 synthesised by grafting the hydrophobic amino acid L-phenylalanine onto the pendant carboxylic acids on PLP (at a stoichiometric percentage of 50 mol% or 75 mol%, respectively).

Treatment of HeLa cells with FITC-labelled PLP *in vitro* showed that the polymer was restricted to intracellular vesicles. Conversely, FITC-labelled PP75 displayed diffused staining in the cytoplasm, supporting the evidence that PP75 has superior endosomal membrane disruptive capabilities (Chen et al., 2009b). In addition, PP75 was shown to facilitate the entry of the calcein into the cytoplasm, predominantly through clathrin-mediated endocytosis (Khormaee et al., 2013). Further studies have shown that the intracellular delivery of apoptin (a protein that induces tumour-specific apoptosis) and siRNA against stathmin (an oncoprotein) for *in vivo* applications is possible using PP75 (Khormaee et al., 2013; Liechty et al., 2009). PP75 has also been shown to deliver model drugs effectively into 3D HeLa multicellular spheroids used as *in vitro* tumour models (Ho et al., 2011).

Most recently, PP50, PLP grafted with phenylalanine at a 50% stoichiometric molar substitution, successfully delivered the pro-apoptotic peptide Bim to cells, as measured by caspase 3/7 activation at pHe 6.5 but not pHe 7.4, and decreased cell viability when compared to Bim or PP50 alone. In addition, PP50 has been reported to enhance the uptake of green fluorescent protein (GFP) (Kopytynski et al., 2020).

PP75, due to its higher stoichiometric percentage of L-phenylalanine grafting, is more membrane-active than PP50 and has thus been proposed as a suitable delivery agent for drug delivery applications (Chen et al., 2009a; Ho et al., 2011). PP50, although having a slightly lower membrane activity than PP75, is still sufficiently membrane-active for the intracellular delivery of therapeutics. Consequently, PP50's applications are more suited to *in vitro* and *ex vivo* delivery of macromolecules and cell engineering, the main focus of this thesis. For such applications, there is a delicate balance between efficient and quick intracellular delivery without causing irreversible damage to the cell. PP50 has demonstrated membrane permeabilisation of erythrocyte membranes at mildly acidic pHe which can be quickly reversed at pHe 7.4 with no permanent damage, confirming its suitability for applications *in vitro*, *ex vivo* and for cell engineering (Chen et al., 2020; Lynch et al., 2011, 2010).

1.3.3.2 PLP-NDA18

PLP-NDA18 (Figure 1-7 and Figure 1-8) is a pH-responsive, comb-like polymer derived from PLP that displays superior membrane anchoring and disruptive capabilities to PLP. PLP-NDA18 is synthesised by grafting the long hydrophobic decylamine, acting as a membrane anchor, onto the pendant carboxylic acid groups on PLP. Chen *et al.* (2017) investigated the effect of grafting different degrees of decylamine (3 mol%, 10 mol% and 18 mol%) on the haemolytic ability of the polymers. The results showed that the increase in grafting percentage of decylamine positively correlated to the polymer's haemolytic activity (PLP < PLP-NDA3 < PLP-NDA10 < PLP-NDA18). The most optimal polymer PLP-NDA18 displayed excellent membrane disruption capabilities even at lower concentrations (0.025 mg/mL). Like PP75, no membrane disruption occurred at physiological pHe. However, unlike PP75, PLP-NDA18's optimum membrane disruption was found at pHe 5.5. Increasing cytotoxic effects were observed at increasing concentrations (> 5 mg/mL) of polymer.

By using the membrane impermeable calcein as a model cargo, diffuse staining was observed in the cytoplasm of HeLa, CHO and A549 cells when treated with calcein and PLP-NDA18. Only punctate green spots, correlating to the sites of intracellular vesicles, were observed when these cells were treated with calcein and PLP (Chen et al., 2017). Although structurally different from PP50, PLP-NDA18 has also demonstrated reversible membrane permeability of erythrocyte membranes without permanent damage to cells. In addition, PLP-NDA18 has shown very rapid (5 minutes) and efficient intracellular delivery of trehalose at mildly acidic pHe (Chen et al., 2020).

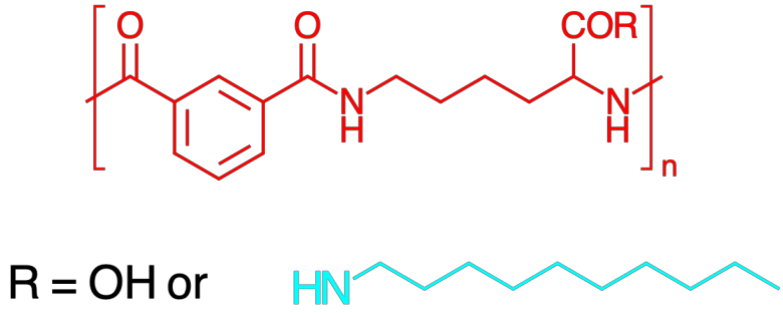

Figure 1-7. Structure of PLP-NDA18 synthesised by grafting the membrane anchoring decylamine at 18 mol% onto the pendant carboxylic acids on PLP.

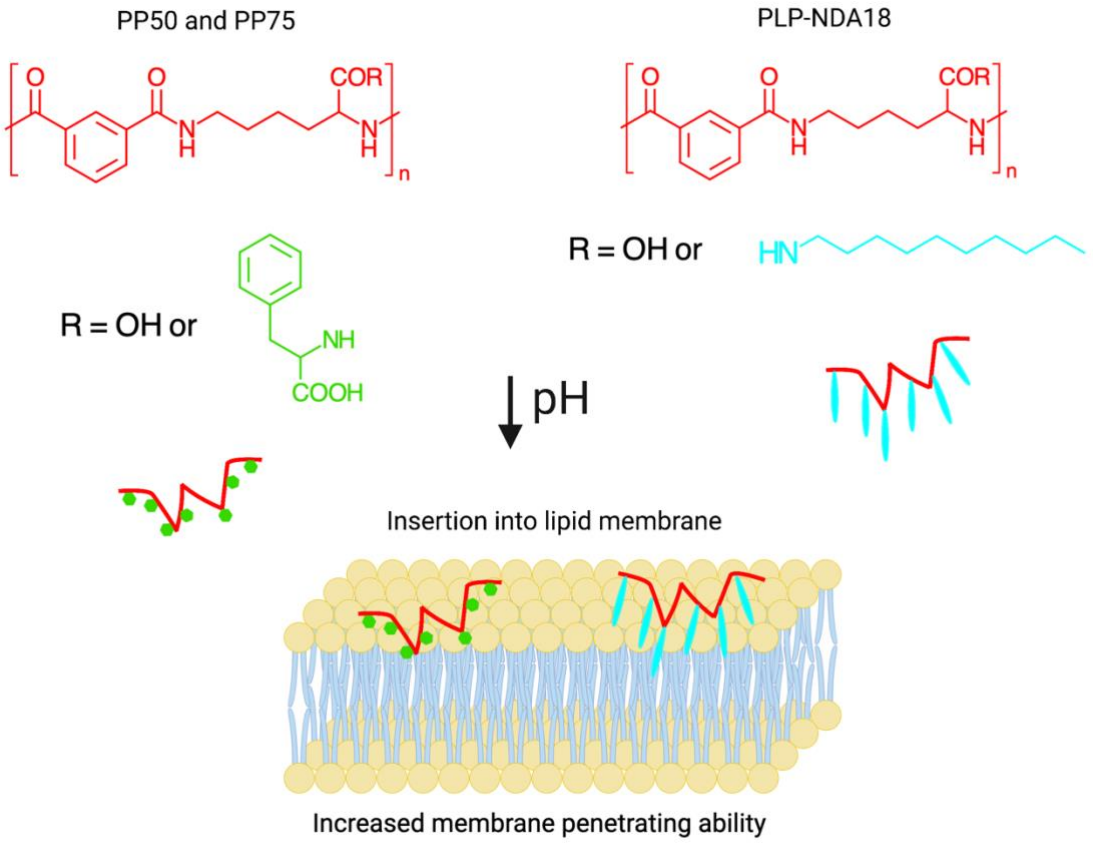

Figure 1-8. pH-responsive polymers for intracellular delivery. The change in pHe to mildly acidic pHe triggers a conformational change in the pH-responsive polymer leading to the insertion and destabilisation of the membrane.

1.4 Intracellular delivery for cell engineering applications

1.4.1 Cell engineering

A cell is the most basic sub-unit of an organism (Nerem, 1991). Cells naturally perform therapeutic tasks by sensing and responding to environmental changes and signals in the body. For example, in response to rising glucose levels, pancreatic ß islet cells produce insulin (Fischbach et al., 2013). With the ability to grow, treat and analyse primary cells, immortalised cell lines and animal cells under controlled laboratory conditions (also commonly known as cell culture), the opportunities to research into the engineering of cells for therapeutic purposes have vastly increased (Nerem, 1991; Xu et al., 2019).

Whilst there is no clear-cut definition for cell engineering, broadly speaking, it can be defined as the intentional alteration of a cell's properties. This could include but is not limited to, manipulating cell function, growth and proliferation, or the way it communicates with other cells (Cameron and Tong, 1993). As such, depending on the therapeutic application, cells can be engineered to express proteins, release cytokines, induce apoptosis and stimulate proliferation (Wang et al., 2015).

Monolayer 2D cell cultures are commonly used to evaluate the performance of intracellularly delivered therapeutics through biologically relevant assays. In addition, *in vitro* cultured 3D spheroids serve as good models for *in vivo* solid tumours (Costa et al., 2016). Compared to normal tissues (pHe 7.4), the pHe of tumour tissues is maintained at ~pHe 6-7 (Dai et al., 2017). For cancer therapy applications, this unique property is advantageous for the delivery of proteins or immunotoxins with pH-responsive polymers whose membrane activity falls in the pH range of the early endosomes.

1.4.2 Cell therapies

Cell therapies are a subset of cell engineering, where the cells themselves act as therapeutic agents. After a cell is engineered to perform a desired biological function, the live cell is introduced into an organism to treat a disease (Liras, 2010; Woodsworth and Holt, 2017). Where a patient's cells are either damaged, defective or missing, cell therapy offers a means to repair or restore lost function (Fodor, 2003).

Most cell therapies are carried out *ex vivo*, whereby the desired cells are isolated and then cultured, treated and/or manipulated *in vitro*. The adoption of *ex vivo* cell manipulation strategies for cell therapies permits the adjustment of extracellular influences i.e., cell culture medium components and pHe to aid in the engineering of cells. For example, in using pH-responsive polymers to deliver therapeutics intracellularly to modify cell function, the pHe can be lowered or growth factors can be added to the culture medium to promote growth, expansion, differentiation or delivery of cargoes (Naldini, 2011; Stewart et al., 2018).

Cell-based therapies can be broadly divided into two categories: allogeneic and autologous cell therapies. Allogeneic cell therapy describes when healthy donor cells are introduced into a patient. Conversely, in autologous cell therapy, the patient's cells are collected, modified and reintroduced back into the same patient (Heathman et al., 2015). The inherent advantage of autologous cell therapies over allogeneic cell therapies is the reduced need for compatible donors and the risk of rejected host cells (Naldini, 2011).

Haematopoietic stem cell (HSC) transplantation is one of the most popular and successful branches of cell therapy. The ability to edit genes in HSCs, which have the ability to self-renew and produce all blood lineages, would enable a continuous supply of permanent gene-corrected progeny in the body (Cavazzana et al., 2019; Naldini, 2011). Clinical trials involving the *ex vivo* gene transfer into CD34+ cells using lentiviral vectors for the treatment of ß-Thalassemia major and Wiskott-Aldrich have been carried out (Naldini, 2015) yielding positive results. However, even with the development of safer vectors, concerns regarding the use of viral vectors for cell therapies remains.

The field of immune cell engineering is rapidly becoming more prominent. In particular, cell membrane engineering. That is, engineering immune cells to express specific surface markers to enhance therapeutic function. For example, the expression of major histocompatibility complex (MHC) on APCs or T cell receptors (TCR) on T lymphocytes (Wang et al., 2015).

1.4.2.1 Antigen Presenting Cells

Professional APCs including DCs, B lymphocytes and macrophages are key players of the immune system that mediate the cellular immune response by recognising and internalising antigens for their presentation in MHCs (Wang et al., 2015). Amongst the professional APCs, DCs are more efficient at T cell stimulation and orchestrating a potent CD8+ T cell response and are thus most routinely used for *ex vivo* manipulation of APCs (Bhargava et al., 2012; Trombetta and Mellman, 2005).

Intracellular protein antigens are initially degraded by proteasomes and delivered to the cytosol before being translocated to the ER where they are loaded and displayed in the peptide binding site of MHC Class I. MHC class I molecules subsequently recognise and interact with TCR to stimulate CD8+ killer T cells. Conversely, extracellular protein antigens traffic to the endo-lysosome and are loaded onto MHC Class II. MHC class II molecules subsequently recognise and interact with TCR to stimulate CD4+ T cells. However, some DCs are capable of cross-presentation – the loading of exogenous antigen peptides on MHC class I molecules (De Charette et al., 2016; Goldberg, 2015; Hubbell et al., 2009; Lai et al., 2011; Laidlaw et al., 2016). In addition to MHC interactions, the expression of co-stimulatory molecules and the release of cytokines are both critical for initiating a strong T cell response (Figure 1-9) (Hubbell et al., 2009; Wang et al., 2015).

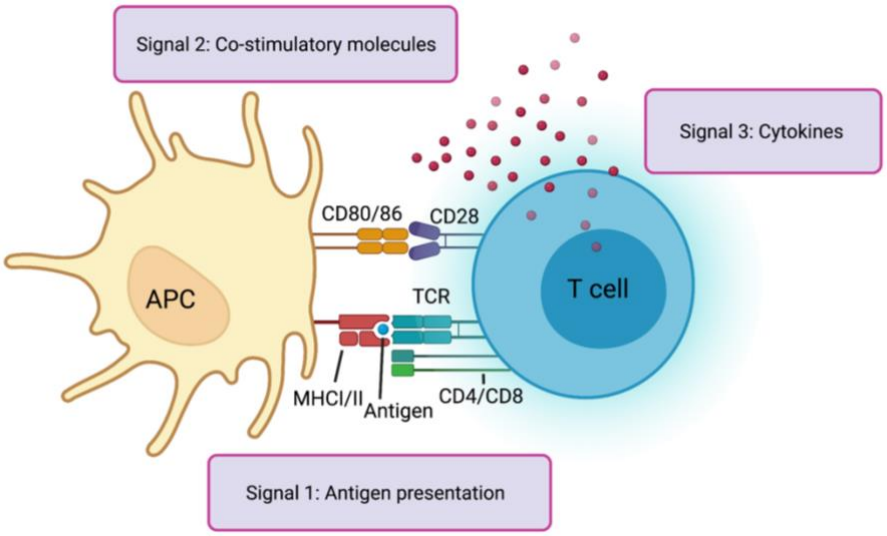

Figure 1-9. Activation of T cells by interaction with APCs. The engagement of the TCR with the appropriate MHC-peptide complex in addition with co-stimulatory molecules and cytokine secretion leads to the activation of T cells. Modified from (Lee et al., 2020) with permission. Abbreviations. APC = antigen-presenting cell. TCR = T cell receptor. MHC = major histocompatibility complex.

Thus, the focus of research has not only been optimising materials to enhance protein antigen uptake *in vitro* into APCs but also ensuring that the correct subcellular targeting is achieved to initiate the direct MHC loading and subsequent priming of T cells.

The first FDA approved (2010) cell-based therapy, Sipuleucel-T (Provenge®), is a prime example of a successful autologous cellular immunotherapy. Here, a patient's APCs are isolated *ex vivo* and incubated with prostatic phosphate antigen (PAP), a tissue antigen expressed by prostate cancer cells. The resulting blood product is reinfused back into the patient with the aim to generate PAP-specific T cells that will evoke a natural immune response against prostate cancer cells (Anassi and Ndefo, 2011; Cheever and Higano, 2011; Heathman et al., 2015).

1.4.2.2 T cells

T lymphocytes are important members of the adaptive immune response and are responsible for coordinating high specific and long lasting responses to help with tumour rejection and pathogen clearance (Fabbri et al., 2003; Sadelain et al., 2017).

Where a person's immune system is not robust enough to generate an efficient T cell response, or when antigen presentation is insufficient, genetically engineered T cells serve as a powerful new therapy to overcome this. When infused back into the body, the *ex vivo* genetic modification of T cells to express either TCR or Chimeric antigen receptors (CARs) enables patients to mount a tumour-specific immune response (Hou et al., 2021).

Chimeric antigen receptors are a class of synthetic receptors that can recognise and kill a pre-defined target (Elahi et al., 2018). Unlike TCRs that are activated by their conjugate MHC molecule, CAR activation is MHC independent (Caliendo et al., 2019). The lead paradigm for CAR T cell therapies and the first FDA approved gene therapy product was the CAR-T targeting the CD19 antigen expressed in malignant B cells. Treatment with this therapy has resulted in remission rates of up to 90% among patients (Hou et al., 2021). Despite showing huge success, there have been concerns over unwanted side effects, including toxicities of healthy B cells which also express the target antigen. For example, B cell aplasia and high relapse rates have been associated with patients treated with CD19 CAR-T cells (Huang et al., 2020; Lim & June, 2017).

Altogether, it is evident that there remains a need for a robust platform to demonstrate efficient targeted intracellular delivery of therapeutics for a range of applications. The PP-family polymers (PP50 and PLP-NDA18) have shown to be promising platforms for the intracellular delivery of macromolecules, possessing many of the desirable qualities of an ideal intracellular delivery system. These bio-inspired and biodegradable polymers offer low cellular toxicity and reversible membrane permeability, whilst showing to deliver a range of cargoes across cell types. In addition, the simple delivery method, of co-incubation with polymer and payload allows payloads to be efficiently delivered into the cell (Chen et al., 2020; Khormaee et al., 2013; Kopytynski et al., 2020; Lynch et al., 2011, 2010).

For those reasons, this group of polymers were chosen as the main subject of the studies presented in this thesis. However, the use of cationic polymers are also introduced and investigated for their role in the intracellular delivery of anionic payloads for cell engineering applications.

1.5 Aims and objectives of project

The aim of this project was to use a series of pH-responsive polymers for the intracellular delivery of macromolecules. Specifically, the author aimed to enhance the current understanding and scope of using the anionic PP50 polymer as an *in vitro* and *ex vivo* platform for the functional delivery of therapeutics. The use of the anionic PLP-NDA18 polymer as an intracellular delivery tool for the delivery of proteins was also briefly explored. In addition, cationic pH-responsive polymers (namely CP1 and CP2) were introduced at the end to address the problem of delivering anionic payloads for cell engineering applications.

Some specific key questions addressed in this project are listed below.

<u>PP50 mediated intracellular delivery of macromolecules</u>

- Do PP50 polymers demonstrate endosomal release or membrane disruption of cellular membranes?
- Can PP50 be fluorescently labelled to visually demonstrate intracellular polymer localisation?
- Can PP50 deliver antibodies to different intracellular target sites?
- Can PP50 deliver anionic and cationic peptides intracellularly?

<u>Development of anionic pH-responsive platforms for the intracellular delivery of proteins *in vitro* for potential cancer therapy and cell engineering applications</u>

- Can PLP-NDA18 and PP50 enhance the cytotoxicity of the ribosome-inactivating membrane-impermeable protein toxin saporin?
- Does co-incubation with saporin result in high efficiency?

- Does PP50 mediated saporin delivery increase cytotoxicity via multiple death pathways?
- Is PP50 mediated saporin delivery accompanied by a decrease in protein synthesis?
- What intracellular delivery mechanisms does PP50 use to deliver saporin to enhance its cytotoxicity?
- Can PP50 penetrate and successfully deliver saporin into multicellular spheroids?

pH-responsive polymers as *ex vivo* cell therapy platforms

- Can ovalbumin peptide be used as a model antigen to demonstrate polymer mediated delivery for cell engineering applications?
- Can pH-responsive cationic or anionic polymers mediate ovalbumin peptide delivery to increase the upregulation of MHC Class I on DCs?
- Is the upregulation of MHC I accompanied by the upregulation of co-stimulatory molecules by DCs?
- Is the upregulation of MHC I accompanied by the secretion of cytokines by DCs?
- Can the upregulation of MHC I molecules on DCs stimulate CD8+ T cells?

1.6 Research gaps and novelties

The work in this thesis builds upon the work previously published on PP50 and PLP-NDA18 as promising intracellular delivery platforms. The research gaps and key novelties of each part are specified below, and also summarised in Table 1-4.

Firstly, the published work introduces PP50 as a promising intracellular delivery platform, capable of delivering different sized dextrans, trehalose, GFP and the therapeutic apoptotic peptide Bim (Kopytynski et al., 2020; Lynch et al., 2011, 2010). Here, we aim to extend the capabilities of PP50 by demonstrating the delivery of other clinically relevant peptides, antibodies and functional proteins. The work presented in this thesis is the first report on the intracellular delivery of cationic and anionic peptides, and the functional delivery of saporin using PP50. The work undertaken in this project will provide a better understanding into the intracellular delivery mechanism and of the use of PP50 for therapeutic payload delivery to

intracellular target sites. As an adaptable platform, PP50 may be used in the future for targeted delivery to address key biological diseases.

Similarly, previous work on PLP-NDA18 has focused on the intracellular delivery of different sized dextrans and trehalose (Chen et al., 2020, 2017). There has been limited understanding of the use of PLP-NDA18 to deliver larger functional proteins to cells. Thus, the intracellular delivery of saporin by co-incubation with PLP-NDA18 adds to the development of PLP-NDA18 as an intracellular delivery platform.

Further, little attention has been dedicated to the investigation of PP50 or PLP-NDA18 as an *ex vivo* tool for cell engineering applications. This project is the first report on the exploration of these polymers as potential cell engineering tools.

Lastly, novel newly synthesised cationic pH-responsive polymers have been tested for their ability to facilitate intracellular delivery of negatively charged payloads for cell engineering applications. This is the first reported work on these polymers. The results generated from this work provides a solid foundation on which to optimise and develop these cationic polymers for applications in disease therapy.

Table 1-4. Summary of research gaps, aims and novelties in the three results chapters.

	Research gap	Sub-project aims	Novelties
Chapter 3 Intracellular delivery of macromolecules using PP50	• Limited understanding about PP50's intracellular delivery mechanism and payload delivery to different intracellular target sites • Peptide delivery currently limited to neutral peptides	• To investigate the mechanism of PP50-meditaed payload entry • Demonstrate cytoplasmic payload delivery and targeted payload delivery to different intracellular sites • Assess the capability of PP50 to deliver anionic and cationic peptides • Further establish PP50 as a suitable non-cytotoxic *in vitro* and *ex vivo* intracellular delivery platform	• First report of anionic and cationic payload delivery by PP50
Chapter 4 Polymer mediated saporin delivery	• No functional delivery of proteins demonstrated by PP50 or PLP-NDA18	• Demonstrate that PLP-NDA18 and PP50 can enhance the cytotoxicity of the membrane-impermeable protein saporin • Investigate the mechanism by which PP50 delivers saporin and initiates cell death • Demonstrate PP50 penetration and saporin delivery into multicellular spheroids	• First report of functional protein delivery by PLP-NDA18 and PP50

Chapter 5 *Ex vivo* manipulation of dendritic cells by anionic and cationic polymers	• Inefficient immune response by APCs for effective T cell stimulation • Limited understanding of the use of PP50 and PLP-NDA18 polymers for *ex vivo* cell engineering applications • Applications of cationic polymers CP1 and CP2 not yet explored	• Investigate the use of pH-responsive polymers to deliver ovalbumin peptide and increase MHC presentation, expression of co-stimulatory molecules and release of cytokines for the stimulation of T cells	• First report of the applications of newly synthesised cationic polymers for intracellular delivery

1.7 Thesis outline

This work presented within this thesis comprises of six chapters, outlined as follows.

Chapter 1 introduces the background of intracellular delivery, highlighting the opportunities and challenges of the delivery of therapeutic macromolecules. An emphasis on *in vitro* and *ex vivo* intracellular delivery and applications for cell engineering is explored. The use of pH-responsive polymers, namely PP50 and PLP-NDA18 is discussed, which provides the focus of the research in this thesis.

Chapter 2 describes the materials and methods used in the subsequent chapters of this thesis. Synthesis and characterisation of PLP and its derivates: PP50 and PLP-NDA18 are described. Cell lines and cell assays to determine successful payload delivery and cytotoxicity are presented.

Chapter 3 describes the versatility of PP50 as an intracellular delivery platform. The pH responsiveness of PP50 is investigated using ovine erythrocytes as model membrane and demonstrated using the co-incubation of PP50 with FITC-dextran at physiological and mildly acidic pHe using HeLa cells. Further, the delivery and cytotoxicity of PP50 to immune cells is shown. Fluorescently labelled polymer and different sized fluorescently labelled payloads are used to demonstrate the capabilities of PP50 to deliver a range of therapeutic molecules to different organelles. In addition, the mechanism elucidating PP50 mediated payload delivery is investigated.

Chapter 4 describes the ability of PP50 to enhance the cytotoxicity of saporin in A549 cells and 3D multicellular spheroids *in vitro*. The death pathway in which saporin acts intracellularly is examined. Finally, the ability of PLP-NDA18 to deliver saporin is measured.

Chapter 5 aims to investigate pH-response polymers for the intracellular delivery of ovalbumin peptide, a model antigen, for cell engineering applications. The ability of PP50, PLP-NDA18 and cationic polymers (CP1 and CP2) are explored to upregulate key markers on DCs for T cell stimulation.

Chapter 6 summarises the research presented in the preceding result chapters. Conclusions are drawn based on the research untaken and recommendations for future work are highlighted.

Chapter 2

Materials and Methods

2.1 Materials

Saporin from *Saponaria officinalis* seeds, amiloride hydrochloride hydrate, Fluorescein isothiocyanate–dextran (FITC-dextran, average Mw 150 kDa), ammonium chloride, Sodium Chloride (NaCl), nystatin, chlorpromazine hydrochloride, decylamine, Methyl beta-cyclodextrin (MβCD), N,N'-Dicyclohexylcarbodiimide (DCC), Dulbecco's modified Eagle's medium (DMEM), Dulbecco's Phosphate-Buffered Saline With MgCl2 and CaCl2 (PBS), Fetal Bovine Serum (FBS), fluorescein isothiocyanate (FITC), 2-Mercaptoethanol, melittin amino acid sequence: (GIGAVLKVLTTGLPALISWIKRKRQQ), penicillin, Lipopolysaccharides from Escherichia coli O55:B5 (cat L2880), dimethyl sulfoxide (DMSO), dimethyl sulfoxide -d_6, 4-(Dimethylamine) pyridine (DMAP), and Hoechst 33342 were purchased from Sigma-Aldrich (Dorset, UK).

Cytochalasin D, LysoTracker® red DND-99, ER-Tracker™ Red dye Mito-Tracker™ Red dye, LysoTracker™ Green DND-26, Alpha minimum essential medium (MEM α), Dead Cell Apoptosis Kit with Annexin V FITC and PI, FIX & PERM™ Cell Permeabilization Kit (cat. no. GAS004), L-Glutamine (200mM), Penicillin-Streptomycin (10,000 U/mL), HEPES, RPMI 1640 Medium (RPMI), Nonessential amino acids, Dynabeads™ Mouse T-Activator CD3/CD28 for T Cell Expansion and Activation (cat. no. 11452D), Trypsin-EDTA (0.25%), Mouse Granulocyte-Macrophage colony-stimulating factor (GM-CSF), Mouse IFN gamma Recombinant Protein (cat. no. PMC4031), Click-iT™ Plus OPP Alexa Fluor™ 488 Protein Synthesis Assay Kit (cat C10456) were purchased from ThermoFisher (Loughborough, UK).

Caspase-Glo® 3/7 Assay, Caspase-Glo® 8 Assay, Caspase-Glo® 9 Assay, CellTiter-Glo® 3D Reagent and CellTiter-Glo® 2.0 Assay were purchased from Promega (Southampton, UK).

Cyanine5 amine (Cy5, cat. no. ab146463), Goat Anti-Rabbit IgG H&L (Alexa Fluor® 488) (cat. no. ab150077), Anti-beta Tubulin antibody (cat. no. ab6046) were purchased from Abcam (Cambridge, UK).

Triton® X-100, L-lysine methyl ester dihydrochloride and L-phenylalanine methyl ester hydrochloride were purchased from Alfa Aesar (Heysham, UK).

Hydrochloric acid (HCl), triethylamine, Dimethylformamide (DMF), Diethyl ether, Sodium hydrogen carbonate, sodium hydroxide (NaOH), sodium citrate dihydrate, potassium carbonate, sodium phosphate, acetone, anhydrous ethanol were purchased for VWR (Lutterworth, UK).

Glass-bottom cell culture dishes (35 mm, cat. no. P35G-1.5-14-C) were purchased from MatTek, (Ashland, MA, USA).

Defibrinated sheep blood (cat. no. SB054) was ordered from TCS Biosciences (Buckingham, UK).

Corning® spheroid microplates (cat. no. CLS4515-5EA), Corning™ Falcon™ Test Tube with Cell Strainer Snap Cap were purchased from Corning (Flintshire, UK).

Brilliant Violet 421™ anti-mouse CD80 Antibody (cat. no. 104726), Alexa Fluor® 647 anti-mouse CD40 Antibody (cat. no. 102912), FITC anti-mouse I-Ab Antibody (cat. no. 116406), PE anti-mouse H-2Kb bound to SIINFEKL Antibody (cat. no. 141604), Purified anti-Nuclear Pore Complex Proteins Antibody (cat. no. 902907), Alexa Fluor® 594 Goat anti-mouse IgG antibody (405326) were purchased from BioLegend (London, UK).

DuoSet enzyme-linked immunosorbent assay (ELISA) Ancillary Reagent Kit 2 (cat. no. DY008), Mouse IL-6 DuoSet® ELISA (cat. no. DY406-05), Mouse TNF-α DuoSet® ELISA (cat. no. DY410-050), Mouse IL-2 Quantikine ELISA Kit (cat. no. M2000) were purchased from R&D Systems (Oxfordshire, UK).

Eppendorf 96-Well Cell Imaging Plates (cat. no. 0030741013) was purchased from Eppendorf (Stevenage, UK).

FITC-OVA (241-270) peptide was synthesised and purchased from Creative peptides (NY, USA).

OVA (323-339) FITC labelled (cat. no. 14805-01), p53 (17-26) FITC labelled (cat. no. 10710-01), Histone H3 (1-21) FAM labelled (cat. no. 14602-01) and (klaklak)2 (cat. no. 14280-01) was purchased from biosynthesis (Lewisville, Texas).

HY-P2495A OVA (241-270) (TFA) was purchased from MedChemExpress (Sollentuna, Sweden).

Polymers $mPEG_{113}$-*b*-($PtBOOC_{90}$-*stat*-PCL_{130}) and $mPEG_{113}$-*b*-$PtBMOC_{110}$-*b*-PCL_{90} (namely CP1 and CP2) were provided by Xinyu Lu, Rongjun Chen research group, Department of Chemical Engineering, Imperial College London (Figure 2-1).

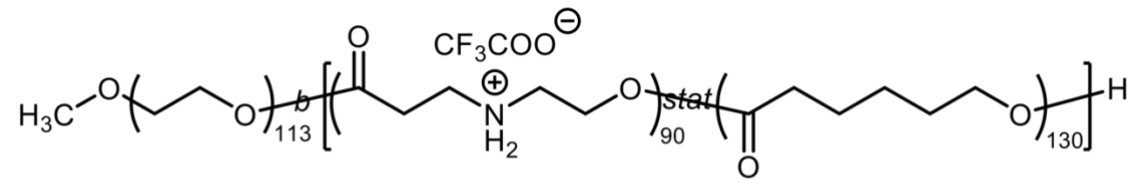

$mPEG_{113}$-*b*-($PtBOOC_{90}$-*stat*-PCL_{130})

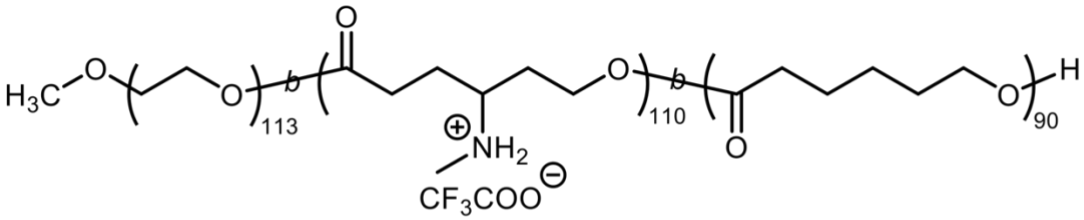

$mPEG_{113}$-*b*-$PtBMOC_{110}$-*b*-PCL_{90}

Figure 2-1. Chemical structures of mPEG113-b-(PtBOOC90-stat-PCL130) (CP1) and mPEG113-b-PtBMOC110-b-PCL90 (CP2). Synthesised by Xinyu Lu (Rongjun Chen group).

2.2 PLP synthesis

The PP50 and PLP-NDA18 polymer backbone were derived from poly(L-lysine isophthalamide) (PLP) (Eccleston et al., 2000, 1999).

Polycondensation

L-lysine methyl ester dihydrochloride (0.15 mol, 35 g) and potassium carbonate (0.6 mol, 83 g) was dissolved in precooled deionised water (dH_2O, 750 mL) and placed in an ice bath under magnetic stirring until all solids disappeared. Iso-phthaloyl chloride (0.15 mol, 30.5 g) was dissolved in dry acetone (750 mL), pre-cooled at -20^oC, and rapidly poured into the aqueous solution. The reaction was allowed to proceed for ~1 hour to allow the PLP methyl ester polymer products to precipitate. The recovered polymer coagulation was washed thoroughly with dH_2O to remove excess solvent and left to oven-dry overnight at 70^oC. The resultant stiff polymer was blended into a white powder.

Ester hydrolysis

The dried PLP methyl ester powder was dissolved in DMSO. NaOH (5% wt) in anhydrous EtOH (0.375 mol, 2.5 molar equivalents to PLP methyl ester) was added to the solution, and the reaction was stirred at room temperature. The resultant precipitated hydrolysed polymer, PLP, was collected by vacuum filtration and re-dissolved in dH_2O.

Purification

HCl (2M) was added to the polymer solution until complete precipitation of the polymer occurred. The precipitated polymer was collected by vacuum filtration and re-dissolved in NaOH (0.2 M). The polymer precipitation with HCl, filtration and re-dissolution with the NaOH process was performed at least 3 times. The final polymer was dialysed against dH_2O with a dialysis membrane (MWCO 12-14 kDa) for one week. The dH_2O was changed daily. After one week, the dialysed polymer solution was adjusted to pH 3.0 with HCl (2M). The precipitated polymer was collected by vacuum filtration, washed with dH_2O and lyophilised until a fine white powder was obtained.

2.3 PP50 synthesis: grafting of PLP with L-phenylalanine

For PP50 synthesis, the stoichiometric ratio of L-phenylalanine to the carboxylic acid groups on the PLP backbone is 50%. PP50 was synthesised according to *Chen et al* (2009a). Briefly, PLP (3 g, 10.87 mmol), L-phenylalanine methyl ester hydrochloride (1.17 g, 5.3 mmol), triethylamine (1.82 mL, 2.4 molar equivalents to L-phenylalanine) and DMAP (0.6 g) was dissolved in a (1:3 v/v) binary anhydrous solvent of DMSO: DMF (15 mL:45 mL) and stirred at room temperature. DCC (3.36 g, 3 molar equivalents to L-phenylalanine) was dissolved in anhydrous DMF (20 mL) and added dropwise to the reaction mixture. The reaction was allowed to proceed for 60 hours at room temperature with continuous stirring. Afterwards, the solution was vacuum filtrated to remove dicyclohexylurea (DCU) side products and solid impurities. NaOH (5 wt%) was dissolved in anhydrous ethanol (28 mL), and the solution was added to the filtrate. The resultant solution was stirred for 3 hours at room temperature to allow polymer hydrolysis to occur. The hydrolysed polymer was then rapidly poured into five volumes of diethyl ether, and the precipitated polymer was collected by vacuum filtration and re-dissolved in dH_2O. The final polymer was dialysed against dH_2O as previously described for one week. For PP50 salt form, the pH was adjusted to pH 7.4 with NaOH (0.2 M) before being lyophilised to produce a fine white powder. For PP50 acidic form, used for NMR analysis, the pH was adjusted to pH 3 with HCl (2M). The polymer precipitate was then collected by vacuum filtration and washed three times using dH_2O before being lyophilised to obtain a fine white powder.

2.4 PLP-NDA18 synthesis: grafting of PLP with decylamine

For PLP-NDA18 synthesis, the stoichiometric ratio of decylamine to the carboxylic acid groups on the PLP backbone is 18%. PLP-NDA18 was synthesised according to Chen *et* al. (2017). Briefly, PLP (3 g) was dissolved in DMF (65 mL) and stirred at room temperature until dissolved. DCC (1.21 g) and DMAP (0.6 mg) were added to the solution with continuous stirring. Decylamine (391 µL) in a minimal amount of chloroform was added to the solution, and the reaction was allowed to proceed for 60 hours. Afterwards, the reaction mixture was filtered by vacuum filtration to eliminate DCU side products. The filtrate was rapidly added to diethyl ether (305 mL), and the precipitated polymer was collected by vacuum filtration. The precipitate was dissolved in a minimal volume of NaOH (2M) and dialysed against dH_2O as previously described for one week. The pH of the polymer solution was adjusted as previously

described for PLP-NDA18 acidic and salt form and lyophilised until a fine white powder was obtained.

2.5 Labelling of PP50 with Cy5

Cy5-PP50 was employed to trace the subcellular localisation of PP50 once delivered intracellularly. Fluorescently labelled PP50 was prepared by grafting Cy5 to the pendant carboxylic acid groups on PP50 at 2%. A low percentage of labelling was chosen to avoid significant changes to the properties of PP50. Briefly, PP50 (100 mg), Cy5 (3.69 g, 2% stoichiometric ratio to PP50's [COOH]) and DMAP (20 mg) was dissolved in 800 µL DMF and stirred at room temperature in a small glass vial, covered from the light. DCC (3 molar equivalents to Cy5) in anhydrous DMF (80 µL) was added to the polymer solution and sealed. The reaction was allowed to proceed for 24 hours. Afterwards, the reaction mixture was centrifuged at 9500 g for 5 minutes to spin down the DCU products. The supernatant was added to sodium bicarbonate (25 mL) and dialysed against dH_2O with a dialysis membrane (MWCO 12-14 kDa) for one week and then lyophilised to obtain a fine blue powder.

2.6 Labelling of saporin with FITC

Saporin was labelled with FITC to visualise the intracellular localisation of saporin after PP50 mediated delivery. FITC (1 mg) was dissolved in DMSO (1 mL). Saporin (1 mg) was dissolved in PBS (1mL) at pH 9. The FITC solution was added dropwise to the saporin solution at a 1:1 ratio and magnetically stirred at 4 °C in the dark overnight. The mixture was dialysed against pH 7.4 for 24 hours (MWCO = 14000 Da) and lyophilised to obtain a fine yellow powder.

2.7 Haemolysis

Sheep RBCs were used as a model membrane to assess the membrane lytic ability of the synthesised polymers. This model can give an insight into a polymer's ability to mediate intracellular payload delivery through direct membrane penetration at certain pHe's or initiate endosomolytic escape within certain pH ranges.

Phosphate buffers (0.1 M) were prepared in the pH range of 5.5-7.4. Citrate buffers (0.1 M) were prepared at pH 4.5 and pH 5.0. The polymer stock solution was added to the phosphate

or citric buffer to achieve the desired concentration for testing. Sheep RBCs were washed at least three times until the supernatant was clear. Briefly, the RBCs were centrifuged at 3500 rpm for 3 minutes. The supernatant was removed and replaced with an equivalent volume of NaCl (150 mM). After the last wash, the supernatant was removed and replaced with an equivalent volume of phosphate buffer pH 7.4. RBCs (10 µL) were then added to polymer buffer solutions or buffer solutions only, which were prepared as negative controls. Positive controls were prepared by adding RBCs to deionised water. All samples were prepared in triplicate (n=3). The samples were incubated at 37°C in a shaking water bath (120 rpm) for 1 hour and then centrifuged at 3500 rpm for 3 minutes. The supernatant was collected, and the absorbance was measured at 540 nm using UV-Vis spectrophotometer GENESYS 10S UV/Vis Spectrophotometer (Thermo Fisher Scientific, USA) to assess the haemoglobin release. The relative haemolysis percentage was calculated using Equation 2-1:

$$\text{Relative haemolysis (\%)} = \frac{\text{(Experimental absorbance) – (negative control absorbance)}}{\text{(Positive control absorbance)}} \times 100$$

Equation 2-1

MEng students Tudor-Octavian Sirbu and Suthinee Phanuvatsuk performed the haemolysis experiments for cationic polymers CP1 and CP2 presented in Figure 5-4 under my supervision.

2.8 Nuclear Magnetic Resonance Spectrometry

Proton Nuclear magnetic resonance (^{1}H-NMR) was utilised to confirm the structures of PP50 and PLP-NDA18. The polymers in their acidic form (5 mg) were dissolved in deuterated DMSO (0.8 mL) before being transferred to an NMR tube and analysed via ^{1}H-NMR at room temperature. The resulting spectrum was analysed via MestRenova software to calculate the degree of L-phenylalanine or decylamine grafting.

2.9 Cell culture

Cell cultures were maintained in a humidified incubator at 37°C with 5% CO_2. All cell culture work was conducted under aseptic conditions.

For long term storage, cells were cryopreserved in liquid nitrogen. Briefly, cells were harvested, and the density was determined using a haemocytometer or cell counter (CytoSMART, Corning). The cells were centrifuged at 1000 rpm or 500 g for 5 minutes and resuspended in a cryopreservation medium containing 10% DMSO (v/v) and 90% FBS (v/v). The final density of cells in the cryopreservation medium was kept between $1x10^6$ to $1x10^7$ cells per mL. Cryogenic storage vials containing 1 mL of cells were transferred to a Mr Frosty™ and placed in a -80°C freezer overnight. Afterwards, the vials were transferred to the liquid nitrogen tank.

Cells were thawed from the liquid nitrogen by placing the cryogenic storage vial in a preheated water bath at 37°C. Once the ice had melted, 1 mL culture medium was added to the cell suspension and centrifuged at 1000 rpm or 500 g for 5 minutes. The medium was removed, and the cell pellet was resuspended in fresh culture medium and transferred into a cell culture flask for incubation.

A549 (human lung cancer cells) and HeLa (human cervical cancer cells) were grown in DMEM supplemented with 10% (v/v) FBS and 1% penicillin/streptomycin.

JAWSII cells (human immature dendritic cells) were grown in MEM α supplemented with 20% (v/v) FBS, 1% penicillin/streptomycin and 5 ng/mL GM-CSF.

Jurkat (human T lymphocyte) and B lymphocytes (human) were generously provided by Professor Xiao-Ning Xu (Department of Infectious Disease, Faculty of Medicine, Imperial College London UK) and were grown in RPMI media supplemented with 10% (v/v) FBS, 1% penicillin/streptomycin, 1% L-glutamine, 1% non-essential amino acids, 1% HEPES and 1% sodium pyruvate.

RF33.70 cells (T-T hybridoma against OVA+ H-2Kb) were generously provided by Dr K L Rock (Department of Pathology, University of Massachusetts Medical School, MA, USA) and were grown in RPMI media supplemented with 10% (v/v) FBS, 1% penicillin/streptomycin, 1% L-glutamine, 1% non-essential amino acids, 1% HEPES and 27 µL 1M Mercaptoethanol.

A459, HeLa and JAWSII cells were detached using Trypsin-EDTA (0.25%) for passaging. RF33.70, B lymphocytes and Jurkat cells were passaged by aliquoting.

2.10 Laser scanning confocal microscopy

Laser scanning confocal microscopy was employed to visualise payload delivery into different intracellular sites within the cell. Images taken were representative of the whole population of cells. All images were taken using a CF6-Leica SP8 Inverted Microscope and were analysed using FIJI version 2.3.0.

FITC-dextran intracellular delivery

FITC-dextran served as a model payload to assess the versatility of the PP50 platform to deliver cargoes to different cell types. HeLa (1 mL, $3x10^5$ cells/mL) were seeded in a 35 mm glass-bottom Mattek dish (USA) overnight and then treated with a PBS solution containing FITC-dextran 150 kDa (10 µM) with PP50 (0.5 mg/mL) at pH 6.5 or pH 7.4 for 30 minutes. Cells incubated with FITC-dextran in the absence of PP50 were used as controls. The cells were then washed with PBS three times and replaced with 1 mL fresh media containing Hoechst 33342 (1 µg/mL, for nuclei visualisation) and LysoTracker® red DND-99 (50 nM, for endosome and lysosome visualisation). Jurkat cells and B lymphocytes (1 mL, $5x10^5$ cells/mL) were treated with a PBS solution containing FITC-dextran 150 kDa (10 µM) with PP50 (0.5 mg/mL) at pH 6.5 for 30 minutes. Cells incubated with FITC-dextran in the absence of PP50 were used as controls. The cells were then washed with PBS three times and replaced with 1 mL of fresh media. Cells were excited using the 488 nm laser for FITC-dextran (green channel), 405 nm laser for Hoechst 33342 (blue channel) and 561 nm for LysoTracker® (red channel).

Antibody intracellular delivery

The ability of PP50 to deliver antibodies to specific intracellular target sites was tested using anti-β-tubulin and anti-nuclear pore complex antibodies.

Anti-β-tubulin antibody

A459 (1 mL, 1.5 x 10^5 cells/mL) were seeded in a 35 mm glass-bottom Mattek dish overnight and then treated with a PBS solution containing anti-β-tubulin antibody (50 µg/mL) with or

without PP50 (1 mg/mL) at pH 6.5 for 2 hours. The cells were washed three times with PBS, replaced with fresh media and incubated for a further 16 hours. Afterwards, the cells were washed with PBS and treated with FIX & PERM™ Cell Fixation & Cell Permeabilization Kit. Briefly, cells were incubated for 15 minutes at room temperature with Fixation Medium A, washed with PBS and then incubated with the Permeabilization Medium B and Alexa 488 fluorochrome-labelled secondary antibody for 30 minutes. Cells were then washed with PBS and replaced with fresh media. A positive control, for comparison, was employed by incubating the cells with Fixation Medium A for 15 minutes at room temperature, followed by incubation with anti-β-tubulin antibody with Permeabilization Medium B for 30 minutes at room temperature. Afterwards, cells were incubated with Alexa 488 fluorochrome-labelled secondary antibody with Permeabilization Medium B for 30 minutes at room temperature and then replaced with fresh media. Cells were excited using the 488 nm laser.

Anti-nuclear pore complex antibody

HeLa (1 mL, 1.5 x 10^5 cells/mL) were seeded in a 35 mm glass-bottom Mattek dish overnight and then treated with a PBS solution containing anti-nuclear pore complex antibody (50 µg/mL) with or without PP50 (1 mg/mL) at pH 6.5 for 1 hour. The cells were washed three times with PBS and treated with FIX & PERM™ Cell Fixation & Cell Permeabilization Kit. Briefly, cells were incubated for 15 minutes at room temperature with Fixation Medium A, washed with PBS and then incubated with the Permeabilization Medium B and Alexa 594 fluorochrome-labelled secondary antibody for 30 minutes. Cells were then washed with PBS and replaced with fresh media. A positive control, for comparison, was employed by incubating the cells with Fixation Medium A for 15 minutes at room temperature, followed by incubation with anti-nuclear pore complex antibody with Permeabilization Medium B for 30 minutes at room temperature. Afterwards, cells were incubated with Alexa 594 fluorochrome-labelled secondary antibody with Permeabilization Medium B for 30 minutes at room temperature and then replaced with fresh media containing Hoechst 33342 (1 µg/mL). Cells were excited using the 405 nm and 594 nm lasers.

Intracellular delivery of FITC-p53

A459 (1 mL, 3 x 10^5 cells/mL) were seeded in a 35 mm glass-bottom Mattek dish overnight and then treated with a PBS solution containing FITC-p53 (11 µM) with PP50 (1 mg/mL) at pH

6.5 for 1 hour. Cells incubated with FITC-p53 in the absence of PP50 were used as a control. The cells were then washed with PBS three times and replaced with 1 mL of fresh media containing Hoechst 33342 (1 μg/mL) and LysoTracker® red DND-99 (50 nM) before analysis. Cells were excited using the 405 nm, 488 nm, and 561 nm lasers.

Intracellular delivery of Histone-FAM

A549 cells (1 mL, 3 x 10^5 cells) were seeded in a 35 mm glass-bottom Mattek dish overnight and then treated with a PBS solution containing PP50 alone at varying concentrations for 30 minutes at pH 6.5. The cells were then washed with PBS and treated with Histone-FAM only (10 μM) at pH 6.5 for 30 minutes. The cells were then washed with PBS three times and replaced with fresh media containing Hoechst 33342 and LysoTracker® before analysis. Cells were excited using the 405 nm, 488 nm, and 561 nm lasers.

Dr Michal Kopytynski (Postgraduate researcher, Department of Chemical Engineering Seed Fund for Translational Research funding) in Dr Rongjun Chen's group performed the above experiment presented in Figure 3-13 and Figure 3-14.

Cy5-PP50 mediated intracellular delivery of FITC-dextran in the presence of endocytosis inhibitors

To elucidate the mechanism of PP50 entry, A549 cells (1 mL, 1.5 × 10^5 cells) were seeded in a 35 mm glass-bottom Mattek dish overnight. The cells were pre-treated with chlorpromazine (3 μg/mL), cytochalasin D (2.5 μM), amiloride (30 μM), nystatin (10 μg/mL) or MβCD (1.5 mg/mL), in serum-free media for 30 minutes. The medium was removed and replaced with PBS containing FITC dextran 150 kDa (10 μM) and Cy5-PP50 (0.5 mg/mL) with inhibitors for 30 minutes at pH 6.5. The cells were washed three times with PBS and replaced with fresh media containing inhibitors and Hoechst 33342 (1 μg/mL). Cells were excited using the 405 nm, 488 nm, and 633 nm lasers.

Co-localisation of Cy5-PP50 and organelle stains

To visualise the intracellular localisation of PP50, A549 cells (1 mL, 1.5 × 10^5 cells) were seeded in a 35 mm glass-bottom Mattek dish overnight and then treated with a PBS solution containing Cy5-PP50 (0.5 mg/mL) for 30 minutes at pH 6.5. The cells were then washed with

PBS three times and replaced with fresh media containing Mito-Tracker red (200 nM), LysoTracker Green (100 nM) or ER-Tracker red (1 µM). Cells were excited using the 488, 561 nm or 633 nm lasers. Co-localisation percentage (Pearson's correlation coefficient) was determined using the Just Another Colocalization Plugin (JACoP) on FIJI. Pearson's correlation coefficient was calculated to quantify colocalisation for at least n=3 separate images for each treatment group.

FITC-saporin intracellular localisation

A549 cells (1 mL, 3 × 10^5 cells) were seeded in 35 mm glass-bottom Mattek dishes and incubated overnight. Afterwards, cells were treated with PBS containing FITC-saporin (0.125 mg/mL) with or without PP50 (0.2 mg/mL) for 1 hour at pH 6.5. The cells were washed three times with PBS, replaced with fresh media, and incubated for 24 hours. After incubation, cells were stained with Hoechst 33342 (1 µg/mL) and excited using the 405 and 488 lasers.

Protein synthesis inhibition assay

The commercially available Click-iT® Plus Alexa Fluor™ 488 OPP Protein Synthesis Assay Kit was employed to determine the level of protein synthesis in cells treated after saporin uptake. A549 cells (0.1 mL, 5 × 10^3 cells) were seeded overnight in a cell imaging plate (Eppendorf). The cells were then treated with sterile-filtered PBS containing free saporin, PP50 or PP50 and saporin at varying concentrations and incubated for 1 hour at pH 6.5. The cells were washed three times with PBS, replaced with media, and incubated for 24 hours before analysis. The cells were then treated with the Click-iT® Plus Alexa Fluor™ 488 OPP Protein Synthesis Assay Kit. All reagents were prepared as per the manufacturer's instructions. Briefly, the media was removed, and cells were incubated for 30 minutes with 20 µM Click-iT® OPP working solution. After incubation, the media was removed and washed with PBS. Then the cells were incubated with 3.7% formaldehyde in PBS for 15 minutes at room temperature. Afterwards, the fixative was removed and the cells were incubated in 0.5% TritionX®-100 for 15 minutes at room temperature. The permeabilisation buffer was removed, and the cells were washed twice with 100 µL PBS. Afterwards, 100 µL of Click-iT® Plus OPP reaction cocktail was added to each well, mixed well and incubated for a further 30 minutes, protected from the light. The reaction cocktail was then removed, and the cells were washed once with 100 µL of Click-iT® Reaction Rinse Buffer. The reaction rinse buffer was removed, and 100 µL per

well of 1X HCS NuclearMask™ Blue Stain working solution was added to the cells and incubated for 30 minutes at room temperature, protected from the light. Afterwards, the Blue stain solution was then removed, and the cells were washed with PBS twice before adding 100 µL PBS to each well. Cells were excited using the 405 nm and 488 nm lasers. The nascent protein synthesis was determined by the signal intensity in the fluorescent channel in the ring around or within the nucleus as defined by NuclearMask™ Blue Stain.

Live staining of multicellular cancer spheroids

A549 cells (0.1 mL, $2.5x10^3$ cells) were seeded in 96-well ultra-low attachment spheroid microplates (Corning) for 72 hours. The resulting spheroids were treated with a PBS solution containing PP50 (5 mg/mL) and saporin (300 nM) and incubated for 1 hour at pH 6.5. The cells were washed three times with PBS, replaced with fresh media, and further incubated for up to 72 hours. Spheroids were stained with Calcein AM (10 µM) and excited using the 488 nm laser at different time points. Spheroids were visualised using Z-stack imaging on FIJI.

Intracellular delivery of FITC-ova (323-339)

B lymphocytes (1 mL, $5x10^5$ cells/mL) were treated with a PBS solution containing FITC-ova (25 µg/mL) with PP50 (0.5 mg/mL) at pH 6.5 for 30 minutes. Cells incubated with FITC-ova in the absence of PP50 were used as controls. The cells were then washed with PBS three times and replaced with 1 mL fresh media. Cells were excited using the 488 nm laser.

Intracellular delivery of FITC-ova30 (241-270)

JAWSII (1 mL, $3x10^5$ cells/mL) were treated with a PBS solution containing polymer solutions: PP50 (0.5 mg/mL), PLP-NDA18 (1 mg/mL), CP1 (1 mg/mL) or CP2 (1 mg/mL) with FITC-ova30 (12 µg/mL) at pH 6.5 for 1 hour. Cells incubated with FITC-ova30 only were used as a control. The cells were washed three times with PBS and replaced with 1 mL fresh media containing Hoechst 33342 and LysoTracker® red DND-99. Cells were excited using the 405 nm, 488 nm, and 561 nm lasers.

2.11 Flow cytometry

All samples were filtered into a 5 mL falcon polystyrene test tube with a cell strainer cap for flow cytometry analysis. Flow cytometry data collection was performed on a BD LSRFortessa and analysed using FlowJo v10.

FITC-dextran cellular uptake

Flow cytometry was employed to quantitatively evaluate the cellular uptake of FITC-dextran. HeLa cells (1 mL, 3 x 10^5 cells/mL) were seeded in a 6-well plate overnight and then treated with a PBS solution containing FITC-dextran 150 kDa (10 μM) with or without PP50 (0.5 mg/mL) at pH 6.5 or pH 7.4 for 30 minutes. The cells were then washed with PBS three times, detached using Trypsin-EDTA, centrifuged (1000 rpm, 5 minutes) and replaced with 0.5 mL fresh PBS. Jurkat cells and B lymphocytes (1 mL, 5x10^5 cells/mL) were treated with a PBS solution containing FITC-dextran 150 kDa (10 μM) with or without PP50 (0.5 mg/mL) at pH 6.5 for 30 minutes. The cells were then washed with PBS three times and replaced with 0.5 mL fresh PBS. All samples were excited at 488 nm, and the emission was collected in the 530/30 nm band.

Cy5-PP50 medicated intracellular delivery of FITC-dextran in the presence of endocytosis inhibitors

Flow cytometry was employed to quantitatively evaluate the cellular uptake of FITC-dextran and Cy5-PP50 in the presence of different endocytosis inhibitors. A549 cells (1mL, 3.0 × 10^5 cells) were seeded in a 35 mm glass-bottom Mattek dish overnight. The cells were pre-treated with chlorpromazine (3 μg/mL), cytochalasin D (2.5 μM), amiloride (30 μM), nystatin (10 μg/mL) or MβCD (1.5 mg/mL), in serum-free media for 30 minutes. The medium was removed and replaced with sterile-filtered PBS containing FITC dextran 150 kDa (10 μM) and Cy5-PP50 (0.5 mg/mL) with inhibitors for 30 minutes at pH 6.5. The cells were washed three times with PBS, detached using trypsin-EDTA, centrifuged (1000 rpm, 5 minutes) and replaced with fresh PBS containing inhibitors. Cells were excited at 488 nm and 561 nm, and the emission was collected at 530/30 and 670/30 bands.

Annexin V/Propidium Iodide

To study cellular apoptosis after the uptake of saporin, FITC-Annexin V/propidium iodide (PI) double staining was employed. Annexin V binds to phosphatidylserine, which is usually only restricted to the inner part of the membrane. During apoptosis, however, phosphatidylserine becomes exposed to the outer membrane. Further, in late apoptotic and necrotic cells, the integrity of the plasma membrane is compromised, allowing PI to enter. Thus FITC-Annexin V/PI staining allows the distinguishment between healthy cells and cells undergoing early or late or necrotic stages of apoptosis (Crowley et al., 2016).

A549 cells (1 mL, 3×10^5 cells) were seeded in a 6 well plate overnight and treated with a PBS solution containing free saporin (1 nM) with or without PP50 (0.2 mg/mL) for 1 hour at pH 6.5. The cells were washed three times with PBS, and fresh culture media added. After 24, 48 or 72 hours of further incubation, the A549 cells were detached using trypsin-EDTA and washed in cold PBS. The cells were centrifuged (1000 rpm, 5 minutes) and re-suspended in 100 µL 1X Annexin-binding buffer. To each sample, 5 µL FITC-Annexin V and 1 µL 100 µg/mL PI working solution was added as prepared per the manufacturer's instructions. The cells were then incubated for 15 minutes at room temperature, and afterwards, 400 µL 1× annexin -binding buffer was added to each sample, mixed gently and kept on ice. Cells were excited at 488 nm and 561 nm, and the emission was collected at 530/30 and 610/20 bands.

Cell surface activation markers

Cell surface levels of MHC I, MHC II, CD80 and CD40 were assessed by staining with anti-MHC I (H-2Kb) PE, anti-MHC II (I-Ab)-FITC, anti-CD40-AF647 and anti-CD80-BV421. Briefly, JAWSII cells (1 mL, 3×10^5 cells) were treated with a PBS solution containing polymer solutions: PP50 (0.5 mg/mL), PLP-NDA18 (1 mg/mL), CP1 (1 mg/mL) or CP2 (1 mg/mL) with ova 30 (100 µM) or ova30 alone at pH 6.5 for 1 hour. After treatment, the cells were washed with PBS, replaced with fresh culture media and incubated for a further 24 or 48 hours. As a positive control, JAWSII cells (1 mL, 3×10^5 cells) were stimulated with LPS (2 µg/mL) or IFN-γ (10 ng/mL) in culture media for 24 or 48 hours. After further incubation, cells were centrifuged (500 g, 5 minutes) and stained with anti- MHC I (H-2Kb) PE (0.625 µL), anti-MHC II (I-Ab)-FITC (4 µL), anti-CD40-AF647 (2 µL) and anti-CD80-BV421 (5 µL) antibodies in 100 µL PBS with 5% FBS on ice for 30 minutes in the dark. After staining, 400 µL PBS was added to each sample,

centrifuged (500 g, 5 minutes), and re-suspended in 0.5 mL PBS. Cells were excited at 488 nm, 633 nm or 405 nm and collected in the emission 586/15, 530/30, 670/14 or 450/50 band.

FITC-saporin intracellular uptake

A549 cells (1 mL, 3×10^5 cells) were seeded in a 6 well plate overnight and treated with a PBS solution containing FITC-saporin (0.125 mg/mL) with or without PP50 (0.2 mg/mL) for 1 hour at pH 6.5. The cells were washed three times with PBS, replaced with fresh media, and incubated for 24 hours. After 24 hours, samples were detached using Trypsin-EDTA, centrifuged (1000 rpm, 5 minutes) and replaced with 0.5 mL fresh PBS. Samples were excited at 488 nm, and the emission was collected in the 530/30 band.

2.12 Caspase- Glo® 3/7, 8 and 9 activation assays

To investigate the cell death mechanism of saporin, A549 cells (0.1 mL, 5×10^3 cells) were seeded in a white flat-bottom opaque 96-well plate and incubated overnight. The cells were either treated with PBS containing free saporin, PP50 or PP50 and saporin combinations at varying concentrations and incubated for various times at pH 6.5. The cells were then washed three times with PBS, replaced with media, and incubated for 24 hours. After 24 hours of further incubation, the media was replaced with 20 µL of serum-free media plus 20 µL of Caspase-Glo® 3/7, 8 or 9 Assay reagent and incubated at room temperature on a plate shaker for 1 hour. The luminescence was measured using a spectrofluorometer (GloMax®-Multi Detection System, Promega). Caspase activation of treated cells were expressed as a percentage of that from corresponding control cells.

2.13 CellTitre-Glo® 2.0 cell viability assay

To assess the cell viability of cells after treatment with PP50 and payloads, the CellTiter-Glo® 2.0 cell viability assay was employed, which detects the amount of ATP present correlating to the number of metabolically active cells. Cells (0.1 mL, $5x10^3$ cells) were treated with a PBS solution containing PP50 at varying concentrations at pH 6.5 for 30 minutes. The cells were washed three times with PBS, replaced with fresh media, and incubated for 24 hours. After 24 hours, the medium was removed and replaced with serum-free media (30 µL) plus CellTiter-Glo® 2.0 Cell reagent (30 µL) per well. The plate was incubated for 10 minutes at

room temperature to stabilise the luminescent signal before the luminescence was read using a spectrofluorometer. Values of viability of treated cells were expressed as a percentage of that from corresponding control cells.

For the cell survival of A549 cells after saporin delivery, A549 cells (0.1 mL, 5×10^3 cells) were seeded in a white flat-bottom opaque 96-well plate and incubated overnight. The cells were either treated with PBS containing free saporin, polymer or polymer and saporin combinations at varying concentrations and incubated for varying times at pH 6.5. The cells were then washed three times with PBS, replaced with media, and incubated for 72 hours. After incubation, the growth medium was removed and treated with the CellTiter-Glo® 2.0 Cell Viability Assay as described above. Values of viability of treated cells were expressed as a percentage of that from corresponding control cells.

For cell survival after saporin delivery in the presence of endocytosis inhibitors, A549 cells (0.1 mL, 5×10^3 cells) were seeded in a white flat-bottom opaque 96-well plate and incubated overnight. The cells were then pre-treated with ammonium chloride (100 μM), nystatin (10 μg/mL), cytochalasin D (2.5 μM), chlorpromazine (3 μg/mL), amiloride (30 μM) or MβCD (1.5 mg/mL) in serum-free media for 30 minutes. The medium was removed and replaced with PBS containing free saporin (1 nM) and PP50 (0.2 mg/mL) with inhibitors for 1 hour. The cells were washed three times with PBS, replaced with media, and further incubated for 72 hours before analysis with the CellTiter-Glo® 2.0 Cell Viability Assay as described above. Controls cells were incubated with inhibitors only under the same conditions. Values of viability of treated cells were expressed as a percentage of that from corresponding control cells.

2.14 CellTiter-Glo® 3D cell viability assay

To determine the cell viability of 3D spheroids after saporin uptake, the CellTiter-Glo® 3D cell viability assay was employed. The CellTiter-Glo® 3D cell viability can penetrate larger spheroids to quantify cell viability based on the detection of ATP. A549 cells (0.1 mL, 2.5×10^3 cells) were seeded in 96-well ultra-low attachment spheroid microplates (Corning) for 72 hours. The resulting spheroids were treated with a PBS solution containing free saporin (300 nM), PP50 (5 mg/mL) or a combination of PP50 and saporin and incubated for 1 hour at pH 6.5. As a negative control, spheroids were treated with PLP (5 mg/mL) and saporin for 1 hour

at pH 6.5. The spheroids were washed three times with PBS, replaced with fresh media, and further incubated for up to 72 hours. After incubation, 50 µL of CellTiter-Glo® 3D Reagent was added to 50 µL of medium containing the spheroids and mixed vigorously (300 rpm) on a plate shaker for 5 minutes to induce lysis of spheroids. The plate was left for 25 minutes at room temperature before reading the luminescence on a spectrofluorometer. Values of viability of treated cells were expressed as a percentage of that from corresponding control cells.

2.15 AlamarBlue cell viability assay

To assess the ability of PP50 to deliver the apoptotic peptide KLAK, the AlamarBlue cell viability assay was utilised. Briefly, HeLa cells (0.1 mL, $1x10^4$ cells) were seeded in a black, flat transparent bottom 96-well plate and incubated overnight. The medium was replaced with PBS containing PP50 alone at varying concentrations for 30 minutes at pH 6.5. The cells were then washed with PBS and treated with KLAK only (100 µM) at pH 6.5 for 2.5 hours. The cells were then washed with PBS three times and incubated for 24 hours. Control cells were treated with either KLAK only or PP50 only under the same conditions. The medium was then replaced with fresh medium containing 10% (v/v) AlamrBlue® reagent and further incubated for another 4 hours. The fluorescence was measured using a spectrofluorometer at emission wavelength 590-640 nm and excitation wavelength 525 nm. Values of viability of treated cells were expressed as a percentage of that from corresponding control cells.

Dr Michal Kopytynski (Postgraduate researcher, Department of Chemical Engineering Seed Fund for Translational Research funding) in Dr Rongjun Chen's group performed the above experiment presented in Figure 3-15.

2.16 ELISAs

IL-6 and TNF-α

Mouse IL-6 and Mouse TNF-α ELSIA Duoset kits were used to analyse the expression levels of IL-6 and TNF-α cytokines in the media 24 or 48 hours after JAWSII treatment. All reagents were prepared and used as per the manufacturer's instructions. Briefly, ELISA 96-well plates were coated with 100 µL Capture Antibody, sealed and incubated overnight. Each well was aspirated and washed with wash buffer (400 µL) three times, inverting the plate and blotting

it against paper towels after each wash. The plates were then blocked by adding 300 µL Reagent Diluent to each well and incubated at room temperature for 1 hour. After incubation, the wells were aspirated and washed with wash buffer (400 µL) three times before adding 100 µL of samples or standards in Reagent Diluent. The plates were sealed and incubated for 2 hours at room temperature. After incubation, the wells were aspirated and washed with wash buffer (400 µL) three times and 100 µL Detection Antibody diluted in Reagent Diluent added to each well. The plates were sealed and incubated for 2 hours at room temperature. After incubation, the wells were aspirated and washed with wash buffer (400 µL) three times and 100 µL Streptavadin-HRP added to each well. The plates were sealed and incubated for 20 minutes at room temperature, protected from the light. After incubation, the wells were aspirated and washed with wash buffer (400 µL) three times, and 100 µL Substrate Solution was added to each well. The plates were sealed and incubated for a further 20 minutes at room temperature, protected from the light. After incubation, 50 µL Stop Solution was added to each well and mixed gently. The absorbance was immediately read at 450 nm on a spectrofluorometer.

IL-2

Peptide presentation in MHC-I was examined by monitoring IL-2 release by the RF33.70 T-cell hybridoma. Treated JAWSII DCs were harvested after 24 hours and diluted by RPMI-1640 complete medium. DCs (2×10^4) and RF33.70 cells (2×10^5) were mixed and incubated in a 96 well plate. As a positive control, anti-CD3/CD28 Dynabeads were added to RF33.70 cells at one bead/RF33.70 cell. As a negative control, RF33.70 cells were incubated without DCs. After 24 hours of incubation, presentation-induced IL-2 secretion was determined using a commercially available Mouse IL-2 Quantikine ELISA Kit.

All reagents were prepared and used as per the manufacturer's instructions. Briefly, 50 µL of Assay Diluent RD1-14 and 50 µL of standard or sample was added to each well. The plate was tapped gently for 1 minute to allow for the mixing of solutions. The plate was sealed and incubated for 2 hours at room temperature. After incubation, each well was aspirated and washed five times using a Wash Buffer (400 µL) and 100 µL of Mouse IL-2 Conjugate added to each well. The plate was then sealed and incubated for 2 hours at room temperature. After incubation, each well was aspirated and washed five times using a Wash Buffer (400 µL) and

100 µL of Substrate solution was added to each well. The plate was incubated for 30 minutes at room temperature, protected from the light. After incubation, 100 µL of Stop Solution was added to each well and mixed thoroughly. The absorbance was immediately read at 450 nm on a spectrofluorometer.

2.17 Statistical analysis

Statistical analysis was performed using GraphPad Prism version 9.2.0 (283). Where appropriate, student's t-tests and ANOVA with Tukey's multiple comparison tests were performed. Statistical significance was determined as * $P \leq 0.05$, ** $P \leq 0.01$, *** $P \leq 0.001$ and **** $P \leq 0.0001$. Statistical analysis was performed on technical repeats unless otherwise indicated.

Chapter 3

PP50 as a versatile pH-responsive platform for the intracellular delivery of macromolecules

This chapter describes the development of PP50 to extend its potential applications as a versatile pH-responsive intracellular delivery platform for *in vitro* and *ex vivo* therapeutic delivery of macromolecules. The pH-dependent membrane destabilising activity of PP50 was examined and confirmed using FITC-dextran as a model payload. The cytotoxicity, mechanism and intracellular localisation of PP50 were further investigated to add to the current knowledge surrounding the polymer's delivery process. In addition, the capabilities of PP50 to deliver a range of peptides and antibodies was explored to demonstrate that PP50 can mediate efficient delivery of a variety of payloads with different properties into cells.

Part of the work presented in this chapter has contributed to the following manuscript: **Morrison G,** Kopytynski M, Chen R. "An anionic pH-responsive polymer to potentiate intracellular delivery of different sized biomacromolecules". To be submitted.

Note: Dr Michal Kopytynski Postgraduate Researcher in Dr Rongjun Chen group (Department of Chemical Engineering Seed Fund for Translational Research funding) contributed to some results in this chapter. Dr Michal Kopytynski prepared samples using his own synthesised PP50, performed experiments and collected the data used in Figure 3-13, Figure 3-14 and Figure 3-15 with input from myself during the design process. Data analysis was performed by Dr Michal Kopytynski and me. The contribution of Dr Michal Kopytynski is specified in the captions of relevant figures.

3.1 Introduction

The efficient intracellular delivery of biologically active payloads across the plasma membrane to specific intracellular sites remains a significant challenge (Jhaveri and Torchilin, 2016).

PP50, consisting of poly(L-lysine iso-phthalamine) (PLP) grafted with the hydrophobic amino acid L-phenylalanine at a stoichiometric percentage of 50 mol%, was designed as a pH-responsive bio-inspired biomimetic polymer to overcome this limitation. PP50 has shown to be non-lytic at neutral pHe but induce membrane destabilisation and enhance the uptake of macromolecules at mildly acidic pHe whilst remaining non-toxic (Kopytynski et al., 2020). Further, the successful delivery of trehalose for cell preservation (Lynch et al., 2010, 2011; Mercado and Slater, 2016a), calcein (Mercado and Slater, 2016b), different sized dextrans, GFP, and the neutral apoptotic peptide Bim (Kopytynski et al., 2020) has rendered PP50 a suitable intracellular delivery system. However, there has been little investigation into the targeted delivery of macromolecules and the delivery of anionic and cationic peptides. In addition, there is still limited understanding surrounding PP50's intracellular delivery mechanism.

This chapter aims to validate PP50 as a suitable intracellular delivery platform for *in vitro* and *ex vivo* applications. In these settings, the pHe can be manipulated to take advantage of the pH-responsive nature of the polymer to potentiate the intracellular delivery of therapeutic macromolecules at mildly acidic pHe. Furthermore, a simple method of co-incubating PP50 with payload can be utilised to aid delivery into the cell as opposed to chemical conjugation or complexation that would be required for *in vivo* settings. The work presented in this chapter confirmed the pH-responsive profile of PP50 using ovine erythrocytes. pH-dependent intracellular delivery was further demonstrated using 150 kDa FITC-dextran. In addition, to elucidate the intracellular delivery mechanism of PP50 mediated FITC-dextran delivery, fluorescently labelled PP50 and FITC-dextran was co-delivered in the presence of several endocytosis inhibitors. Further, the co-localisation of fluorescently labelled polymer against several organelle stains was assessed to determine the intracellular localisation of PP50.

To expand the scope of using PP50 for the delivery of therapeutic agents, the intracellular delivery of fluorescently labelled antibodies was examined to determine whether PP50 could facilitate targeted delivery to different intracellular localisations within the cell. Lastly, to expand the previously published work on neutral peptide delivery, PP50 mediated cationic and anionic peptide uptake was studied.

3.2 Results and Discussion

3.2.1 PP50 pH-responsive interaction with biological membranes

Ovine erythrocytes are the simplest mammalian cell. Whilst they contain no nuclei or organelles, their lipid domain is structurally similar to that found in most mammalian cells (Smith, 1987). The integrity of the RBC membrane can be quantified by measuring the levels of haemoglobin retained within or leaked from (haemolysis) the RBC after being in contact with a specific molecule or material. Therefore, RBCs were used as a model membrane to examine the pH-dependent membrane destabilising activity of PP50.

The importance of understating the pH range for which the polymer is active is essential for two reasons. Firstly, the erythrocyte membranes could represent the endo-lysosomal vesicle lipid membranes. During intracellular payload delivery, if PP50 and therapeutic payload become entrapped within the endosomal pathway, endosomal escape and payload delivery into the cytoplasm should be facilitated if the polymer is responsive within the range of the early to late endosomes. Secondly, the erythrocyte membranes could represent the outer cell lipid bilayer. For the applications of *in vitro* intracellular delivery of payloads and *ex vivo* cell engineering, where the pHe of the cell environment can be controlled, cross membrane delivery may be facilitated if the extracellular pHe is altered to a pHe where the polymer is membrane active. To investigate this, the relative haemolysis of PP50 as a function of pHe at 0.5 mg/mL and 1 mg/mL was examined (Figure 3-1).

The relative haemolytic activity of PP50 as a function of concentration yielded different haemolysis profiles. The maximum haemolysis for PP50 (1 mg/mL) was observed at pHe 5.5 (76.8 ± 3.1%), the pH of the late endosomes. Above pHe 5.5, a sharp decrease in haemolysis is observed. However, PP50 (1 mg/mL) still displayed high haemolysis within the pH range of

the early endosomes. Conversely, the maximum haemolysis for PP50 (0.5 mg/mL) was observed at pHe 6.5 (57.7 ± 0.9%), the pH of the early endosomes. PP50 (0.5 mg/mL) showed similar haemolysis levels ranging from early to late endosome (pH 7.0 to 5.5). Interestingly, both PP50 concentrations showed similar levels of haemolysis at pHe 6.5. Reduced haemolysis was observed for both concentrations at physiological pHe (7.4). In addition, negligible haemolysis was shown below pHe 5.0 due to the precipitation of the polymer (Chen et al., 2009b). This suggests that the haemolytic activity of PP50 is influenced by pHe and concentration.

It is important to recognise that the maximum pHe (5.5) observed for PP50 (1.0 mg/mL) may not be the most suitable pHe to use for intracellular delivery. Upon cell membrane injury, whether through endocytosis or direct membrane penetration, the cell can die or reseal its membrane (Stewart et al., 2016). Whilst the pHe can be modified to optimise payload delivery, a harsh pHe environment, further away from physiological pHe, may trigger irreversible cell damage or cause unwanted off-target effects.

Therefore, the mildly acidic pHe 6.5 was chosen for the subsequent experiments with the hypothesis that PP50 would still be sufficiently membrane-active and accommodate payload delivery across the cell but not reduce cell viability or cause cell perturbation.

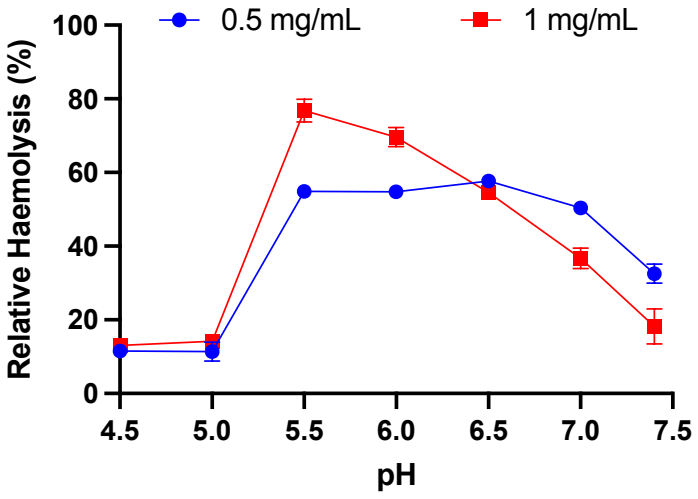

Figure 3-1. pHe-dependent relative haemolysis of PP50 at 0.5 mg/mL and 1 mg/mL. Mean ± SD, n=3.

3.2.2 Intracellular delivery of FITC-dextran by co-incubation with PP50 to adherent cells

To validate the hypothesis that the mildly acidic pHe 6.5 is sufficient to accommodate the intracellular delivery of payloads into cells, PP50 mediated delivery of FITC-dextran into HeLa cells was investigated (Figure 3-2). FITC-dextran was chosen as a model payload due to FITC's popularity as a fluorescent probe for detection. FITC-dextran has been widely used to measure successful intracellular delivery by other delivery platforms (Chen et al., 2017; Hur and Chung, 2021; R. Wang et al., 2018; Wu et al., 2015). A larger size (150 kDa) was employed to test the capability of PP50 to deliver larger sized molecules across the cell membrane. Successful delivery could represent the ability of PP50 to deliver functional antibodies into cells. For comparison, delivery at pHe 7.4 was compared. An endo-lysosomal stain was employed to visualise whether the payload was entrapped within the endosome or lysosomal compartments. Flow cytometry was used to quantitatively measure the cellular uptake in cells (Figure 3-3).

It should be noted that FITC is a pH-sensitive probe. In pH environments below pH 7.0, such as the endosomes and lysosomes, which have mildly acidic pHs, fluorescein is quenched (Hermanson, 2013; Lorenz and Gruenstein, 1999). The fluorescent signal may be underestimated in these environments, which is essential to recognise when analysing results.

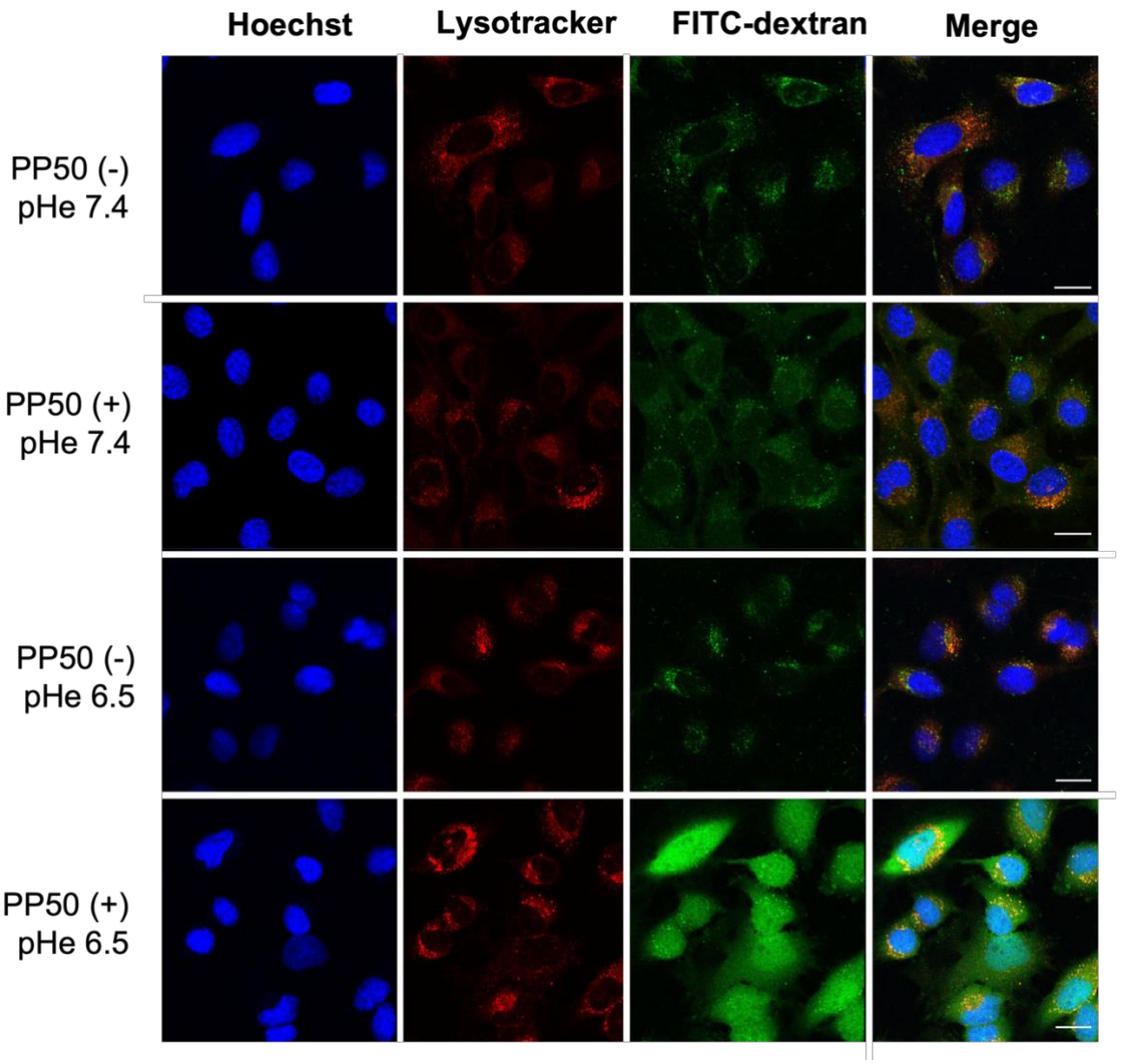

Figure 3-2. Representative laser scanning confocal microscopy images of the intracellular uptake and distribution of FITC-dextran in HeLa cells. Cells were incubated with 150 kDa FITC-dextran (10 µM) in the absence or presence of PP50 (0.5 mg/mL) for 30 minutes at pHe 6.5 or pHe 7.4. Scale bar = 20 µm.

As shown in Figure 3-2, FITC-dextran delivery (green channel) at pHe 7.4, both in the presence and absence of PP50, showed limited delivery, as observed by the dim green fluorescence within the cells. More diffuse staining was observed for PP50 (+) than PP50 (-) at pHe 7.4. However, flow cytometry analysis revealed no significant difference in the mean fluorescence intensity (MFI) between cells with or without PP50 at pHe 7.4. The punctate staining of FITC-dextran, co-localised with the endo-lysosomes (red channel), indicates the payload entrapped inside the endosome or lysosomal compartments.

PP50 mediated delivery of FITC-dextran was considerably improved, as hypothesised, at pHe 6.5, exhibited by a strong green diffused fluorescence in the cytoplasm and nucleus. Larger molecules (> ~40 kDa) are greatly limited in their ability to transport across the nuclear pore (Lin and Hoelz, 2019). Here, it was observed that FITC-dextran (150 kDa in size) was co-localised inside the nuclei after co-incubation with PP50 (Figure 3-2). The precise mechanism by which FITC-dextran enters the nucleus after PP50 mediated delivery is not yet well understood and requires further investigation. Delivery of FITC-dextran at pHe 6.5, in the absence of PP50, resulted in punctate spots co-localised with the endo-lysosomes, similar to that at pHe 7.4. Flow cytometry confirmed that PP50 mediated delivery at pHe 6.5 was significantly ($P \leq 0.0001$) higher than PP50 mediated delivery at pHe 7.4 and pHe 6.5 in the absence of PP50.

Whilst this experiment does not indicate whether PP50 mediated FITC-dextran delivery at pHe 6.5 was initiated through endocytosis and subsequent endosomal escape into the cytoplasm or membrane disruption, it does show the potential of PP50 as a promising pH-responsive intracellular delivery agent when the extracellular pHe is manipulated. Thus, the extracellular pHe of 6.5 was used for all subsequent experiments.

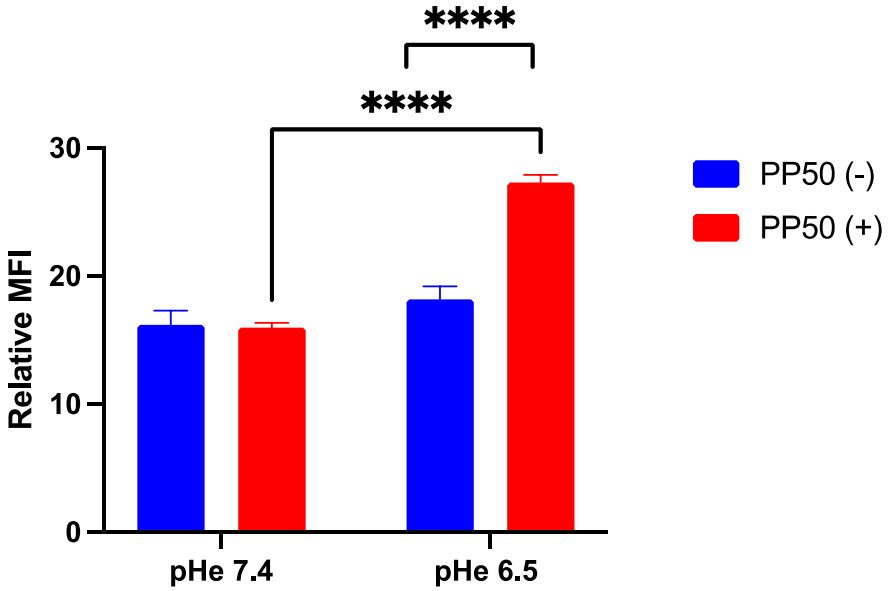

Figure 3-3. Cellular uptake of FITC-dextran in HeLa cells was quantitatively analysed by flow cytometry after incubation with 150 kDa FITC dextran (10 µM) in the absence or presence of PP50 (0.5 mg/mL) for 30 minutes at pHe 6.5 or pHe 7.4. Results are represented as relative MFI compared to blank HeLa cells. Mean ± SD, n=3. **** $P \leq 0.0001$.

3.2.3 PP50 cytotoxicity

An optimal delivery system should facilitate the uptake of macromolecules into the cell interior whilst remaining non-toxic to the cell itself. Mercado *et al.* (2016b) evaluated the cellular metabolic activity, membrane integrity and morphology in osteosarcoma cells treated with PP50. It was found that concentrations up to 2 mg/mL PP50 were well tolerated by cells and did not bring about cytotoxic or morphological changes.

Using the Alamar Blue assay, Kopytynski *et al.* (2020) determined that HeLa cells treated with 150 kDa FITC-dextran (10 µM) and PP50 (up to 2mg/mL) after 30 minutes of treatment at pHe 6.5 and pHe 7.4 in PBS did not produce any major cytotoxic effects. Even after 3 hours PP50 (1 mg/mL) treatment was still well tolerated by cells.

Here, the cytotoxicity of HeLa cells was confirmed after treatment with PP50 concentrations up to 5 mg/mL in PBS at pHe 6.5 and pHe 7.4 using the CellTitre-Glo® 2.0 cell viability assay (Figure 3-4). The viability of HeLa cells treated with PP50 was comparable to the cells treated with PBS buffer (negative control) throughout the concentration range tested, even at the

higher concentration of 5 mg/mL, validating that PP50 is well tolerated by HeLa cells at pHe 6.5 and pHe 7.4.

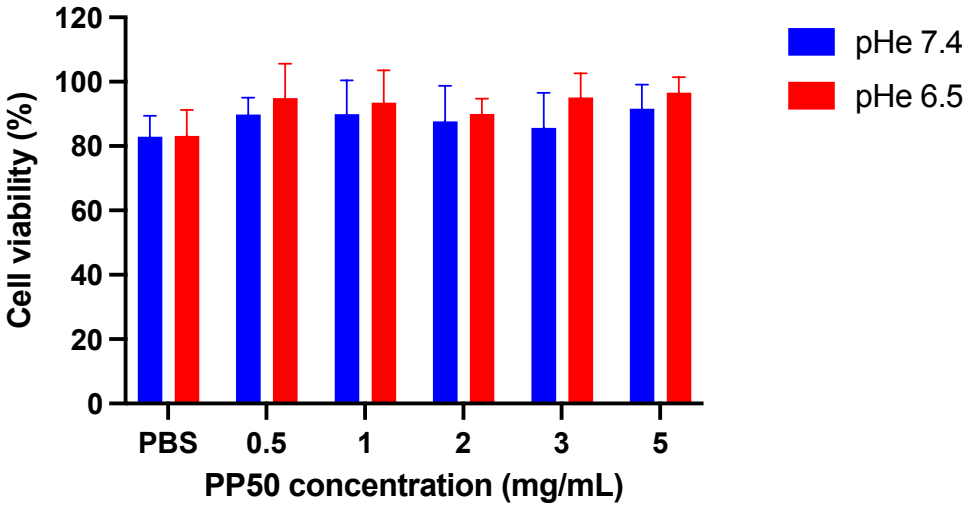

Figure 3-4. Cell viability of HeLa cells treated with varying concentrations of PP50 in PBS at pHe 6.5 and pHe 7.4 for 30 minutes as determined by the CellTitre-Glo® 2.0 cell viability assay. Mean ± SD, n = 4.

3.2.4 FITC-dextran delivery to immune cells

Next, the intracellular delivery of FITC-dextran to immune cells: Jurkat cells (T lymphocytes) and B lymphocytes were investigated (Figure 3-5). For applications in cell engineering, specifically in cell therapies, the intracellular delivery of therapeutic biomolecules to immune cells is of high importance but is often harder to achieve. Figure 3-5A and B displays the considerably increased uptake and brighter green fluorescence in Jurkat and B lymphocytes co-incubated with PP50 and FITC-dextran compared to treatment with FITC-dextran alone. Flow cytometry analysis confirmed the enhanced uptake of FITC-dextran using PP50 (Figure 3-5C). It was observed that in both Jurkat and B lymphocytes, some cells displayed a brighter green fluorescence. The successful delivery of FITC-dextran to a range of cell types, including adherent, suspension, immune and cancer cells, further demonstrates the versatility of PP50 as a delivery platform. Regarding the cell viability of immune cells treated with PP50 at pHe 6.5, the cell survival dropped slightly to 90.3 ± 5.8% and 87.7 ± 5.4% for B lymphocytes and Jurkat cells, respectively (Figure 3-5D). However, this still suggests that PP50 mediated delivery is well tolerated by immune cells.

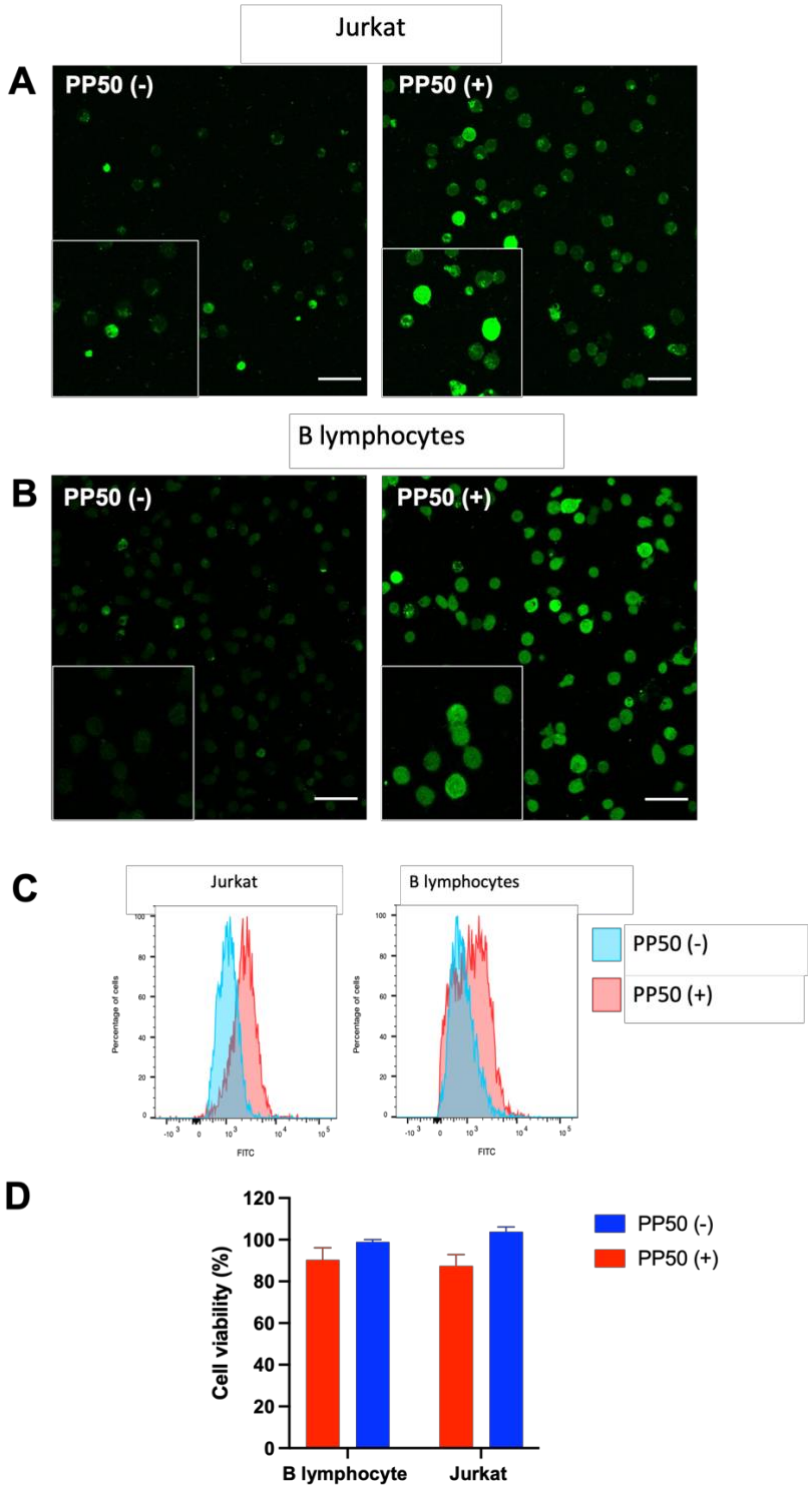

Figure 3-5. Representative laser scanning confocal microscopy images of A) Jurkat cells and B) B lymphocytes treated with 150 kDa FITC dextran (10 µM) in the absence or presence of PP50 (0.5 mg/mL) for 30 minutes at pHe 6.5. Scale bar = 40 µm. C) Flow cytometry analysis and D) Cell viability of B lymphocytes and Jurkat cells treated with PP50 (0.5 mg/mL) in PBS at pHe 6.5 for 30 minutes determined by the CellTitre-Glo® 2.0 cell viability assay. Mean ± SD, n = 3.

3.2.5 Mechanisms underlying PP50 mediated FITC-dextran uptake

To further understand the possible mechanism in which PP50 mediated FITC-dextran uptake occurs, polymer and payload uptake experiments in the presence of a range of inhibitors of various cellular internalisation pathways were performed (Table 3-1). In addition, PP50 was grafted with Cy5 to visualise polymer uptake. HeLa cells were pre-treated with inhibitors (30 minutes) and were then incubated with inhibitors throughout the duration of Cy5-PP50 and FITC-dextran treatment. Reduced Cy5-PP50 staining (red channel) and cytoplasmic delivery of FITC-dextran (green channel) in any sample, compared to the control, would suggest that PP50 is reliant on that given pathway for internalisation and FITC-dextran delivery.

Previously published data on PP75 revealed that internalisation can occur through CME or CIE in U251 cells but predominantly does through CME (Khormaee et al., 2013). Mercado et al. (2016) reported that PP50 mediated calcein uptake was partially inhibited by CME, CIE and micropinocytosis inhibitors in SOAS-2 cells at neutral pHe. As no inhibitor could completely inhibit calcein delivery, it was concluded that PP50 is internalised through multiple endocytic pathways. However, little is understood as to whether the same mechanism would occur at pHe 6.5 or if the mechanism is payload and cell dependent. Endocytosis is a complex process still not fully understood. Whilst inhibitors are a common way of investigating the underlying mechanisms elucidating intracellular delivery, there are limitations in their use, including their lack of specificity and toxicity at high concentrations (Rennick et al., 2021).

Table 3-1. Uptake inhibitor overview.

Inhibitor	Uptake pathway inhibited	Dose
Nystatin	Lipid raft mediated endocytosis	10 μg/mL
MβCD	Lipid raft mediated endocytosis	1.5 mg/mL
Cytochalasin D	Macropinocytosis and actin polymerisation	2.5 μM
Chlorpromazine	CME	3 μg/mL
Amiloride	Macropinocytosis	30 μM

It was observed that cytoplasmic delivery of FITC-dextran was achieved in all samples treated with inhibitors (Figure 3-6). Quantitative analysis confirmed that the MFI was not reduced in

these samples. Nystatin and MβCD (both lipid raft mediated endocytosis inhibitors) significantly ($P \leq 0.05$) increased the uptake of FITC-dextran (Figure 3-7A). Plausibly, there was also a significant ($P \leq 0.01$) increase in the uptake of Cy5-PP50 in cells treated with nystatin and MβCD.

In the presence of inhibitors, cells may adapt or overcompensate by upregulating an alternative pathway or mechanism typically less relevant to aid delivery (Francia et al., 2019). If one pathway is blocked, PP50 may mediate delivery via another pathway. This may explain the upregulation of Cy5-PP50 and FITC-dextran delivery in cells treated with nystatin and MβCD.

For cells treated with cytochalasin D, there was a marked decrease in Cy5-PP50 fluorescence, significantly ($P \leq 0.001$) lower than the control (Figure 3-6, Figure 3-7). Cells treated with chlorpromazine were also found to have a significant ($P \leq 0.01$) decrease in Cy5-PP50 fluorescence. Interestingly, contrary to the results of cells treated with nystatin and MβCD, a reduction of Cy5-PP50 fluorescence was not correlated to a reduction in FITC-dextran fluorescence. This suggests that lower concentrations of PP50 can still aid high levels of payloads into cells. This hypothesis is consistent with previous studies, reporting that 1 mg/mL, 0.1 mg/mL and 0.025 mg/mL PP75 produced similar membrane lytic abilities at pHe 6.5 after 60 minutes as measured by haemolysis (Chen et al., 2009b).

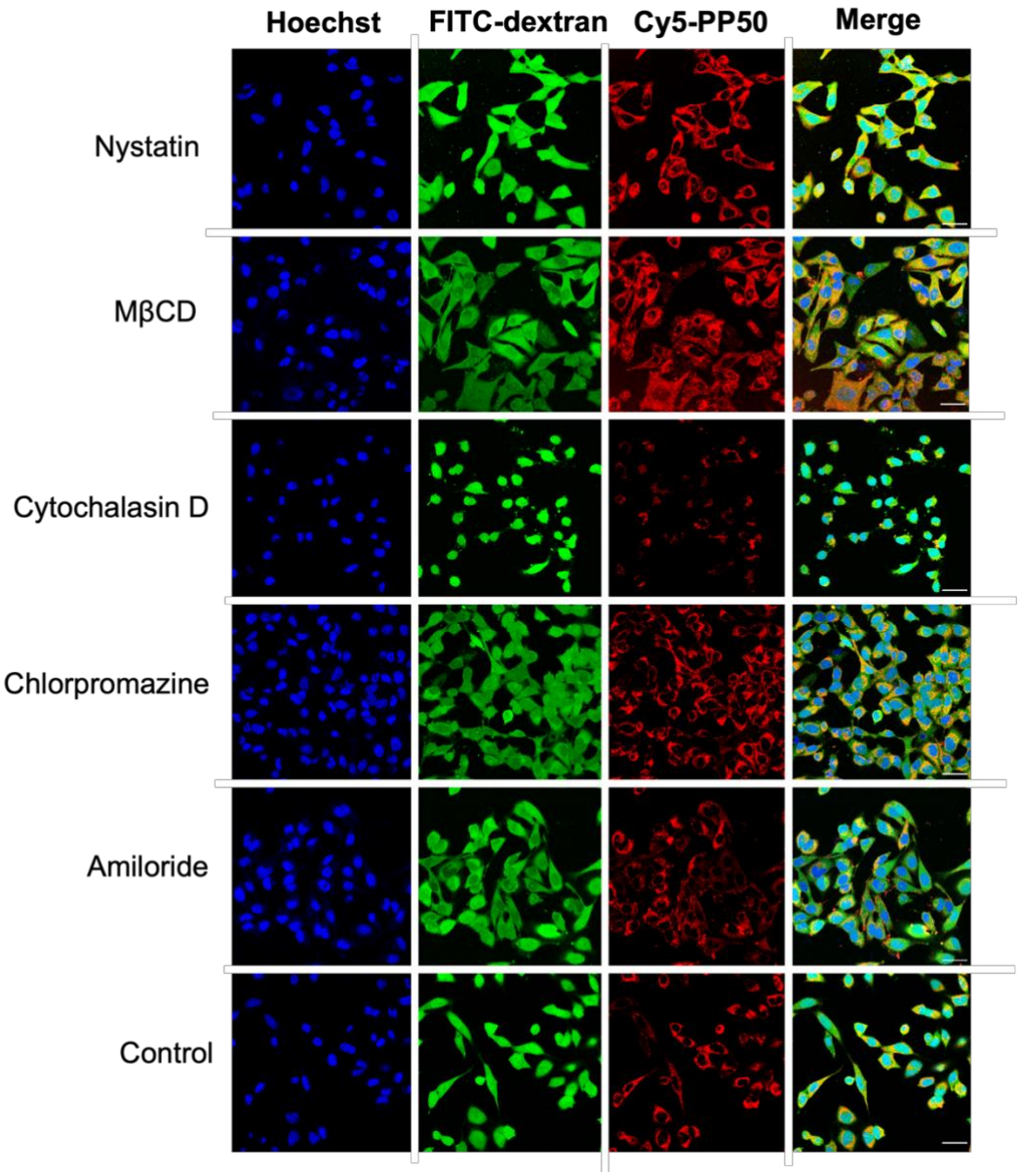

Figure 3-6. Effects of endocytosis inhibitors on the intracellular uptake and distribution of FITC-dextran in HeLa cells. Cells were pre-treated with nystatin (10 µg/mL), MβCD (1.5 mg/mL), cytochalasin D (2.5 µM), chlorpromazine (3 µg/mL) or amiloride (30 µM) for 30 minutes followed by treatment of 150 kDa FITC-dextran (10 µM) and Cy5-PP50 (0.5 mg/mL) in the presence of inhibitors for 1 hour at pHe 6.5. Control cells were treated with FITC-dextran and Cy5-PP50 without inhibitors. Scale bar = 40 µm.

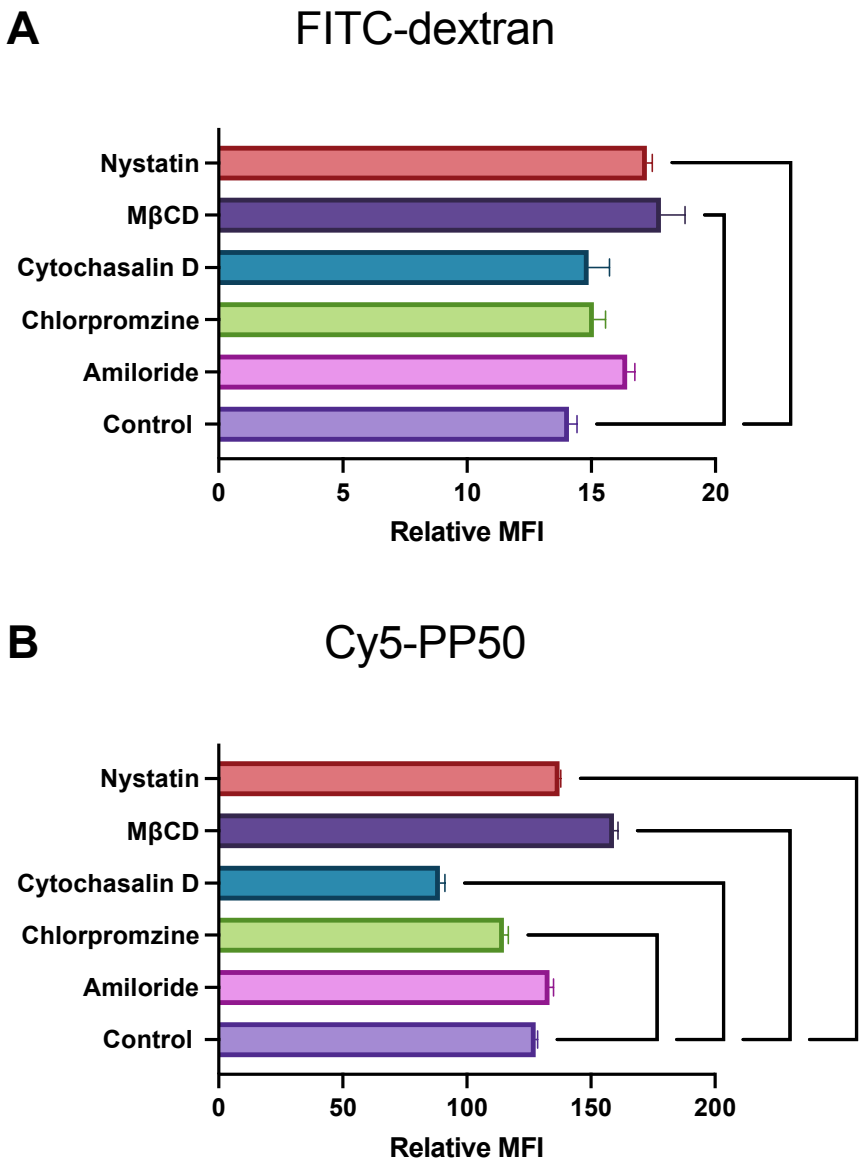

Figure 3-7. Relative MFI of the uptake of (A) FITC-dextran and (B) Cy5-PP50 in HeLa cells as measured by flow cytometry. Cells were pre-treated with nystatin (10 µg/mL), MβCD (1.5 mg/mL), cytochalasin D (2.5 µM), chlorpromazine (3 µg/mL) or amiloride (30 µM) for 30 minutes followed by treatment of 150 kDa FITC-dextran (10 µM) and Cy5-PP50 (0.5 mg/mL) in the presence of inhibitors for 1 hour at pHe 6.5. Control cells were treated with FITC-dextran and Cy5-PP50 without inhibitors. Mean ± SD, n=3. *P ≤ 0.05 **P ≤ 0.01*** P ≤ 0.001.

At least three possible broad categories exist to explain the mechanism behind the intracellular delivery of FITC-dextran using PP50 at pHe 6.5: (I) polymer and payload enter via endocytosis, traffic through the endosomal pathway and subsequent endosomal escape into

the cytoplasm is initiated by PP50 (II) direct membrane translocation of polymer and payload into the cytoplasm (III) a combination of both. This experiment shows that PP50 mediated FITC-dextran cytoplasmic delivery is successful in the presence of all endocytosis inhibitors studied, which suggests that direct translocation is a possible mechanism. However, Cy5-PP50 does, to some extent, rely on micropinocytosis, actin polymerisation or CME for entry which further indicates that a combination of one or more endocytosis pathways in conjunction with direct membrane translocation could be used for FITC-dextran delivery. As previously mentioned, the mechanism of PP50 mediated delivery could be dependent on the size and characteristics of the payload to be delivered. This will be revisited in Chapter 4, where the intracellular mechanism of PP50 mediated saporin delivery is explored.

3.2.6 Intracellular localisation of Cy5-PP50

Based on the previous findings, showing various levels of Cy5-PP50 distributed within the cell, the intracellular localisation and staining pattern of Cy5-PP50 was further investigated. No nuclear localisation of the polymer was previously observed (Figure 3-6), suggesting that PP50 alone cannot cross the nuclear membrane within 1 hour of incubation. Cells were incubated with Cy5-PP50 at pHe 6.5 for 1 hour and then subsequently stained with the LysoTracker (to visualise the endo-lysosomes), ER-Tracker (to visualise the ER) or Mito-Tracker (to visualise the mitochondria) before analysis. It was speculated that Cy5-PP50 would not reside in the endo-lysosomes. As revealed in the previous experiments (Figure 3-6), FITC-dextran was successfully delivered to the cytoplasm and nucleus. Few punctate spots were observed, suggesting efficient endosomal escape by PP50 if multiple endocytosis pathways were utilised.

Cy5-PP50 (magenta channel) showed negligible co-localisation with the endo-lysosomes, as hypothesised (Figure 3-8), with a Pearson's coefficient of 0.216 ± 0.030. Partial co-localisation (Pearson's coefficient 0.587 ± 0.075) was found between Cy5-PP50 and the ER, significantly ($P \leq 0.001$) higher than the endo-lysosomes. Cy5-PP50 co-localisation with the mitochondria (Pearson's coefficient 0.854 ± 0.058), however, was found to be significantly higher than the ER ($P \leq 0.01$) and the endo-lysosomes ($P \leq 0.0001$). The similar intensity plot profiles (Figure 3-8B) further confirmed this co-localisation.

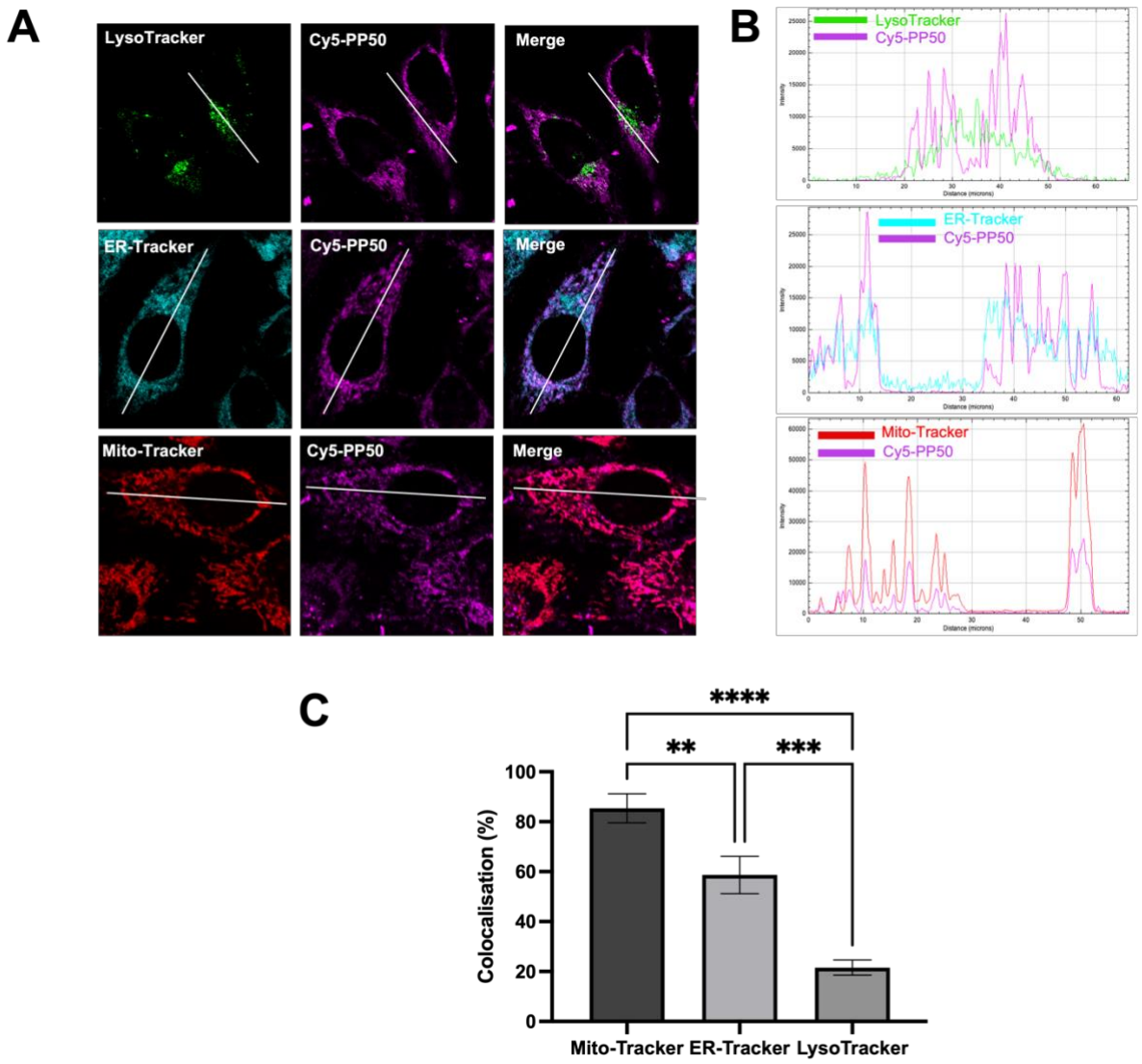

Figure 3-8. Co-localisation studies of Cy5-PP50 (1.0 mg/mL) with endo-lysosomes, ER and mitochondria after 1 hour incubation at pHe 6.5. The cells were subsequently stained with LysoTracker green (green channel), ER-Tracker red (cyan channel) or Mito-Tracker red (red channel). B) Fluorescent intensity profiles in the cross-sectional area indicated by the white line in each channel. C) Co-localisation percentage of merged images in A) calculated using the Pearson's correlation coefficient percentage. At least three different images were used for each marker to calculate the Pearson's correlation coefficient. **P ≤ 0.01 *** P ≤ 0.001 **** P ≤ 0.0001.

One possible explanation for the Cy5-PP50 localisation is due to the presence of carboxyl groups on PP50 which may have caused preferential accumulation in the ER or mitochondria. Wan *et al.* (2018) found that carboxyl-containing polymers were able to target the ER lumen. Pala *et al.* (2020) found that carboxylic acid incorporation enhanced the mitochondrial uptake of phosphonium cations.

Alternatively, Cy5, and other cyanine dyes, have been shown to locate in the mitochondria at high concentrations (above 1 μM) (Nödling et al., 2020). Thus, another explanation for the Cy5-PP50 mitochondrial accumulation is that the Cy5 labelling lead to the mitochondrial localisation of PP50. Jiang *et al.* (2020) revealed that upon Cy3-conjugation, anionic polymers exhibited rapid mitochondria accumulation, significantly more than cationic or charge-neutral polymers. When the anionic polymers were conjugated with other dyes, they did not exhibit mitochondrial localisation. Nödling *et al.* (2020) showed that Cy5 conjugated to R8, a short penetrating peptide increased the subcellular localisation of the conjugate to the mitochondria. Further, the conjugation of KLA, a proapoptotic anti-microbial peptide, with Cy5 increased its targeting to the mitochondria. Whilst further experiments are required to confirm this, the data presented here suggests that Cy5 may be used to increase PP50's potential as a mitochondrial targeting agent to direct cell impermeable payloads to the mitochondria. This is to be further explored in the future.

3.2.7 Intracellular targeted delivery of antibodies

The ability of a delivery platform to deliver functional payloads to specific intracellular target sites within the cell is of great importance. Anti-NPC and anti-β-tubulin antibodies were chosen as model antibodies to assess the capabilities of PP50 as an intracellular targeting agent. Anti-NPC was selected to target the nuclear pore complex whilst anti-β-tubulin was chosen to target β-tubulin, a cytoskeletal element.

Cells were co-incubated with PP50 and either anti-NPC or anti-β-tubulin antibody for different times and afterwards fixed and permeabilised with a secondary antibody to visualise the intracellular staining pattern. Cells fixed and permeabilised with secondary antibodies alone produced no visible staining (data not shown).

Figure 3-9 reveals the successful targeted delivery of anti-NPC antibody by PP50 as demonstrated by the bright red fluorescent circle around the nuclei, identical to that of the positive control group. Bright red fluorescent dots were also visualised in the cytoplasm. However, this was also similar to that of the positive control group. Anti-NPC antibody alone, PP50 (-), could not cross the cell membrane. The fast delivery kinetics (1 hr treatment time) shows the promising ability of PP50 to deliver larger macromolecules with high specificity efficiently.

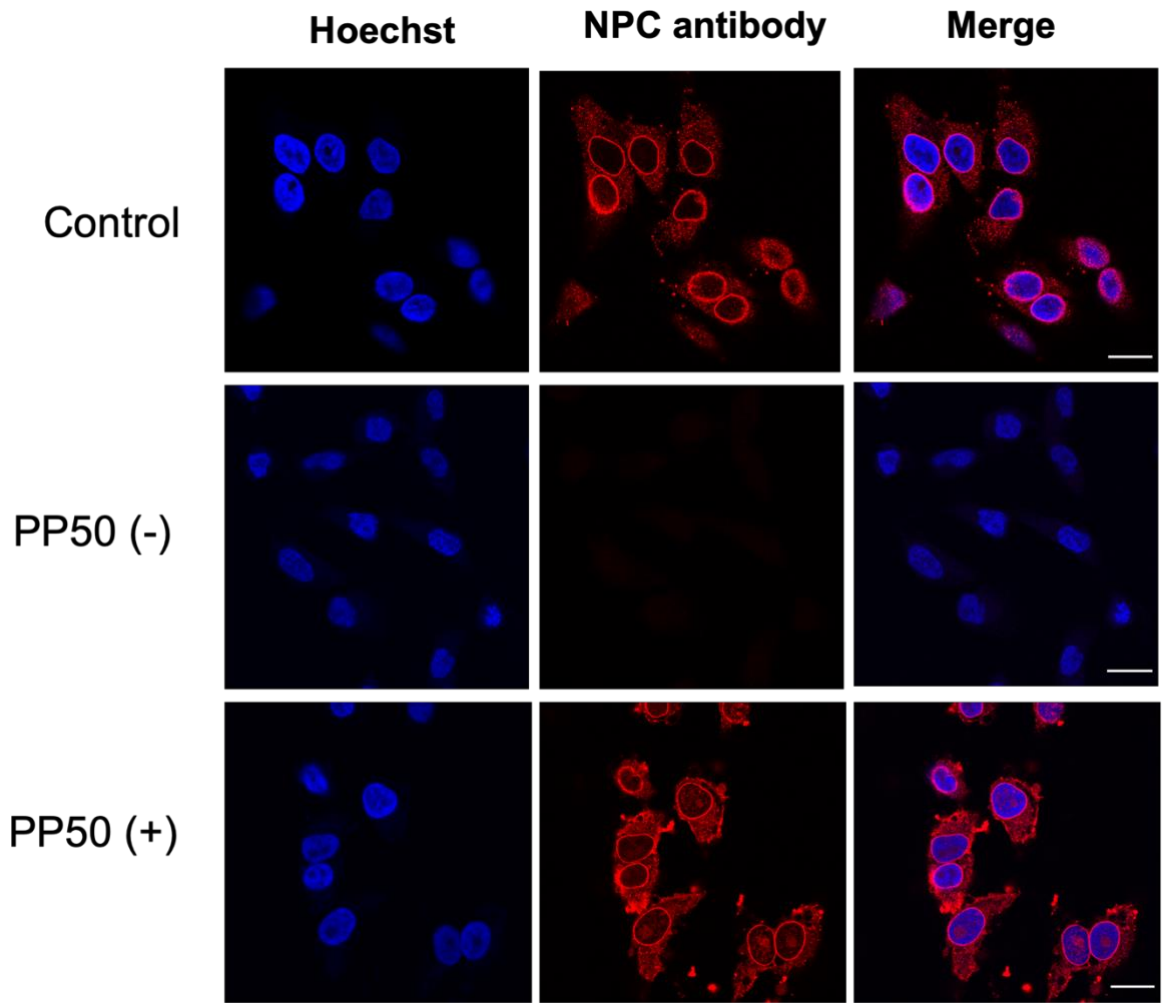

Figure 3-9. Representative laser scanning confocal microscopy images of HeLa cells fixed and permeabilised after treatment with anti-NPC antibody (50 µg/mL) in the presence or absence of PP50 (1 mg/mL) for 1 hour at pHe 6.5. The antibodies were tagged using an Alexa Fluor 594 secondary antibody. Control cells were fixed and permeabilised with anti-NPC and Alexa Fluor 594 secondary antibodies. Scale bar 40 µm.

PP50 mediated anti-β-tubulin antibody delivery resulted in faint intracellular green fluorescence after 2 hours of treatment and 16 hours further incubation (Figure 3-10). Partial binding to actin (white arrow) was observed in some cells. Compared to anti-NPC antibody, the longer treatment and additional incubation time required to deliver anti-β-tubulin shows the potential need to optimise parameters based on payload and intracellular targeting site.

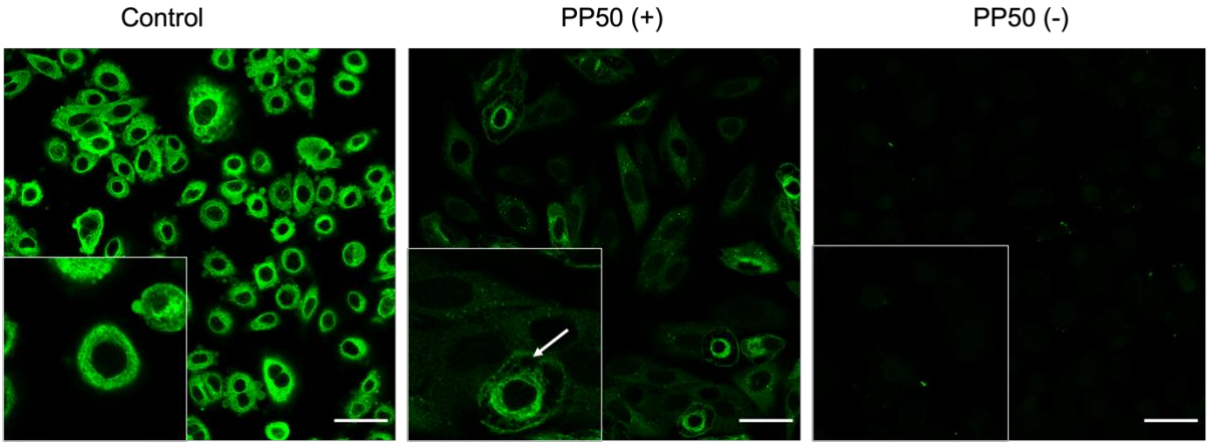

Figure 3-10. Representative laser scanning confocal microscopy images of A549 cells fixed and permeabilised after treatment with anti-β-tubulin antibody (50 µg/mL) in the presence or absence of PP50 (1 mg/mL) for 2 hours at pHe 6.5. Cells were further incubated for 16 hours before analysis. The antibodies were tagged using an Alexa Fluor 488 secondary antibody. Control cells were fixed and permeabilised with anti- β-tubulin and Alexa Fluor 488 secondary antibody. Scale bar 40 µm. The positive control cells were imaged with a different laser power to the PP50 (+) and PP50 (-) treated cells, so the fluorescence intensity is not directly comparable.

3.2.8 Peptide delivery

Kopytynski *et al.* (2020) previously reported that Bim, a neutral apoptotic peptide, was successfully delivered at mildly acidic pHe but not at pHe 7.4 by co-incubation with PP50. To further explore the use of PP50 to enhance the uptake of peptides intracellularly, the next aim was to examine the delivery of anionic or cationic peptides by co-incubation with PP50 at the mildly acidic pHe 6.5 (Table 3-2).

Table 3-2. Peptide delivery overview.

Peptide	**Molecular weight (Da)**	**Net charge at pH 6.5** ("Peptide Property Calculator," 2022)
FITC-ova	2276.5	-0.5
FITC-p53	1753.1	-1
KLAK	1523	6
Histone H3 FAM	2854.2	7

3.2.8.1 Anionic peptides

Ovalbumin is the main protein component in egg white (Huntington and Stein, 2001). FITC-ova (323-339) contains the amino acids 323-339 of the ovalbumin sequence and binds to MHC Class II proteins. It is often used in research as a model peptide antigen to study MHC class II binding (Diebold et al., 2001). Here, the delivery of FITC-ova was studied using B lymphocytes as disease-relevant APCs. Figure 3-11 shows that strong green fluorescence was observed throughout the cells in B lymphocytes co-incubated with PP50 and FITC-ova. B lymphocytes treated with FITC-ova in the absence of polymer exhibited much lower intracellular fluorescence. Interestingly, it appears that on some cells treated with FITC-ova only, a bright green fluorescence is observed on the cell membrane, which is not observed on cells treated with FITC-ova and PP50. The reason for this is unknown.

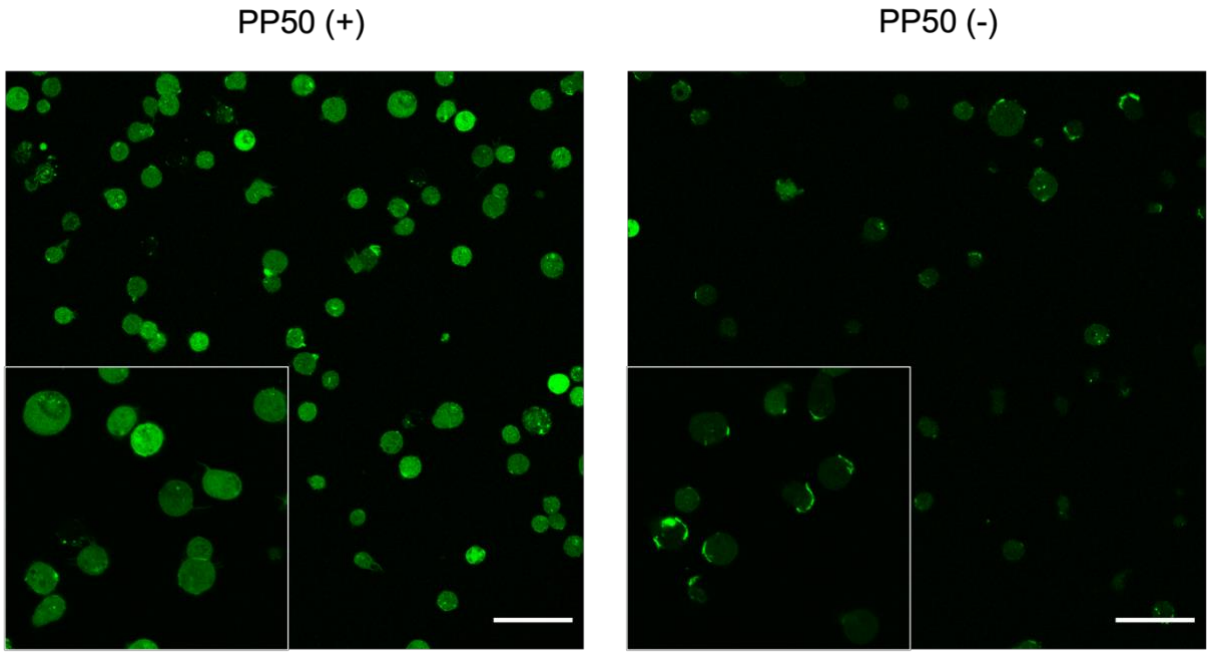

Figure 3-11. Representative laser scanning confocal microscopy images of the intracellular uptake of FITC-ova in B lymphocytes. Cells were incubated with FITC-ova (25 µg/mL) in the absence or presence of PP50 (0.5 mg/mL) for 30 minutes at pHe 6.5. Scale bar = 40 µm.

Similarly, the FITC-p53 peptide (which contains the mdm2 binding domain of p53) was efficiently internalised in A549 cells by co-incubation with PP50 (Figure 3-12). Whilst green cytoplasmic fluorescence was observed throughout the cells, the green punctate spots co-localised with the lysotracker suggests that some FITC-p53 was entrapped after endocytosis. No diffused cytoplasmic fluorescence was observed in cells treated with FITC-p53 in the absence of polymer.

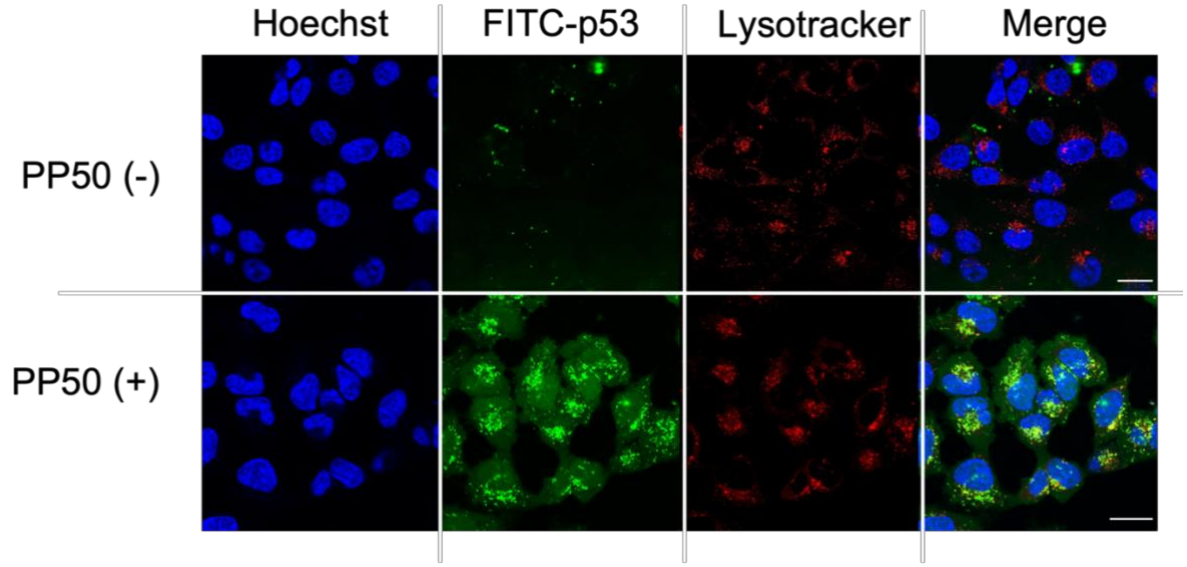

Figure 3-12. Representative laser scanning confocal microscopy images of the intracellular uptake of FITC-p53 in A549 cells. Cells were incubated with FITC-p53 (10 µM) in the absence or presence of PP50 (1.0 mg/mL) for 1 hour at pHe 6.5. Scale bar = 20 µm.

3.2.8.2 Cationic peptides

For the delivery of cationic peptides, the uptake of Histone-FAM peptide in A549 cells was first investigated by co-incubation with PP50, as previously studied with neutral and anionic peptides. As shown in Figure 3-13, Histone-FAM co-incubation with 0.5 mg/mL PP50 for 30 min resulted in a brighter green fluorescence compared to cells incubated with Histone-FAM alone suggesting an increased cellular uptake of Histone-FAM. It is interesting to note that the fluorescence was not diffused within the cells. This might be due to the anionic polymer interacting with the cationic peptide, hindering the diffusion of the resulting complexes. In addition, the polymer's interaction with the cell membrane could be reduced as result of the polymer-peptide interactions. Further studies would be required to confirm this.

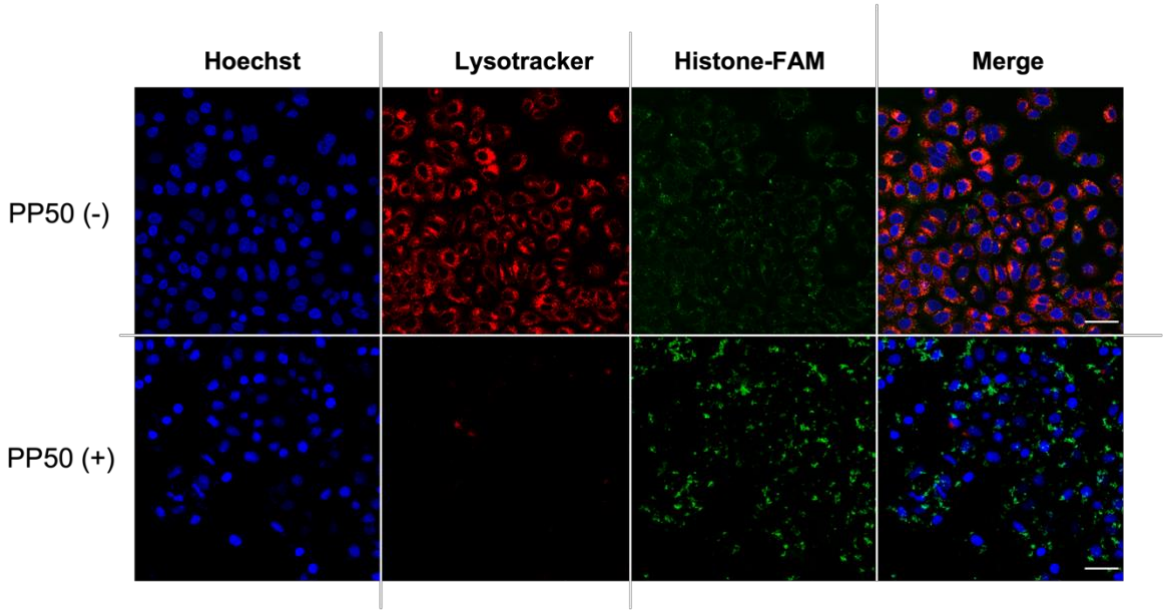

Figure 3-13. Representative laser scanning confocal microscopy images of the intracellular uptake of Histone-FAM in A549 cells. Cells were incubated with Histone-FAM (10 µM) in the absence or presence of PP50 (0.5 mg/mL) for 30 minutes at pHe 6.5. Scale bar = 40 µm. *Sample preparation, performance of experiments* and *images were collected by Dr Michal Kopytynski in Dr Chen's group*.

Evans *et al.* (2019) found that the uptake of cationic amphipathic CPP-based peptides was greatly increased when cells were pre-treated with the anionic polymer poly(propyl acrylic acid) alone first followed by subsequent treatment with peptide alone, as opposed to co-incubation of polymer and peptide. To test this delivery strategy for the uptake of Histone-FAM, HeLa cells were pre-treated with PP50 alone at pHe 6.5 for 30 minutes followed by subsequent treatment with Histone-FAM alone at pHe 6.5 for 30 minutes.

In striking contrast to co-incubation, the sequential treatment of PP50 and Histone-FAM resulted in a greater uptake of peptide (Figure 3-14). Further, it was observed that pre-treating with increasing concentrations of PP50 resulted in higher uptake of Histone-FAM into the cell interior. It is postulated that pre-treatment with PP50 alone allows the polymer to permeabilise the cell membrane without interacting with payload, providing a gateway to the cell interior (Lynch et al., 2011). Consequently, subsequent treatment with Histone-FAM alone would enable efficient peptide uptake.

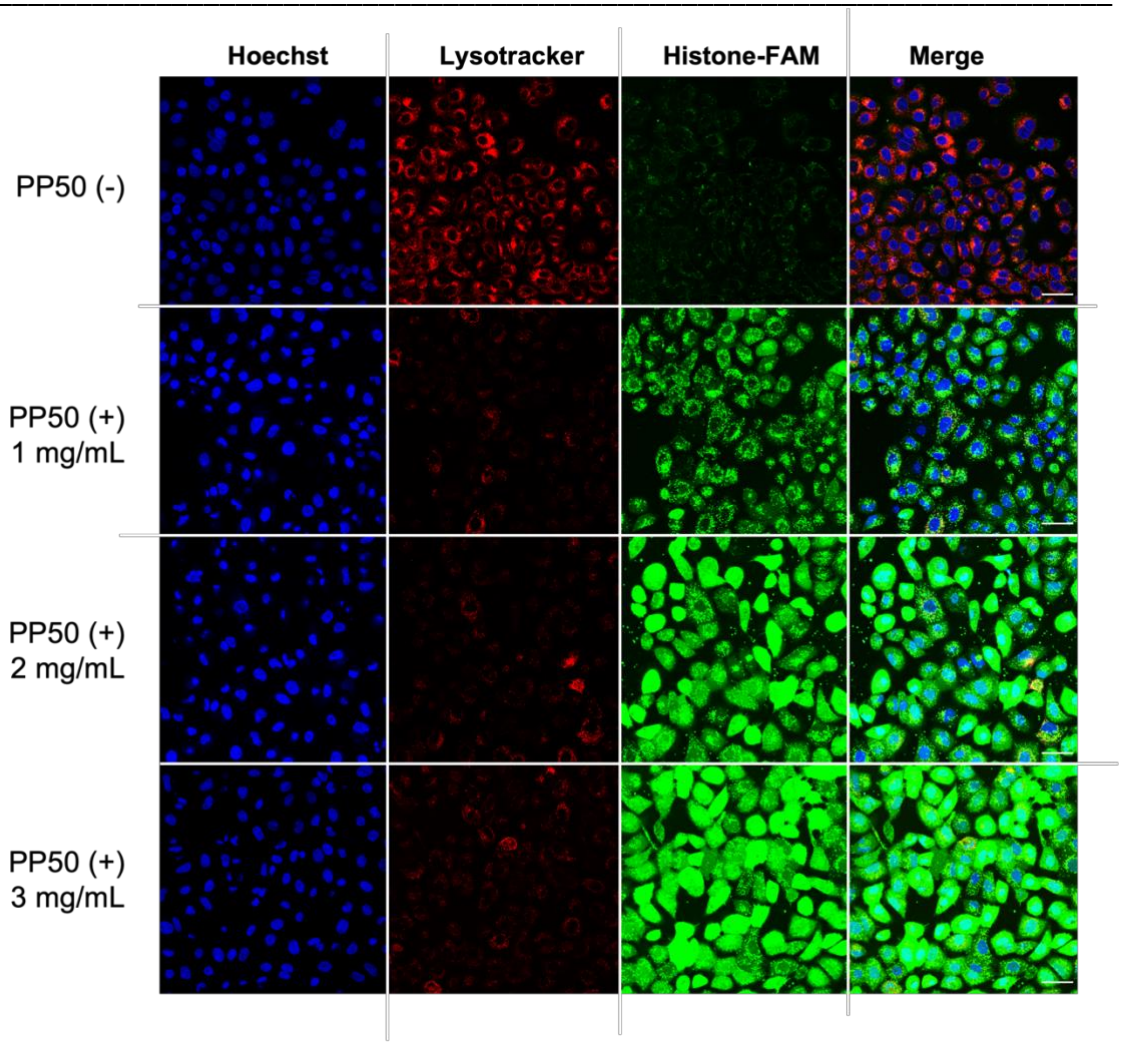

Figure 3-14. Representative laser scanning confocal microscopy images of the intracellular uptake of Histone-FAM (10 µM) in A549 cells. Cells were pre-treated with varying concentrations of PP50 only for 30 minutes at pHe 6.5, washed and then incubated with Histone-FAM only for 30 minutes at pHe 6.5. Scale bar = 40 µm. *Sample preparation, performance of experiments* and *images were collected by Dr Michal Kopytynski in Dr Chen's group.*

To further test the sequential treatment strategy for the uptake of cationic peptides, KLAKLAKKLAKLAK (KLAK) delivery was next explored. KLAK is a 14 amino acid proapoptotic polycationic therapeutic antibacterial agent and α helix forming peptide that disrupts cellular membranes. When efficiently internalised, KLAK triggers mitochondrial permeablisation, generation of reactive oxygen species and mitochondria-dependent apoptosis, ultimately resulting in cell death (Moktan and Raucher, 2012; Qiao et al., 2017).

Like many other macromolecules, its internalisation is crucial for it to exert its therapeutic activity, but KLAK has low efficiency in bypassing the cell membrane. As a result, several strategies, including conjugation with Cy5 (as previously discussed), cell-penetrating peptides and antibodies, have been employed to facilitate its uptake (Moktan & Raucher, 2012; Qiao et al., 2017; Nödling et al., 2020). Based on the previous knowledge obtained from delivering the cationic peptide Histone-FAM (Figure 3-14), for the delivery of KLAK, HeLa cells were pre-treated with PP50 for 30 minutes, washed and then treated with KLAK only for 2.5 hours. Cell survival was determined using the AlamarBlue assay.

As shown in Figure 3-15, treatment with KLAK only decreased cell viability to 67.0 ± 4.2%. However, the sequential treatment of PP50 and KLAK (PP50/KLAK) enhanced the uptake of KLAK, as quantified by the reduced cell viability compared to KLAK only. In particular, the cell viability of cells pre-treatment with 2 mg/mL PP50 and then KLAK (38.8 ± 1.4%) was significantly ($P \leq 0.05$) lower than KLAK only. Unlike sequential delivery with Histone-FAM, no trend was observed with the polymer pre-treatment concentration and uptake of KLAK. This suggests that the optimal pre-treatment polymer concentration for sequential delivery may need to be optimised depending on the peptide of interest to be delivered. Treatment of cells with PP50 alone did not reduce the viability of cells, once again demonstrating the non-toxic nature of the polymer. It would be of interest to further explore whether the delivery of Cy5-PP50, which has been shown to accumulate in the mitochondria (Figure 3-8), further enhances the uptake of KLAK.

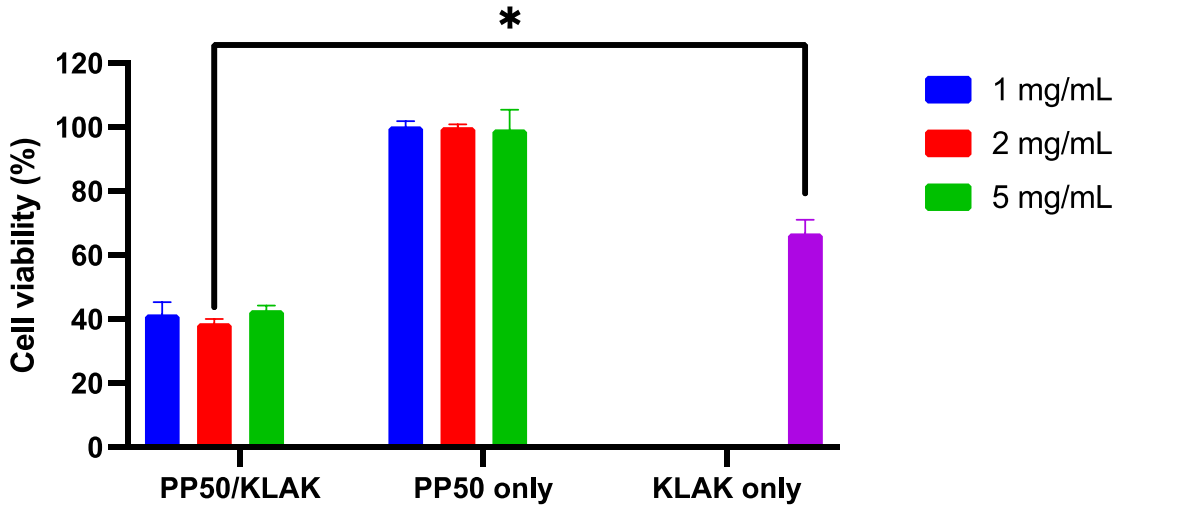

Figure 3-15. Cell viability of HeLa cells treated with the apoptotic peptide KLAK (100 uM). Cells were pre-treated for 30 minutes with PP50 at varying concentrations followed by a wash and addition of KLAK only for 2.5 hours. Controls were treated with either KLAK only or PP50 only. Cell viability was quantified 24 hours after treatment using the AlamarBlue assay. Mean ± S.D. (n=3). *P ≤ 0.05. *Sample preparation, performance of experiments* and *images were collected by Dr Michal Kopytynski in Dr Chen's group.*

3.3 Conclusions

The proposal of PP50 as a versatile *in vitro* and *ex vivo* delivery platform capable of facilitating the intracellular delivery of various macromolecules into the cell interior motivated the research presented in this chapter.

The pH-responsive membrane activity was demonstrated using haemolysis, revealing that PP50 exhibits limited membrane lytic activity at pHe 7.4 but substantially increased membrane destabilising abilities at mildly acidic pHe. pHe dependent payload delivery was further demonstrated in HeLa cells by co-incubation of PP50 with the model payload FITC-dextran, confirming successful delivery at pHe 6.5 but limited uptake of payload at pHe 7.4. Successful uptake of FITC-dextran was also shown in immune cells (B lymphocytes and Jurkat cells) commonly used for cell engineering applications.

Cytotoxicity of PP50 and mechanism underlying polymer mediate uptake was investigated, drawing comparisons with previously published data. Intracellular localisation of PP50

conjugated to Cy5 was explored, revealing the co-localisation of PP50 with the mitochondria, highlighting a potential application of Cy5-PP50 as a mitochondrial targeting agent.

To demonstrate the potential of PP50 to deliver macromolecules to specific intracellular sites, the delivery of anti-NPC and anti-β-tubulin antibodies using PP50 were assessed. Successful PP50 mediated delivery was demonstrated in each case, but the difference in delivery parameters used for each antibody highlights the potential need for optimisation according to the payload of interest.

Finally, to build upon the previously published data on the delivery of neutral peptides, the uptake of anionic and cationic peptides was explored using PP50. The intracellular uptake of FITC-ova in B lymphocytes and FITC-p53 in A549 cells was enhanced by co-incubation of polymer and peptide. However, for the delivery of cationic peptides (Histone-FAM and KLAK), pre-treatment of polymer alone and then subsequent treatment of payload alone greatly increased peptide uptake compared to co-incubation.

Taken together, the data discussed in this chapter provides a solid foundation for using pHe as a trigger to facilitate the intracellular delivery of functional therapeutic payloads using PP50.

Chapter 4

Applications of anionic pH-responsive polymers for intracellular delivery of functional proteins

This chapter describes the intracellular delivery of the cell membrane-impermeable functional protein saporin using the anionic polymers PP50 and PLP-NDA18. For PP50 mediated delivery, the cell death mechanisms and cellular uptake of saporin were investigated in-depth and discussed in comparison to currently published literature to give an overall understanding of the capabilities of PP50 as a delivery platform. In addition, the ability of PLP-NDA18 to enhance the cytotoxicity of saporin was explored to add to the previously published work on PLP-NDA18 as a drug delivery system.

Part of the work presented in this chapter has contributed to the following manuscripts: **Morrison G,** Kopytynski M, Chen R. "Polymer-based intracellular delivery platform enhances the cytotoxicity of saporin through multiple death pathways". To be submitted.

Chen S, **Morrison G,** Kopytynski M, Chen R. "Comb-like pseudopeptidic polymer-mediated pH-triggered rapid intracellular delivery of cargos from a wide size range". To be submitted.

4.1 Introduction

Ribosome inactivating proteins (RIPs) are a family of potent toxins that irreversibly inhibit protein synthesis, ultimately resulting in cell death (Walsh et al., 2013). This advantageous property has led RIPs to be widely studied as cancer-targeting agents.

RIPs are grouped into type I and type II proteins. Type I RIPs possess RNA N-glycosidase enzymatic activity that brings about depurination of adenine at position 4324 in the 28 S rRNA

(Narayanan et al., 2005). However, the full extent of their therapeutic potential is severely hindered by their lack of binding receptor chains (Wang et al., 2016). Consequently, type I RIPs have no efficient means of entering target cells, rendering them cell impermeable.

Saporin-S6 (saporin) is a 30 kDa type I RIP isolated from the seeds of *Saponaria officinalis* (Zhang et al., 2020). If given a method of entry into the cell, saporin is highly potent. As such, the use of lipid nanoparticles, antibodies and dendrimers have been utilised to aid the uptake of saporin into the cell interior (Bonardi et al., 1993; Lai et al., 2008; Martínez-Jothar et al., 2019; Shen et al., 2021; Zhang et al., 2020).

There is conflicting evidence regarding the mechanism of saporin uptake and the biological pathways involved in cell death. For example, the extrinsic and intrinsic apoptotic pathway, activation of caspases, DNA damage and inhibition of protein synthesis are all reported potential pathways contributing to the death of cells once saporin entry is initiated (Bagga et al., 2003a; Cavallaro and Soria, 1995; Narayanan et al., 2005; Polito et al., 2009; Sikriwal et al., 2008). However, it is important to note that the pathways involved may not be mutually exclusive and may depend on the cell line and delivery platform used (Narayanan et al., 2005).

In Chapter 3, the versatility of PP50 as an intracellular delivery platform was explored to deliver a range of macromolecules at pHe 6.5. To build upon this, in this chapter, the ability of PP50 to enhance the cytotoxicity of the therapeutic RIP saporin was studied in A549 cells using the co-incubation method at pHe 6.5. The time-dependent and concentration-dependent *in vitro* cytotoxicity was measured using the CellTitre-Glo® 2.0 cell viability assay.

To understand the cell entry mechanism of PP50 and saporin, cytotoxicity measurements were performed in the presence of endocytosis inhibitors. FITC was conjugated to saporin to visualise its intracellular localisation in the cell. The cell death mechanism induced by saporin was investigated by measuring the activation of caspase 8, caspase 9 and caspase 3/7. In addition, time-dependent apoptosis and inhibition of protein synthesis were assessed to draw conclusions on the biological pathways involved in cell death. The results were compared to the pertinent literature. Further, the ability of PP50 to enhance the delivery of saporin into

A549 multicellular spheroids *in vitro* was evaluated. Lastly, the ability of the pH-responsive anionic polymer PLP-NDA18 was examined for its ability to enhance the cytotoxicity toward A549 cells.

4.2 Results and Discussion

4.2.1 PP50 mediated uptake of saporin

The ability of PP50 to enhance the uptake and cytotoxicity of saporin was investigated in A549 cells. Successful delivery was quantitatively measured by determining the cell viability of A549 cells as saporin has been reported to induce cell death after entry into the cell interior (Polito et al., 2009). Cells were firstly co-incubated with PP50 and saporin (PP50/saporin) at three different PP50 concentrations: 0.2 mg/ml (PP50-0.2), 0.1 mg/ml (PP50-0.1) or 0.025 mg/ml (PP50-0.025) for 1 hour and then further incubated for 72 hours before analysis. The dose-dependent cytotoxicity of free saporin (i.e. not co-incubated with PP50) was also compared. Cell viability was measured using the CellTitre-Glo® 2.0 cell viability assay. Figure 4-1A shows the successful delivery of saporin as measured by the decreased cell viability in cells treated with PP50-0.2/saporin and PP50-0.1/saporin. For PP50-0.2/saporin and PP50-0.1/saporin, the saporin concentration required to decrease the cell viability by half (IC_{50}) was 0.036 nM and 0.085 nM, respectively.

In comparison, PP50-0.025 was unable to aid the delivery of saporin into the cell. This is likely due to the PP50 concentration being too low to induce membrane destabilisation and subsequent payload entry into the cell interior. Free saporin was also not cytotoxic, confirming that saporin is a cell impermeable toxin (Bolshakov et al., 2020).

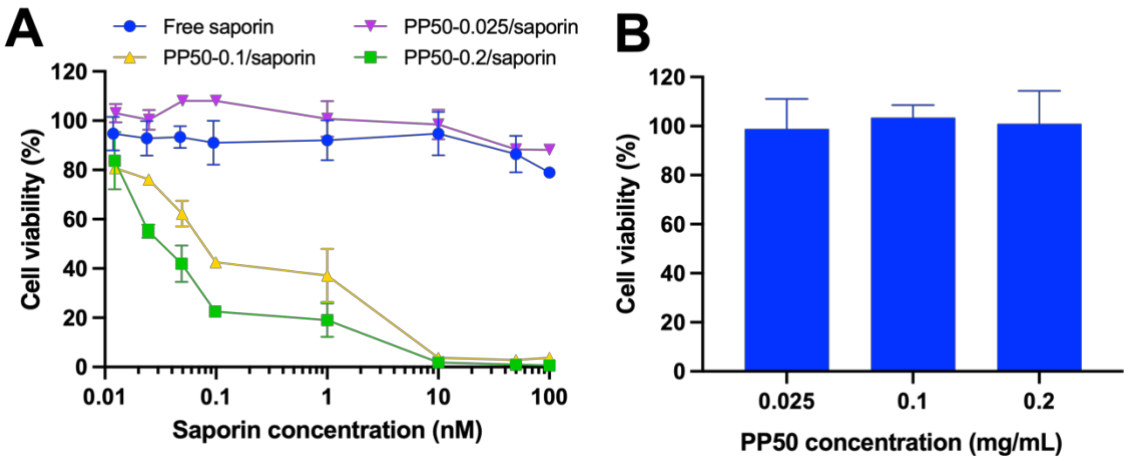

Figure 4-1. A) Cytotoxicity of A549 cells treated with free saporin or PP50/saporin at varying PP50 concentrations. Cell viabilities were evaluated after 1 hour of treatment plus 72 hours of further incubation to the indicated concentrations of saporin. Mean results ± SD, n=3 B) Cytotoxicity of A549 cells treated with PP50 alone at various concentrations for 1 hour plus 72 hours further incubation. Mean results ± SD, n=6. Viability was determined by the CellTitre-Glo® 2.0 cell viability assay.

To confirm that the cytotoxicity induced was due to the uptake of saporin and not PP50 induced toxicity, the cell viability of A549 cells incubated with PP50 alone at the concentrations used within this study was also measured (Figure 4-1B). The results validate the claim that PP50 enhances the cytotoxicity of saporin, but the PP50 delivery platform is not toxic itself.

Next, to explore the time-dependent cytotoxicity of PP50/saporin, cells were treated with PP50/saporin (saporin concentration 1 nM) for various time durations and then further incubated for 72 hours before analysis (Figure 4-2). In cells treated with the highest PP50 concentration (PP50-0.2/saporin), only 21 minutes of treatment time was required to reduce the cell viability by half (IT_{50}). For PP50-0.1/saporin, the effects of saporin cytotoxicity were only observed at 1 hour. PP50-0.025 and free saporin once again had no effects on cell viability.

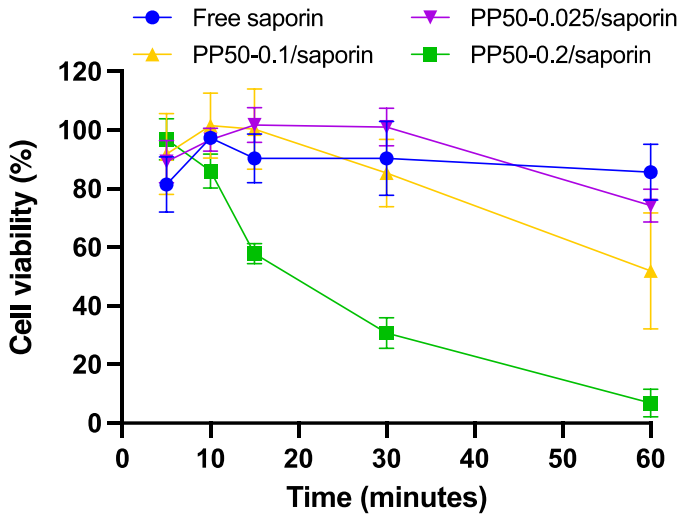

Figure 4-2. Cytotoxicity of A549 cells treated with free saporin or PP50/saporin at varying PP50 concentrations with cells were exposed to 1 nM saporin as determined by the CellTitre-Glo® 2.0 cell viability assay. Cell viabilities were acquired after the indicated treatment times plus 72 hours further incubation. Mean results ± SD, n=4.

4.2.2 Caspase activation

The two main pathways of caspase activation involved in triggering apoptosis are the extrinsic and intrinsic pathways. The former consists of the activation of caspase 8 mediated by the death receptor on the cell membrane. The latter involves the release of cytochrome c from the mitochondria and subsequent activation of caspase 9. Caspases 8 and 9 are initiator caspases that converge into the activation of the executioner caspase 3/7 (Boatright and Salvesen, 2003). Therefore, to elucidate the cell death mechanism induced by saporin, caspase 8, 9 and 3/7 activity was measured in cells treated with PP50/saporin or free saporin. Activation was measured after 1 hour of treatment and 24 hours of further incubation. Figure 4-3A shows that PP50-0.2/saporin and PP50-0.1/saporin were able to induce the activation of all three caspases. Consistent with the cytotoxicity results, PP50-0.2/saporin demonstrated the highest caspase 8, 9 and 3/7 activations. The higher activation of caspase 3/7, compared to caspases 8 and 9, is likely due to caspases 8 and 9 feeding into caspase 3/7, the downstream effectors of apoptosis. Similar to the cell viability results, free saporin and PP50-0.025/saporin were unable to initiate caspase activation.

In the time-course experiment (Figure 4-3B), using 1 nM saporin, PP50-0.2/saporin exhibited significantly ($P \leq 0.05$) higher caspase 8 and 3/7 activation and significantly ($P \leq 0.01$) higher caspase 9 activation than free saporin after 1 hour.

These results are consistent with Polito *et al*. (2009), who reported that the activation of caspase 3/7, 8 and 9 in L540 (Hodgkins lymphoma cells) was triggered by saporin. In addition, a reduction in protein synthesis in L540 cells was measured after exposure to saporin. On the other hand, Sikriwal *et al*. (2008) demonstrated that saporin induced caspase-dependent apoptosis in U937 (human histiocytic lymphoma cells) was through the mitochondrial cascade (measured by the upregulation of caspases 3 and 9) but not through the extrinsic pathway. Most interestingly, Sikriwal *et al*. (2008) reported that this activation was independent of protein synthesis inhibition, despite saporin being termed a potent inhibitor of protein synthesis. These conflicting reports suggest that the cell death mechanism caused by saporin may differ according to the cell type or delivery mechanism used.

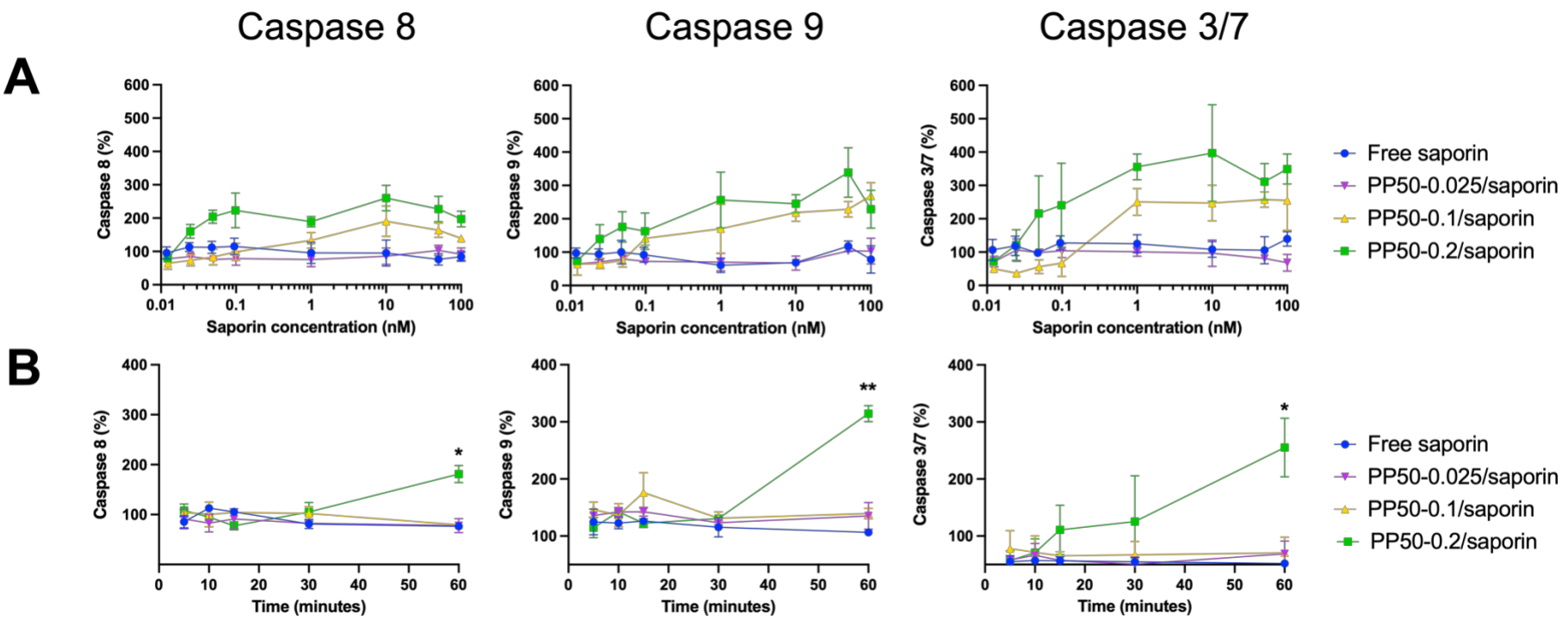

Figure 4-3. Caspase 3/7, 8 and 9 activation in A549 cells treated with A) free saporin or PP50/saporin at varying PP50 concentrations. Caspase activation was evaluated after 1 hour treatment plus 24 hours further incubation to the indicated concentrations of saporin or B) with free saporin or PP50/saporin at varying PP50 concentrations with cells were exposed to 1nM saporin. Caspase activation was acquired after the indicated treatment times plus 24 hours further incubation. Caspase activity is expressed as the percentage of control values obtained from A549 cells grown in the absence of saporin. Mean results ± SD, n=3. *P ≤ 0.05 **P ≤ 0.01.

4.2.3 Inhibition of protein synthesis

To determine whether the uptake of saporin in A549 cells and subsequent activation of the intrinsic and extrinsic pathways is dependent on protein synthesis inhibition, the Click-iT® Plus OPP protein synthesis assay was employed to measure the levels of protein synthesis after treatment with PP50/saporin. The optimum PP50 polymer concentration (PP50-0.2), which showed the highest caspase activation and decrease in cell viability when co-incubated with saporin, was used for the subsequent experiments. As a control, free saporin and PP50 alone were also tested. Levels of protein synthesis were measured after 1 hour of treatment plus 24 hours of further incubation to determine if protein synthesis inhibition coincided with caspase activation.

Figure 4-4A displays the decrease in green fluorescence, representing the inhibition of protein synthesis in cells treated with PP50-0.2/saporin. Even at low levels of saporin (1 nM), the fluorescence within the cell is remarkedly lower than the control. Treatment with PP50-0.2 alone or free saporin at the concentrations measured did not result in reduced protein synthesis levels. Semi-quantitative fluorescence intensity analysis (Figure 4-4B) verified a significant reduction in protein synthesis levels in cells treated with PP50-0.2/saporin with saporin concentrations of 1 nM ($P \leq 0.0001$), 10 nM ($P \leq 0.0001$) and 100 nM ($P \leq 0.001$) compared to controls. This data sheds increased light on the cell death pathway, confirming that the caspase activation induced by PP50-0.2/saporin in A549 cells is accompanied by an inhibition of protein synthesis.

Surprisingly, there have been reports of saporin induced cytotoxicity, measured by protein synthesis inhibition, in the absence of a delivery vehicle. For example, Bagga *et al.* (2003b) showed a decrease in protein synthesis in U937 (human histiocyte lymphoma), HUT102 (human cutaneous T-cell lymphoma), J774A.1 (mouse monocyte-macrophage) and L929 (mouse fibroblast) cells after treatment with free saporin for 36 hours. In this study, the concentration of saporin required to inhibit cellular protein synthesis was 150 nM (U937), 100 nM (HUT102), 0.67 nM (J774A.1) and 20 nM (L929). Here, in the present study, free saporin (up to 100 nM) was shown not to inhibit protein synthesis in A549 cells after 1 hour treatment plus 24 hours further incubation.

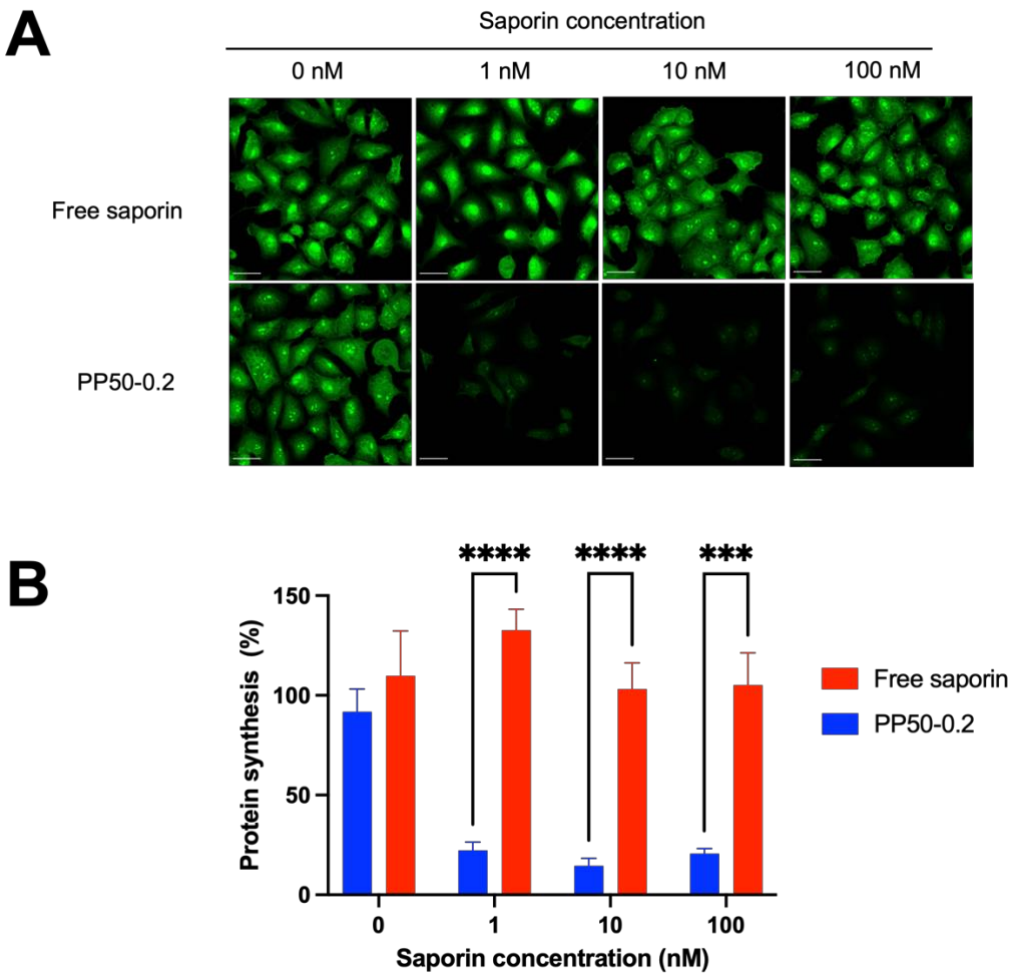

Figure 4-4. Protein synthesis levels in A549 cells treated with free saporin, PP50-0.2 alone or PP50-0-2/saporin. Protein synthesis levels were measured using the Click-iT® Plus OPP protein synthesis assay after 1 hour treatment plus 24 hours further incubation to the indicated concentrations of saporin. A) Nascent protein synthesis is detected by Alexa Fluor 488 signal within the nucleus. Scale bar = 45 µm B) Semi-quantitative fluorescence intensity analysis via FIJI. Mean results ± SD, n=6 individual cells. ***P ≤ 0.001 **** P ≤ 0.0001.

4.2.4 Induction of apoptosis

To confirm the time-dependent induction of apoptosis in A549 cells, cells were treated with PP50-0.2/saporin, free saporin or PP50-0.2 alone for 1 hour. Cells were stained with Annexin V-FITC and PI staining after 24, 48 or 72 hours of further incubation. A low saporin

concentration, 1 nM, was used as previous data had shown it was sufficient to inhibit protein synthesis when co-incubated with PP50-0.2 (Figure 4-4).

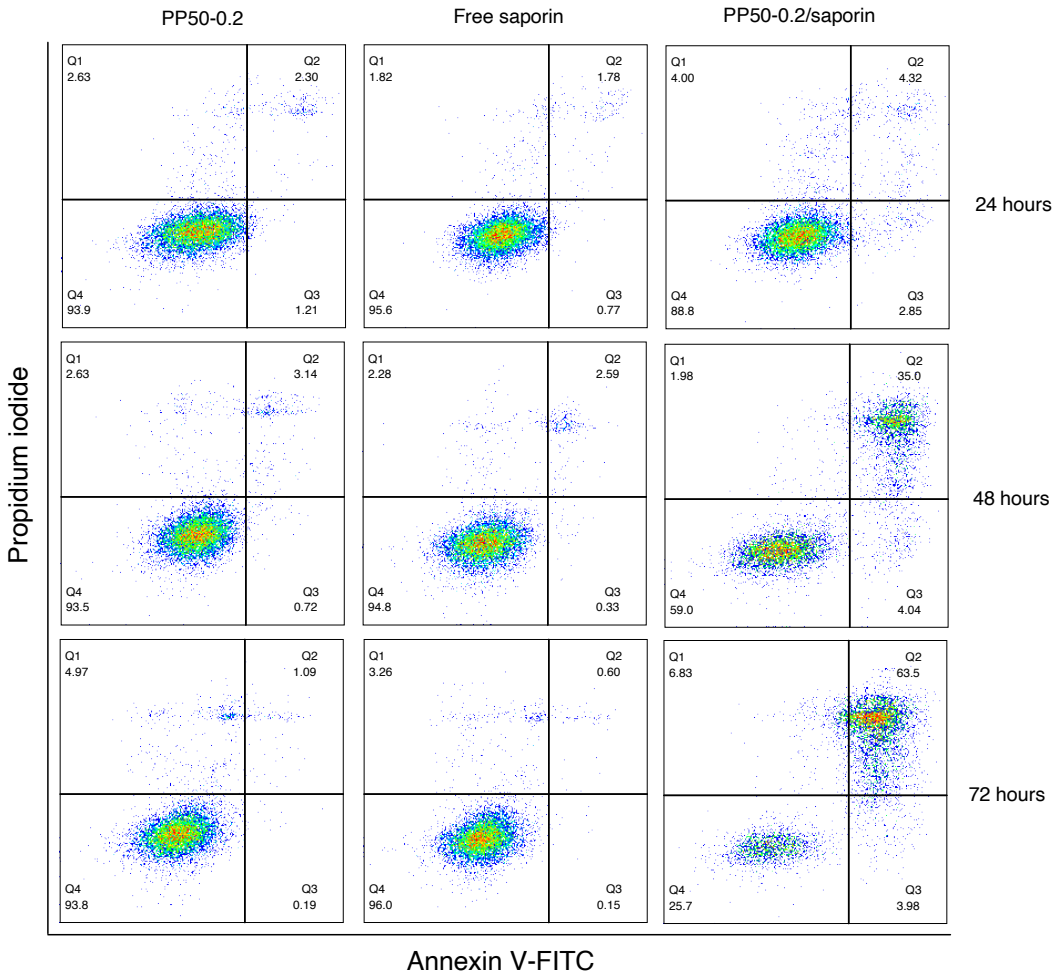

Figure 4-5. Effects of PP50-0.2/saporin (saporin concentration 1 nM), free saporin (1 nM) and PP50-0.2 alone on the induction of apoptosis in A549 cells after 1 hour of treatment plus 24, 48 or 72 hours of further incubation. The apoptotic cell population was quantified using flow cytometry using Annexin V-FITC/PI double staining.

Figure 4-5 reveals the time-dependent and gradual onset of apoptosis over the course of 72 hours in PP50.02/saporin treated cells as indicated in the Annexin V-FITC+/PI+ quadrant signifying late apoptotic or necrotic cells. After 24 hours of further incubation, where caspases 8, 9 and 3/7 are activated and protein synthesis levels are decreased, the percentage of

Annexin V-FITC+/PI+ cells remain low (4.32%). However, after 48 hours and 72 hours of further incubation, the levels of late apoptotic or necrotic cells increase to 35.0% and 63.5%, respectively. It is also likely that Annexin V-FITC +/PI- cells are in the early stages of apoptosis and will eventually progress to late apoptotic or necrotic cells. Taken together, this indicates that caspase activation and inhibition of protein synthesis are prerequisites for the induction of apoptosis. Treatment with PP50-0.2 alone or free saporin resulted in a consistently high level of viable cells even after 72 hours of further incubation (93.8% and 96.0%, respectively).

The visual analysis of cells exposed to PP50-0.2/saporin and stained with Annexin V-FITC/PI revealed fluorescent patterns of cells undergoing early and late stages of apoptosis (Figure 4-6). In contrast, cells treated with free saporin or PP50-0.2 alone showed low levels of fluorescent signal. A greater number of cells were also observed in these samples than cells treated with PP50-0.2/saporin, which is in agreeance with the cell viability data earlier presented (Figure 4-1).

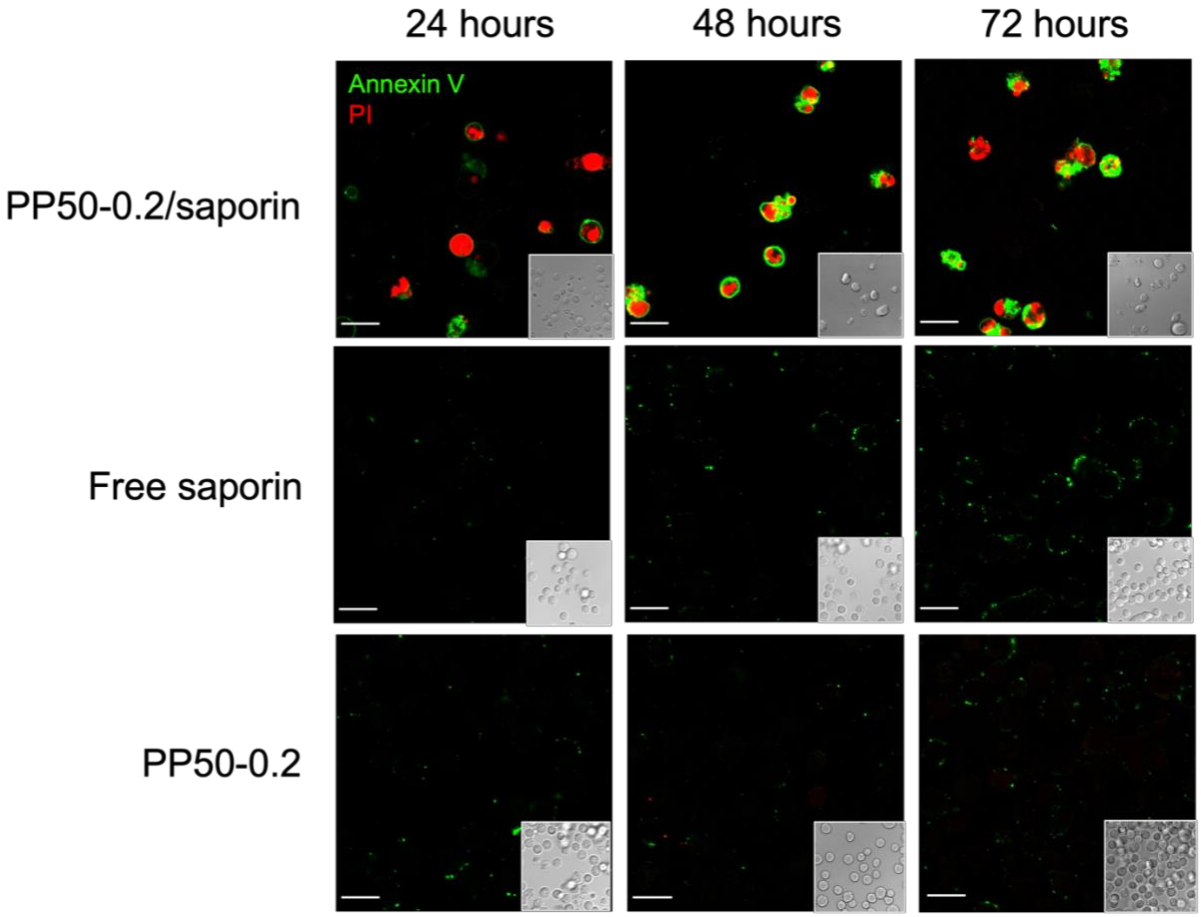

Figure 4-6. Representative confocal microscopy images of A549 cells treated with PP50-0.2/saporin, free saporin or PP50-0.2 alone for 1 hour plus 24, 48 or 72 hours of further incubation. Fluorescent and phase contrast channels depicting the signals for Annexin V-FITC (apoptotic cells) in green and PI (dead cells) in red. Scale bar = 20 µm.

4.2.5 Intracellular localisation of saporin

To visualise the intracellular localisation of saporin, A549 cells were treated with FITC labelled saporin (FITC-saporin) and PP50-0.2 for 1 hour. The intracellular fluorescence was observed by confocal microscopy after 24 hours of further incubation. Figure 4-7A shows the uptake, cytoplasmic and nuclear delivery of FITC-saporin in cells treated with PP50-0.2/FITC-saporin as indicated by the strong green diffuse fluorescence distributed within the cell. The fluorescent intensity plot profile (Figure 4-7B) in the cross-sectional area indicated by the white line in Figure 4-7A further confirms the localisation of FITC-saporin in the nuclei. The delivery efficiency of PP50-0.2/FITC-saporin compared to FITC-saporin alone was further

quantitively evaluated by flow cytometry (Figure 4-7C), confirming a higher uptake of FITC-saporin when treated in the presence of the PP50-0.2 delivery platform.

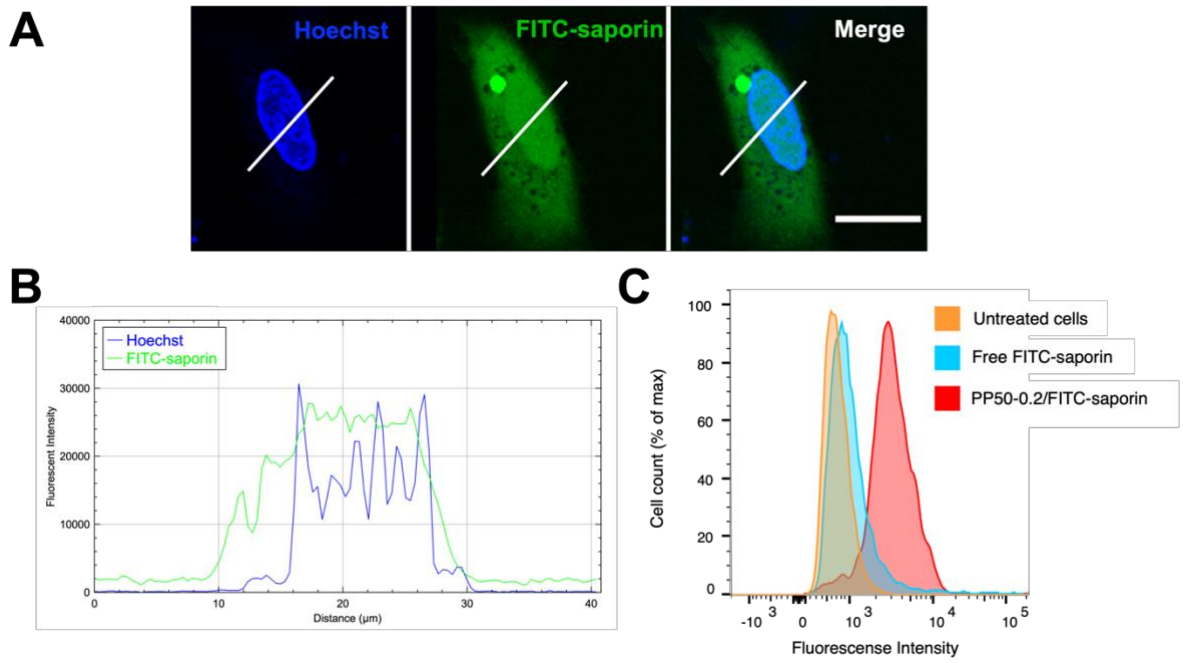

Figure 4-7. A) Intracellular localisation of FITC-saporin in A549 cells. Cells were treated with PP50-0.2/FITC-saporin (FITC-saporin concentration 125 µg/mL) for 1 hour. Images were taken after 24 hours of further incubation. Scale bar = 20 µm B) fluorescence intensity plot produced from the cross-section (white line indicated on image A). C) Flow cytometry analysis of the uptake of FITC-saporin in cells treated with PP50-0.2/FITC-saporin or FITC-saporin alone.

Lai *et al*. (2008) visualised the nuclear and cytoplasmic accumulation of dendrimer conjugated saporin in Ca9.22 human gingival cells after treatment with photochemical internalisation. Bolognesi *et al.* (2012) also observed the nuclear localisation of saporin in HeLa cells. The nuclear localisation of FITC-saporin in the nuclei when co-delivered with PP50-0.2, despite saporin not containing a nuclear localisation sequence, suggests that DNA damage may be additionally involved in the cell death mechanism. Further experiments would be required to confirm this.

4.2.6 Mechanism of cell entry of PP50-0.2/saporin

Next, to further understand the cell entry mechanism used by PP50-0.2 to facilitate the uptake of saporin, PP50-0.2/saporin delivery was measured in the presence of endocytosis inhibitors. The ability of an inhibitor to block the cellular uptake of PP50-0.2/saporin was quantified by an increase in cell viability compared to PP50-0.2/saporin alone (no inhibitor), which has shown to be cytotoxic. Cells were initially pre-treated with cytochalasin D (2.5 μM), chlorpromazine (3 μg/mL), amiloride (30 μM), MβCD (1.5 mg/mL), nystatin (10 μg/mL) or ammonium chloride (100 μM) for 30 minutes. Then, similar to the cell viability experiments, cells were treated with PP50-0.2/saporin in the presence of inhibitors for 1 hour, and viability was assessed after 72 hours of further incubation.

Figure 4-8 reveals that almost complete inhibition of saporin uptake was detected in cells treated with PP50-0.2/saporin in the presence of cytochalasin D as indicated by the high cell viability (90.3 ± 4.9%). Partial inhibition of saporin uptake was measured in cells treated with PP50-0.2/saporin in the presence of MβCD (cell viability 44.8 ± 13.5%). Cytochalasin D is a micropinocytosis and actin polymerisation inhibitor, whilst MβCD is an inhibitor of lipid raft mediated endocytosis (Auriac et al., 2010; He et al., 2018). This suggests that PP50-0.2/saporin uptake primarily depends on macropinocytosis and actin polymerisation and may, secondarily, depend on lipid raft mediated endocytosis for entry.

To ensure that the cytotoxicity induced was due to the uptake of PP50-0.2/saporin and not the inhibitor being toxic itself, the cell viability of cells incubated with inhibitors alone under the same conditions was also measured. Figure 4-8B confirms that treatment with inhibitors alone for the same time period did not affect cell viability.

Taken together, the enhanced uptake of saporin by PP50 is summarised in Figure 4-9.

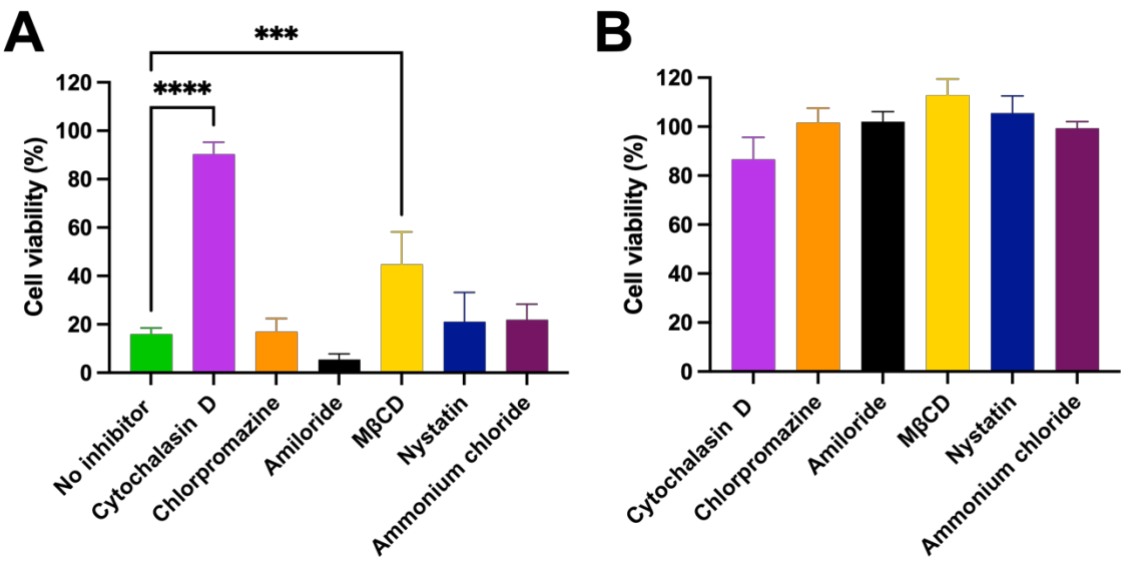

Figure 4-8. A) Cytotoxicity of A549 cells treated with PP50-0.2/saporin alone or PP50-0.2/saporin in the presence of various inhibitors (saporin concentration 1 nM). Cells were pre-treated with cytochalasin D (2.5 µM), chlorpromazine (3 µg/mL), amiloride (30 µM), MβCD (1.5 mg/mL), nystatin (10 µg/mL) or ammonium chloride (100 µM) for 30 minutes followed by treatment with PP50-0.2/saporin in the presence of inhibitors for 1 hour followed by 72 hours of further incubation. Control cells (no inhibitor) were treated with PP50-0.2/saporin without inhibitors. B) Cytotoxicity of A549 cells treated with inhibitors alone under the same conditions. Viability was determined by the CellTitre-Glo® 2.0 cell viability assay after 72 hours of further incubation. Mean results ± SD, n = 4. *** $P \leq 0.001$ **** $P \leq 0.0001$.

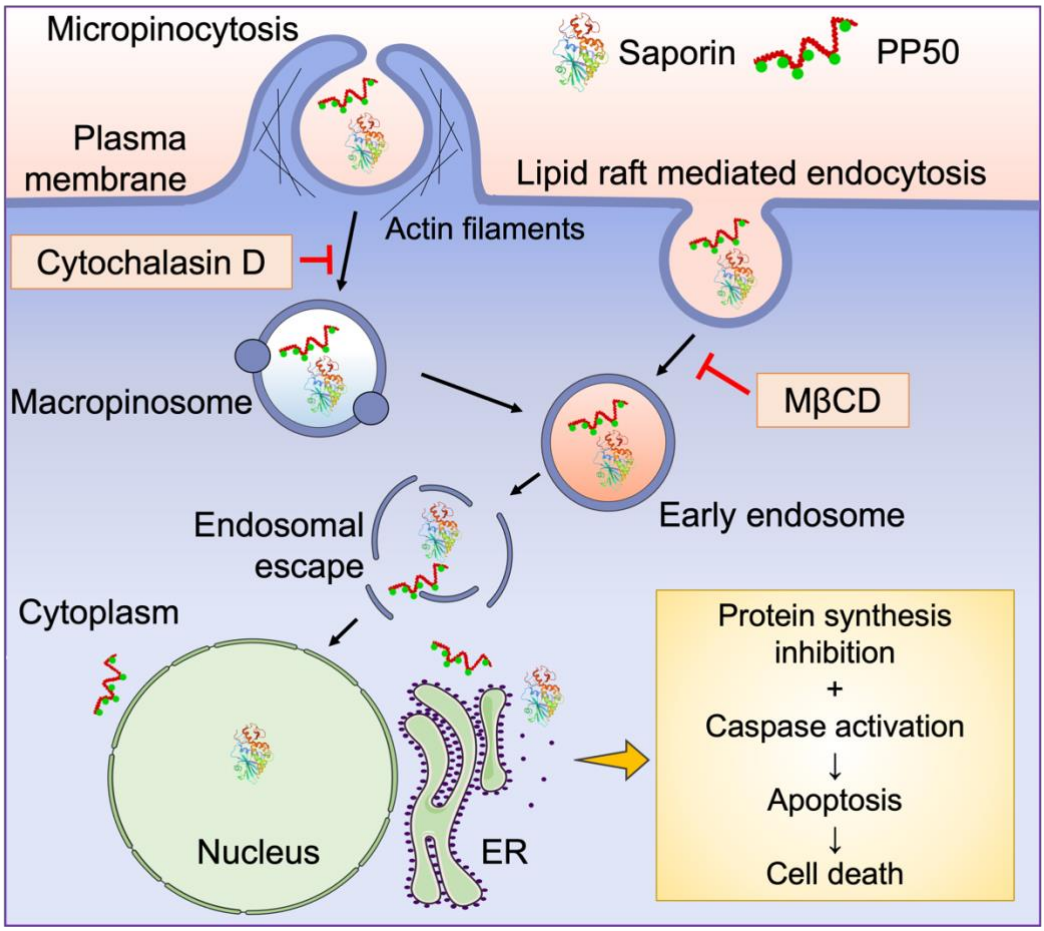

Figure 4-9. Schematic of the intracellular delivery of PP50 mediated saporin uptake.

4.2.7 PP50 mediated saporin delivery to multicellular spheroids

Multicellular 3D tumour spheroids are spherical aggregates of cancer cells. They serve as biologically relevant *in vitro* models, more closely mimicking the structural architecture and dynamic microenvironment of *in vivo* tumours than 2D monolayer cells (Cui et al., 2017; Lazzari et al., 2017). Kopytynski *et al*. (2020) previously demonstrated the delivery of 150 kDa FITC-dextran into A549 multicellular spheroids at pHe 6.5 by co-incubation with PP50.

The next aim was to test the ability of PP50 to enhance the uptake of saporin in A549 spheroids *in vitro*. As in the 2D monolayer experiments, delivery was performed within the active range of the polymer, at pHe 6.5. This pHe more closely represents the pHe tumour microenvironment for delivery into spheroids than at physiological pHe (Hao et al., 2018). In this experiment, a higher PP50 concentration at 5 mg/ml (PP50-5) and a higher concentration

of saporin (300 nM) was used to ensure efficient 3D penetration into spheroids. A549 spheroids were grown for 3 days and then treated with PP50-5/saporin, free saporin or PP50-5 for 1 hour. The co-treatment of PLP (poly(L-lysine isophthalamide) with no grafting of L-phenylalanine) at 5mg/ml (PLP-5) with saporin (PLP-5/saporin) under the same conditions was also investigated to show the enhanced delivery capabilities of PP50 in comparison to the parent polymer. Cell viability was quantified using the CellTitre-Glo®-3D cell viability assay and visualised by staining PP50-5/saporin treated spheroids with the live stain Calcein AM over 3 days.

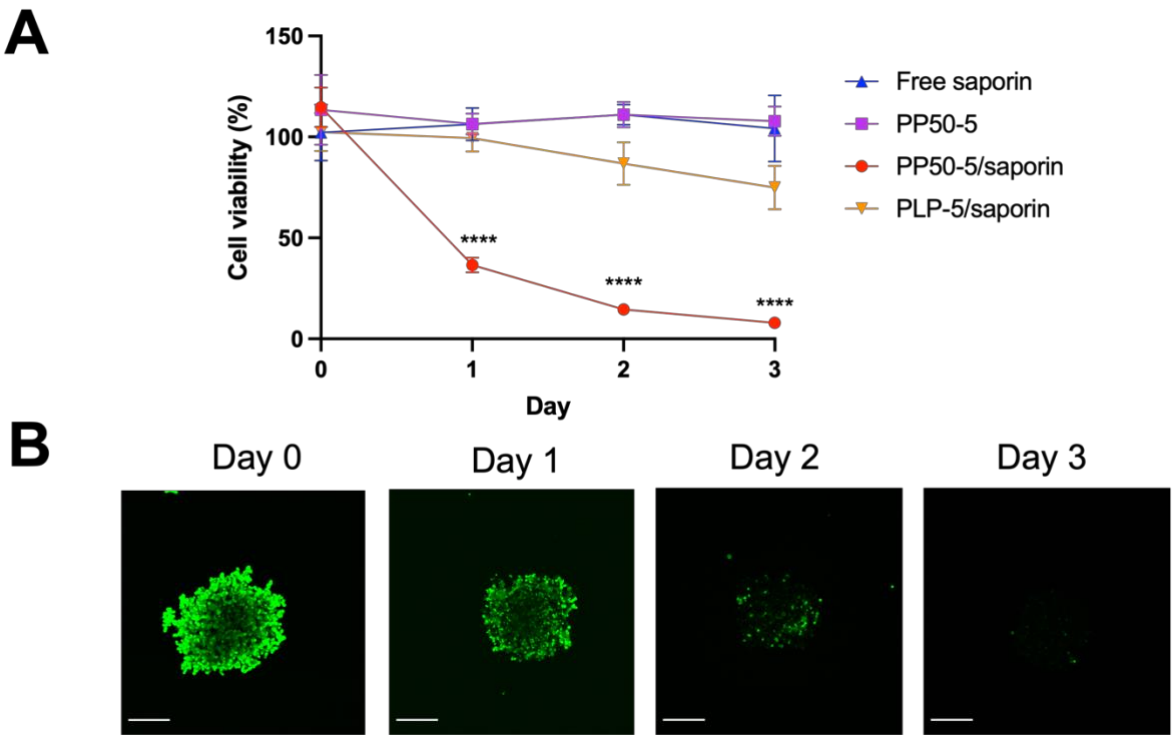

Figure 4-10. A) Cytotoxicity of A549 multicellular spheroids treated with PP50-5/saporin, PLP-5/saporin, PP50-5 alone or free saporin (saporin concentration 300 nM). Cell viability was measured over 3 days and determined by the CellTitre-Glo®-3D cell viability assay. Mean results ± SD, n=7. ****P ≤ 0.001 B) Calcein AM (live stain) of A549 multicellular spheroids treated with PP50-5/saporin over 3 days. The distribution of green fluorescence was measured using Z-stack scanning. Scale bar = 200 µm.

Figure 4-10A shows the enhanced cytotoxicity of saporin by PP50-5. By day 1, the cell viability of spheroids treated with PP50-5/saporin had decreased to 36.6 ± 3.6%, significantly ($P \leq 0.0001$) lower than the controls. The cell viability continued to decrease to 14.5 ± 2.5% at day 2 and to 7.9 ± 2.5% at day 3. The cell viability of spheroids treated with free saporin (300 nM) or PP50-5 alone remained above 100% after day 3. A slight decrease was measured in spheroids treated with PLP-5/saporin to 86.8 ± 10.4% at day 2 and to 74.9 ± 10.7% at day 3. This indicates the limited potential of the parent polymer PLP without side-chain modifications as an intracellular delivery system due to its the low cell membrane activity (Chen et al., 2009b, 2009a). Figure 4-10B further verifies the enhanced cytotoxicity of saporin by PP50-5 as visualised by the decrease in green fluorescence (signifying live cells) over 3 days after treatment. This data highlights the possibility of extending PP50's use as an intracellular delivery platform for *in vivo* applications.

4.2.8 PLP-NDA18 mediated uptake of saporin

PLP-NDA18 is another pH-responsive polymer derived from the parent polymer PLP, synthesised by grafting decylamine at an actual percentage of 18 mol% relative to the carboxyl groups pendant to the PLP backbone. Decylamine acts as a hydrophobic membrane anchor to enhance polymer-membrane interaction and provide stronger membrane binding and insertion for improved intracellular delivery. Due to PLP-NDA18's long alkyl side chains, it has been reported to cause deeper and more pronounced membrane curvature and membrane permeability compared to PP50 with L-phenylalanine side chains. A key desirable feature is PLP-NDA18's ability to facilitate more rapid and efficient delivery of macromolecules such as trehalose than PP50 (Chen et al., 2017, 2020b). Here, to extend the work on PLP-NDA18 as an intracellular delivery platform, the ability of PLP-NDA18 to enhance the uptake and cytotoxicity of the functional protein saporin in A549 cells was assessed at pHe 6.5. Initially, PLP-NDA18 (1 mg/mL) was co-incubated with saporin (PLP-NDA18/saporin) for 2 hours, and the cell viability was measured 48 hours after treatment. The cytotoxicity of free saporin under the same delivery conditions was compared as a control.

Figure 4-11 shows the dose-dependent cytotoxicity of saporin when co-incubated with PLP-NDA18 compared to free saporin. The IC_{50} was found to be 0.079 nM, demonstrating the ability of PLP-NDA18 to greatly enhance the cytotoxicity of saporin.

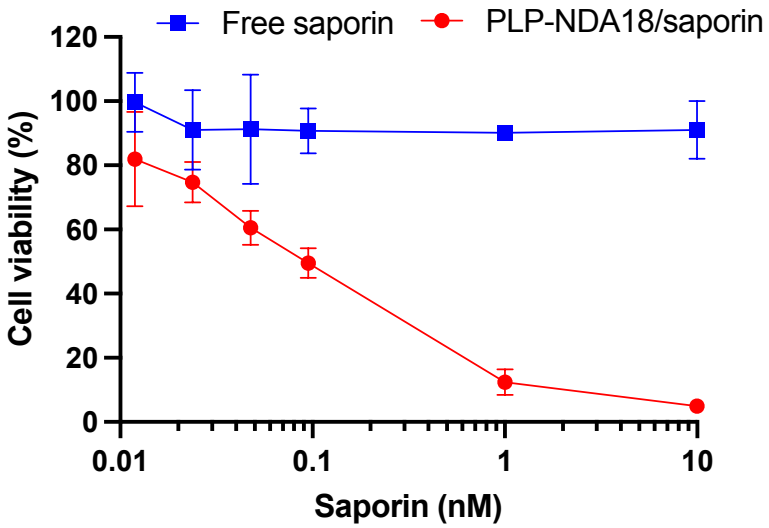

Figure 4-11. Cytotoxicity of A549 cells treated with free saporin or PLP-NDA18 (1 mg/mL) co-incubated with saporin at the indicated concentrations. Cell viabilities were evaluated after 2 hours of treatment plus 48 hours of further incubation. Mean results ± SD, n=3. Viability was determined by the CellTitre-Glo® 2.0 cell viability assay.

To confirm that the enhanced cytotoxicity of saporin was due to the intracellular delivery of saporin and not unwanted polymer toxicities, the cell viability of PLP-NDA18 alone at varying concentrations was measured. As shown in Figure 4-12, a decrease in cell viability was not measured in cells treated with PLP-NDA18 alone at the concentrations used in this study, verifying that PLP-NDA18 enhances the cytotoxicity of saporin, but the PLP-NDA18 delivery platform is not toxic itself.

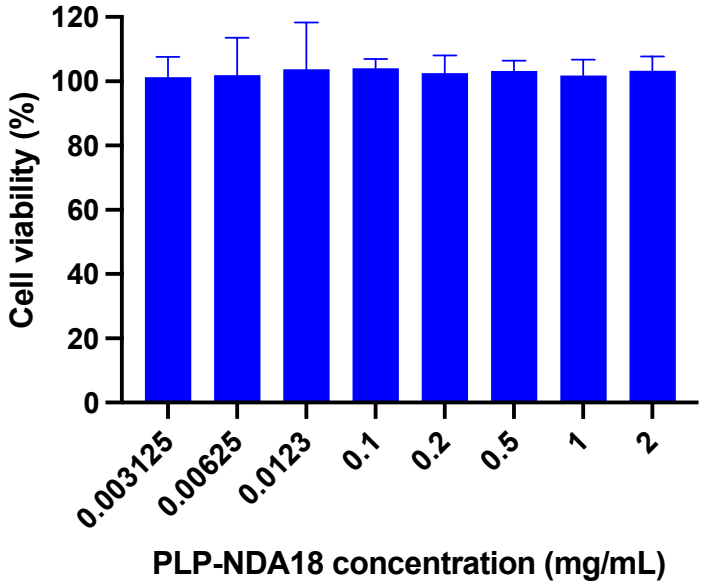

Figure 4-12. Cytotoxicity of A549 cells treated with PLP-NDA18 alone at various concentrations for 2 hours plus 48 hours of further incubation. Mean results ± SD, n=4. Viability was determined by the CellTitre-Glo® 2.0 cell viability assay.

Next, the delivery kinetics of PLP-NDA18 mediated saporin uptake was assessed. Using a low saporin concentration of 1 nM, the delivery of PLP-NDA18/saporin was compared to free saporin over 2 hours of treatment time. Figure 4-13 displays the time-dependent cytotoxicity of PLP-NDA18/saporin. The IT_{50} was found to be 9.1 minutes, revealing the extremely fast delivery kinetics of PLP-NDA18. This is in agreement with the previously published report showing the very rapid and efficient loading of the small molecule trehalose at mildly acidic pHe. It was also found that PLP-NDA18 mediated considerably more rapid and efficient trehalose intracellular delivery than PP50 (Chen et al., 2020).

In the present study, the IT_{50} for the PLP-NDA18 mediated and PP50 mediated delivery of saporin was 9 minutes and 21 minutes respectively. This suggests that PLP-NDA18 can also mediate more rapid and efficient intracellular delivery of saporin than PP50. However, it is imperative to note that a direct comparison between the two polymers is difficult to make due to slightly different treatment parameters, including polymer concentration and treatment time, used for saporin delivery.

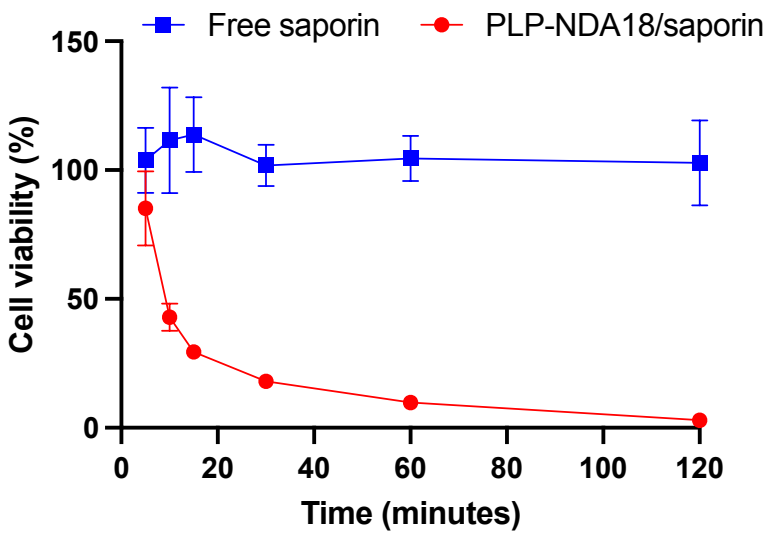

Figure 4-13. Cytotoxicity of A549 cells treated with free saporin or PLP-NDA18 (1 mg/mL) co-incubated with saporin (1nM) as determined by the CellTitre-Glo® 2.0 cell viability assay. Cell viabilities were acquired after the indicated treatment times plus 48 hours further incubation. Mean results ± SD, n=3.

Lastly, the concentration-dependent ability of PLP-NDA18 to deliver 1 nM saporin intracellularly was investigated. Figure 4-14 reveals the efficiency of low concentrations of PLP-NDA18 to improve the uptake of saporin, suggesting that PLP-NDA18's membrane destabilising ability is effective at low concentrations. The cell viability was reduced to 52.9 ± 10.0% when 1 nM saporin was co-incubated with a low PLP-NDA18 concentration at 0.003125 mg/mL, and then sharply decreased to 9.8 ± 7.0% with decreasing the PLP-NDA18 concentration to 0.0125 mg/mL. At 0.0125 mg/mL, PP50 was unable to efficiently deliver 1 nM saporin to A549 cells, as measured by a high cell viability after 1 hour of treatment and 72 hours of further incubation (Figure 4-1). This suggests that PLP-NDA18 can mediate more efficient intracellular delivery of saporin than PP50 at lower concentrations.

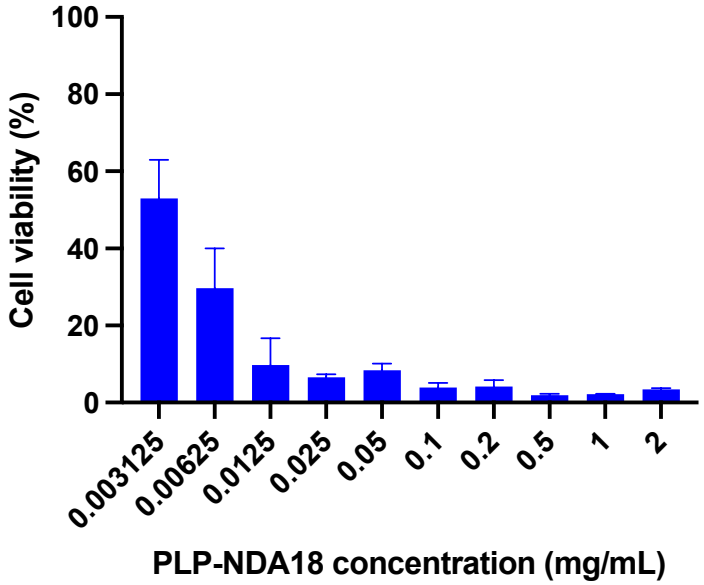

Figure 4-14. Cytotoxicity of A549 cells treated with free saporin or PLP-NDA18 at varying concentrations co-incubated with saporin (1 nM) as determined by the CellTitre-Glo® 2.0 cell viability assay. Cell viabilities were acquired after 2 hours of treatment plus 48 hours of further incubation. Mean results ± SD, n=4.

4.3 Conclusions

The aim of this chapter was to add to the knowledge surrounding type I RIP toxins by using PP50 and PLP-NDA18 as intracellular delivery platforms to enhance the uptake of the cell impermeable saporin into A549 cells. Successful uptake of saporin was determined by increased cytotoxicity, measured by a decrease in cell viability, compared to free saporin when saporin was co-incubated with either PP50 or PLP-NDA18 delivery platforms. Importantly, polymers alone were found to be non-cytotoxic to A549 cells.

The cell death mechanism of saporin has been well reported in the literature but with inconsistent findings, suggesting that its mechanism of action is dependent on the cell line and delivery platform used. Thus, this study specifically aimed to understand the cell death mechanism induced by the PP50 mediated saporin uptake in A549 cells. It was found that inhibition of protein synthesis and activation of caspases 8, 9 and 3/7 began earlier than the onset of apoptosis, indicating that these events are critical to triggering apoptosis and subsequent cell death in A549 cells. The accumulation of FITC-saporin in the cytoplasm and

nucleus when co-incubated with PP50 further suggests that a DNA dependent apoptotic mechanism may also be involved. It was revealed that PP50 mediated saporin uptake was primarily reliant on macropinocytosis and actin polymerisation for internalisation but may, secondarily, be dependent on lipid raft mediated endocytosis for entry. Additional studies are required to fully assess the cell death mechanism induced by PLP-NDA18 mediated saporin uptake in A549 cells.

Whilst a direct comparison between PP50 and PLP-NDA18 as intracellular delivery systems is difficult to make, the data suggests that PLP-NDA18 can mediate more rapid and efficient intracellular delivery of saporin than PP50, consistent with the published literature (Chen et al., 2020). Both delivery platforms, however, have shown their superior performance in enhancing the uptake and targeted delivery of saporin compared to free saporin alone. This further gives evidence of the potential of PLP-NDA18 and PP50 as *in vitro and ex vivo* delivery platforms for the intracellular delivery of therapeutics.

Lastly, the successful delivery of saporin in A549 spheroids by co-incubation with PP50 suggests that the applications of PP50 can extend beyond *in vitro* and *ex vivo* tools to *in vivo* cancer therapy applications.

Chapter 5

Ex vivo manipulation of dendritic cells for cell engineering applications

The chapter explores the potential of using pH-responsive polymers (PP50, PLP-NDA18, CP1 and CP2) for their applications in cell engineering. The polymer's ability to engineer JAWSII DCs by enhancing antigen presentation was investigated using the model antigen peptide ova30. In addition, the expression of co-stimulatory molecules and cytokine production was used as a measure of successful DC maturation and activation. The results were compared to stimulation of DCs with LPS and IFN-γ. IL-2 release after the co-culturing of DCs with RF33.70 cells was used also as an indicator of successful antigen presentation and enhanced engineering of surface molecules. Conclusions were drawn discussing pH-responsive polymers and their roles as intracellular delivery agents, with applications to cell engineering.

Note: The two novel cationic polymers CP1 and CPs were designed, synthesised and provided by Xinyu Lu (PhD student, Rongjun Chen group). MEng students Tudor-Octavian Sirbu and Suthinee Phanuvatsuk performed the haemolysis experiments for CP1 and CP2 presented in Figure 5-4 under my supervision. The contribution of Tudor-Octavian Sirbu and Suthinee Phanuvatsuk is also specified in the captions of relevant figures.

5.1 Introduction

APCs, including DCs, B lymphocytes and macrophages, are a specialised subset of immune cells that mediate the cellular immune response by capturing, processing and presenting antigens for recognition by T lymphocytes (T cells) (Szeto et al., 2015). DCs have been classified as the most potent APC, often termed "professional APCs". These DCs present antigens as MHC I or II, which subsequently trigger CD8+ or CD4+ T cell activation, respectively (Cebrian et al., 2016). Endogenous or exogenous foreign antigens loaded in the cytosol can be presented by MHC I for recognition by CD8+ T cells. Conversely, antigens loaded in the

endo-lysosomes are directed for presentation by MHC II for recognition by CD4+ T cells. Thus the loading onto MHC I molecules is highly advantageous for activating cytotoxic CD8+ T cells, as these cells are key in their immune response to tumours (Farhood et al., 2019). In addition to the correct MHC presentation, the expression of co-stimulatory molecules including CD40, CD80 and CD86 on DCs and the release of cytokines act to amplify the initial activation signal (Hubo et al., 2013).

Accordingly, much attention has been geared towards the *ex vivo* manipulation of APCs to increase antigen uptake. Tumour antigen-loaded APCs, when re-introduced into a patient, have the potential to activate their immune system to evoke a long-lasting tumour-specific CD8+ T cells response. For example, Provenge is a cellular immunotherapy that aims to manipulate DCs *ex vivo* to express key tumour antigens. Once activated, these cells are returned to the patient as an immune modulator (Anassi and Ndefo, 2011).

The model protein antigen ovalbumin, bearing the epitope SIINFEKL, has been extensively used in research to investigate efficient MHC I presentation in APCs (He et al., 2019; Szeto et al., 2015). Gong *et al*. (2020) showed the successful delivery of $ova_{241\text{-}270}$ peptide (ova30) and subsequent surface presentation of MHC I in DC2.4 DCs using a polymer-peptide conjugate-based nanotransformer. Further, in conjugation with a high expression of CD86, CD40, CD80 and release of cytokines TNF-α and IL-Iβ, they demonstrated antigen-specific T cell proliferation via cross-presentation.

The earlier success of the anionic polymer PP50 mediated antibody and peptide delivery (Chapter 3) and protein delivery (Chapter 4) suggests that PP50 may be a suitable *ex vivo* intracellular delivery platform for loading tumour antigens onto APCs. Therefore, in the present study, the ova30 peptide was utilised to assess the ability of PP50 to deliver tumour antigens intracellularly to upregulate MHC I on JAWSII DCs. In addition, the anionic polymer PLP-NDA18, which has shown previous success for the intracellular delivery of proteins (Chapter 4), and two novel pH-responsive cationic polymers (CP1 and CP2) synthesised by Xinyu Lu (Rongjun Chen group) were also used to investigate antigen delivery and MHC I upregulation. For CP1 and CP2 mediated ova30 delivery, the upregulation of MHC II, expression of co-stimulatory molecules CD40 and CD80 and the release of cytokines TNF-α

and IL-6 were measured. The results are discussed with comparison to DC stimulation with LPS and IFN-γ. Lastly, the ability of tumour loaded DCs to activate RF33.70 was assessed by measuring IL-2 secretion to give an overall picture of the capabilities and limitations of pH-responsive polymers for cell engineering applications (Figure 5-1).

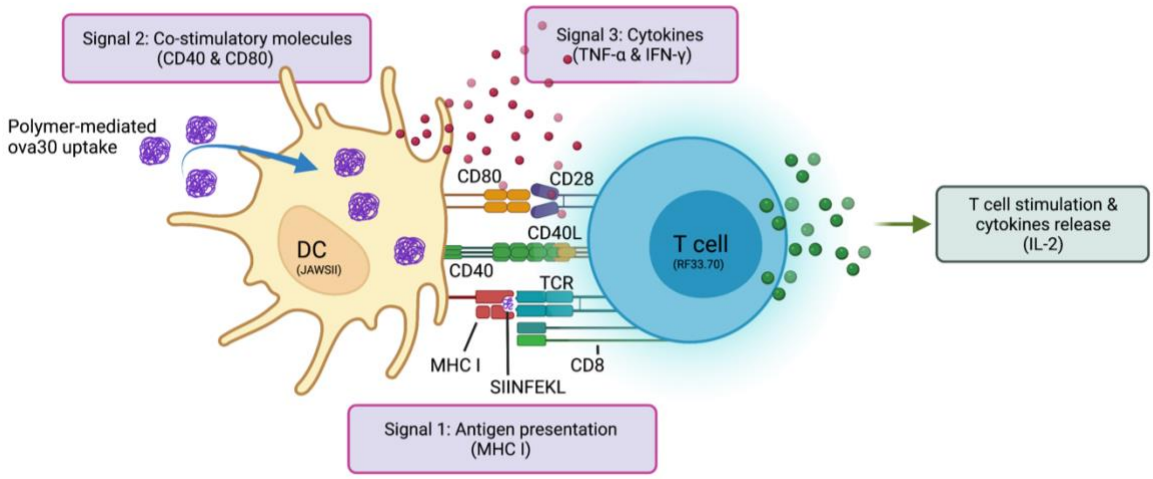

Figure 5-1. Schematic illustrating the intracellular delivery of ova30 for the upregulation of MHC I, expression of co-stimulatory molecules and release of cytokine for T cell stimulation.

5.2 Results and Discussion

5.2.1 PP50 and PLP-NDA18 mediated intracellular distribution of FITC-ova30 and MHC I presentation

The chicken ovalbumin protein-derived peptide called ova30, consisting of the amino acids 241-270 of the ovalbumin protein, was selected as the model antigen in this study. JAWSII cells (DCs) were chosen as biologically disease-relevant cells that can present the ova epitope SIINFEKL after successful cytoplasmic delivery of ova30. Firstly, the ability of PP50 and PLP-NDA18 to facilitate the cytoplasmic delivery of ova30 by co-incubation was assessed using FITC labelled ova30 (FITC-ova30). DCs were co-incubated with FITC-ova30 and PP50 (PP50/FITC-ova30) or PLP-NDA18 (PLP-NDA18/FITC-ova30) for 2 hours. Treatment was at pHe 6.5 as per previous experiments (Chapters 3 and 4). The intracellular fluorescence was observed by confocal microscopy and compared to DCs treated with FITC-ova30 only.

Figure 5-2 shows the localisation of FITC-ova30 (green channel) in the endosomes as observed with the high co-localisation with the lysotracker stain (red channel) in cells treated with FITC-ova30 only. Similarly, in DCs treated with PP50/FITC-ova30, FITC-ova30 was also restricted to the endosome. Based on previous data, this suggests that a high concentration of PP50 was not present in the endosomes with FITC-ova30. PP50 is membrane active within the endosomal range of pH 5.5-6.5 (data presented in Chapter 3) and at low concentrations e.g. 0.1 mg/mL (data presented in Chapter 4). Therefore, if PP50 was entrapped within the endosome with FITC-ova30, upon acidification of the endosome, PP50 should become membrane-active and initiate endosomal escape. However, no cytoplasmic delivery was observed. Little fluorescent signal was also observed in the cytoplasm of DCs treated with PLP-NDA18/FITC-ova30.

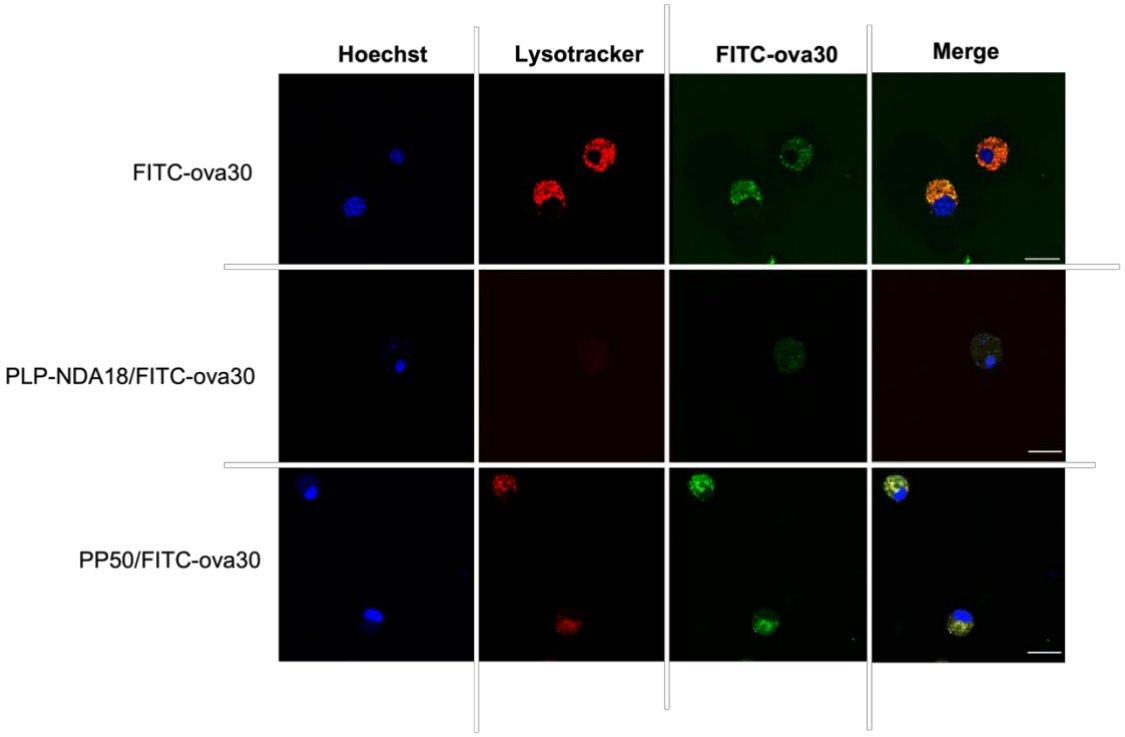

Figure 5-2. PP50 and PLP-NDA18 mediated delivery of ova30 in JASWII cells. DCs were co-incubated with FITC-ova30 (12 µg/mL) and PP50 (1 mg/mL) or PLP-NDA18 (1 mg/mL) for 2 hours at pHe 6.5 and the distribution of FITC-ova30 observed under confocal microscopy. Scale bar 20 µm.

The intracellular distribution of FITC-ova30 can only give an indication as to whether PP50 or PLP-NDA18 can enhance the uptake of ova30, and upregulation of MHC I. Antigens delivered

to the cytoplasm are usually presented by MHC I molecules for presentation to CD8+ T cells whilst antigen delivered to the endo-lysosomes are presented to MHC II molecules for presentation to CD4+ T cells (Szeto et al., 2015). For the treatment of tumours, it is more desirable to increase the activation of cytotoxic CD8+ T cells and thus, the upregulation of MHC I by DCs are required.

To quantitatively measure the presentation of MHC I, DCs were stained with SIINFEKL H-2Kb antibody after 2 hours of treatment and 24 or 48 hours of further incubation. Figure 5-3 confirms the unsuccessful upregulation of MHC I by DCs treated with PLP-NDA18/ova30 (Figure 5-3A) and PP50/ova30 (Figure 5-3B), consistent with the confocal data showing little cytoplasmic delivery of FITC-ova30. It was found that DCs treated with free ova30 showed a small increase in MHC I presentation. This may be due to the effects of cross-presentation, whereby DCs are able to present endocytosed antigens on MHC I (Ito et al., 2014). The adjustment of parameters (polymer concentration and treatment time) did not yield any significant positive results (data not shown).

PLP-NDA18 and PP50 are anionic polymers (Chen et al., 2020, 2017; Khormaee et al., 2013; Kopytynski et al., 2020). The ova30 peptide antigen also bears a net negative charge (-5 at pHe 6.5) (“Peptide Property Calculator,” 2022). As the cell membrane is negative, it could be speculated that there is some form of repulsion between the cell membrane, polymer and peptide hindering efficient intracellular delivery. In Chapter 3, it was demonstrated that PP50 was able to facilitate the intracellular delivery of other negatively charged peptides, including p53 and ova (amino acid sequence 323-339). However, these peptides were only slightly negatively charged (-1 and -0.8 at pHe 6.5) (“Peptide Property Calculator,” 2022). The greater negative charge of ova30 in this study may contribute to the unsuccessful intracellular delivery of the antigen. This suggests that alternative strategies, apart from simple co-incubation, should be explored for the intracellular delivery of more negatively charged payload using anionic PP50 or PLP-NDA18.

For the intracellular delivery of negatively charged nucleic acids, positively charged cationic materials are often employed to interact with the cell membrane and facilitate uptake of macromolecules (Bishop et al., 2015). Thus, two novel cationic polymers (namely, CP1 and

CP2) synthesised and provided by Xinyu Lu (Rongjun Chen group) were studied for their ability to enhance the uptake of ova30 and upregulation of MHC I.

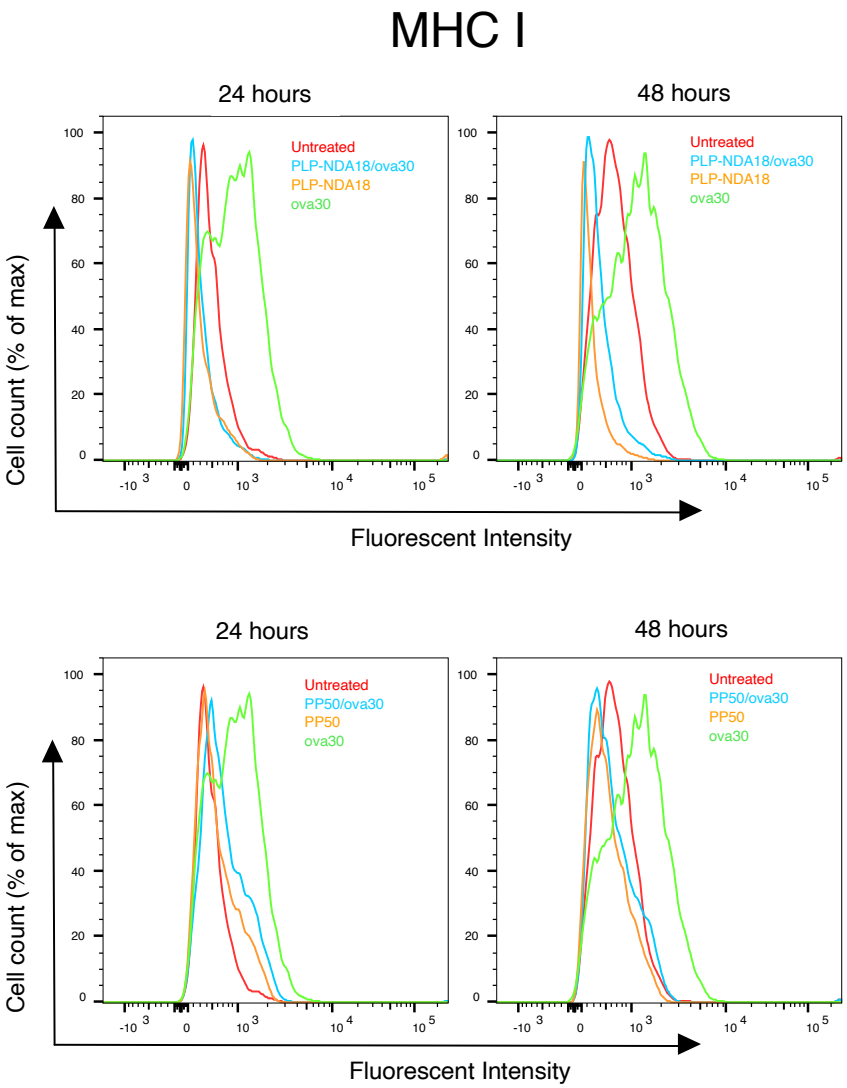

Figure 5-3. MHC I upregulation (SIINFEKL-H2Kb) on JAWSII cells treated with A) PLP-NDA18 (1 mg/mL) or B) PP50 (1mg/mL) co-incubated with ova30 (100 µM) at pHe 6.5 for 2 hours treatment. MHC I levels were assessed after 24 or 48 hours of further incubation compared to untreated cells or cells treated with ova30 or polymers only.

5.2.2 Haemolytic activity of CP1 and CP2

The haemolytic activity of CP1 and CP2 at 1.0 mg/mL was determined as a function of pHe to assess their ability to disrupt lipid bilayer membranes. As shown in Figure 5-4, CP1 achieved a maximum degree of haemolysis of 97.8 ± 1.4% at pHe 6.5 whilst CP2 achieved a maximum degree of haemolysis of 71.8 ± 2.0% at pHe 6.0. Both polymers displayed haemolytic activity

between the pH range (5.5-7.4) typical of the endosomal compartments. CP1 showed superior membrane lytic abilities between pHe 5.5 and pHe 7.0 than CP2. However, at pHe 7.4, CP1 showed a marked decrease in haemolysis (32.2 ± 1.3%) compared to CP2 (67.0 ± 1.9%).

Based on these results, CP1 and CP2 were both deemed suitable candidates to test for the intracellular delivery of ova30 at pHe 6.5.

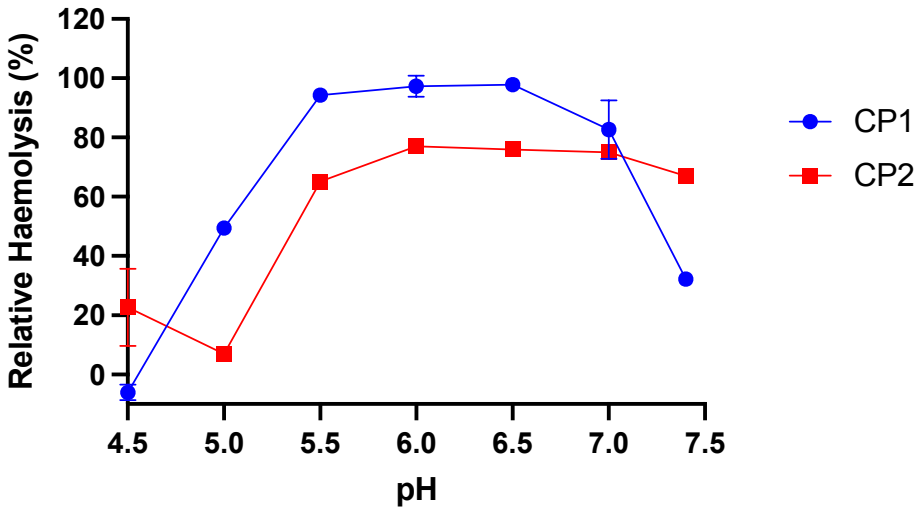

Figure 5-4. pH-dependent relative haemolysis of CP1 and CP2 at 1 mg/mL. Mean ± SD, n=3. *Data was collected by MSc students Tudor-Octavian Sirbu and Suthinee Phanuvatsuk* under my supervision.

5.2.3 Cationic polymer mediated intracellular distribution of FITC-ova30 and MHC Class I presentation

Confocal microscopy was employed to determine if enhanced cytoplasmic delivery of FITC-ova30 could be achieved by co-incubation with CP1 (CP1/FITC-ova30) or CP2 (CP2/FITC-ova30) (Figure 5-5). As previously described, FITC-ova30 fluorescence was co-localised with the endo-lysosomal stain, suggesting entrapment of payload in the endosomes. Gong *et al.* (2020) also showed that even after 24 hours of treatment, FITC-ova30 alone (5 µg/mL) was restricted to the endosomal compartments, and little fluorescence was observed in the cytoplasm. Co-incubation with CP1 or CP2 induced enhancement of the FITC-ova30 fluorescence signal. Stronger green fluorescence was observed in DCs treated with CP1/FITC-

ova30. However, the fluorescence does not completely appear to be diffused throughout the cytoplasm. On the other hand, there is stronger evidence of cytoplasmic delivery in DCs treated with CP2/FITC-ova30. As cytoplasmic delivery is required for MHC I upregulation (Szeto et al., 2015), this data suggests that both CP1 and CP2, particularly the latter, may be suitable polymers for the cytoplasmic delivery of ova30 and subsequent MHC I upregulation.

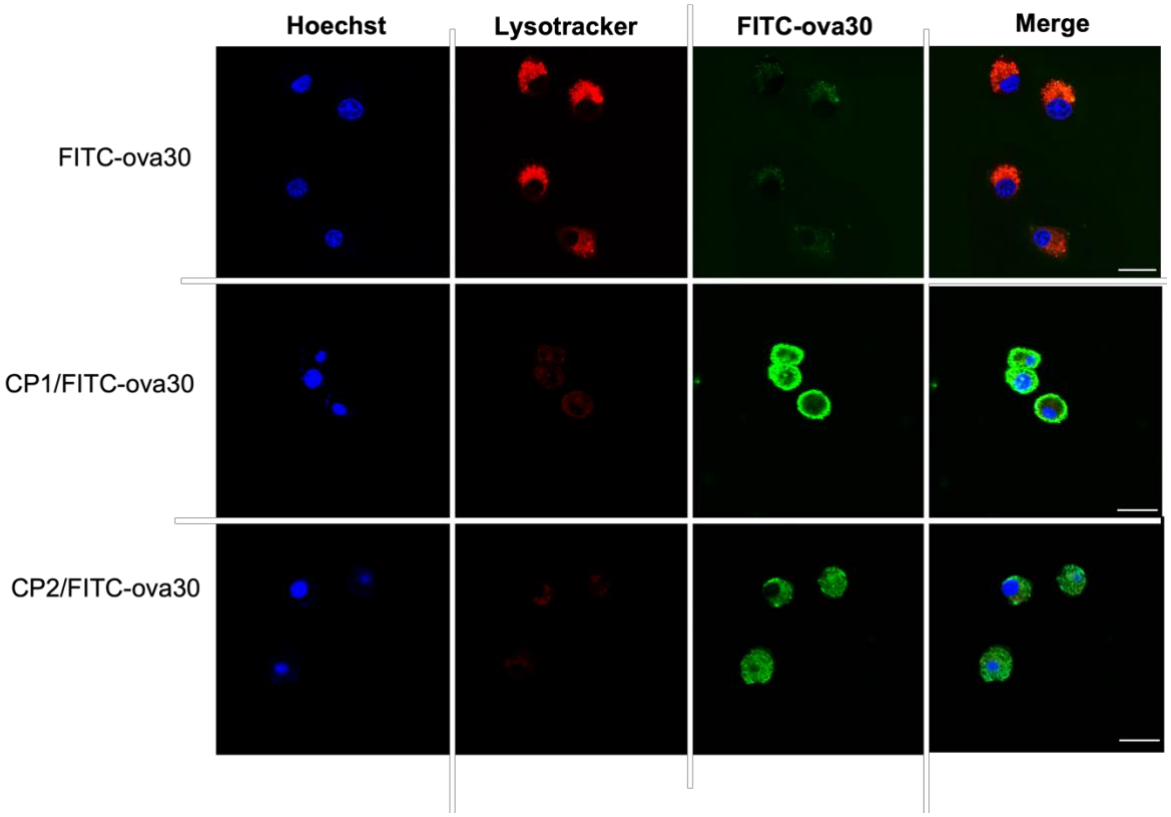

Figure 5-5. CP1 and CP2 mediated delivery of ova30 in JASWII cells. DCs were co-incubated with FITC-ova30 (12 µg/mL) and CP1 (1 mg/mL) or CP2 (1 mg/mL) for 1 hour at pHe 6.5 and the distribution of FITC-ova30 observed under confocal microscopy. Scale bar 20 µm.

MHC I upregulation was measured by staining DCs with SIINFEKL H-2Kb antibody (Figure 5-6). The results were compared to stimulation with LPS (2 µg/mL) and IFN-γ (10 ng/mL). As shown in Figure 5-6A, treatment with CP1/ova30 did not increase the upregulation of SIINFEKL H-2Kb more than ova30 alone. After 24 hours, levels of SIINFEKL H-2Kb was comparable in DCs treated with CP1/ova 30, ova30 alone and CP1 alone. After 48 hours, the levels of SIINFEKL H-2Kb decreased in DCs treated with ova30 whilst the MHC I levels of DCs stimulated with LPS greatly increased.

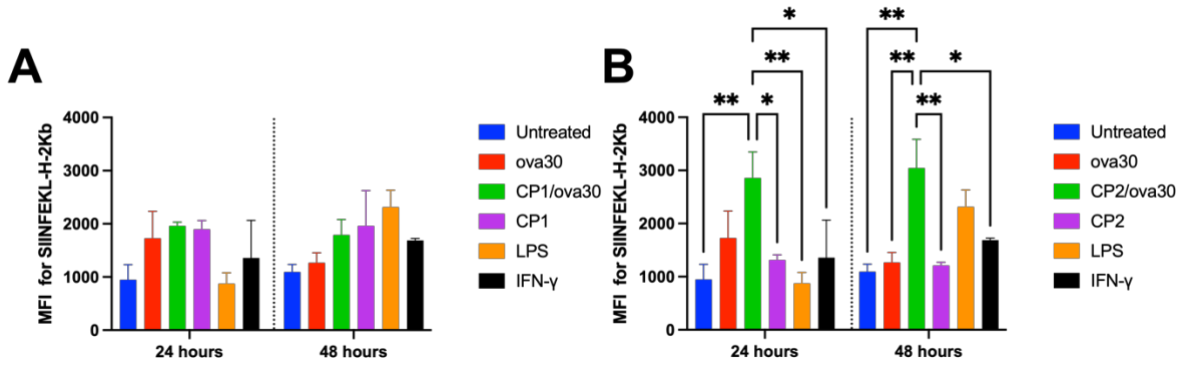

Figure 5-6. Surface presentation of MHC-I-ova30 (SIINFEKL-H2Kb) on JAWSII cells. DCs were treated with A) CP1 (1 mg/mL) or B) CP2 (1mg/mL) co-incubated with ova30 (100 µM) at pHe 6.5 for 1 hour treatment. MHC I levels were assessed after 24 or 48 hours of further incubation compared to untreated DCs or DCs incubated with ova30 or polymers only under the same conditions. Positive controls LPS (2 µg/mL) or IFN-γ (10 ng/mL) were incubated with DCs for 24 or 48 hours before staining. Mean ± SD, n=3 from three independent experiments. * $P \leq 0.05$ ** $P \leq 0.01$.

Figure 5-6B reveals the increased surface levels of SIINFEKL-H2Kb in DCs treated with CP2/ova30 24 hours and 48 hours after treatment. At 24 hours, this expression was significantly higher than untreated DCs ($P \leq 0.01$), CP2 alone ($P \leq 0.05$), LPS ($P \leq 0.01$) and IFN-γ ($P \leq 0.05$). After 48 hours, SIINFEKL-H2Kb regulation induced by CP2/ova30 was also significantly higher than DCs treated with ova30 alone ($P \leq 0.01$). This data further supports the observation in Figure 5-5 showing cytoplasmic delivery of FITC-ova when co-incubated with CP2.

Zapala *et al*. (2011) reported that resting (unstimulated or untreated) JAWSII cells are characterised by high levels of MHC I. However, IFN-γ can exert significant stimulatory effects on the expression of MHC I. Here, IFN-γ was found to increase the surface presentation of SIINFEKL-H2Kb after 24 and 48 hours of stimulation, but not significantly greater than untreated DCs. IFN-γ induced higher surface levels of SIINFEKL-H2Kb than LPS after 24 hours, but at 48 hours, LPS stimulated DCs displayed higher MHC I levels.

5.2.4 MHC II presentation

Although cytoplasmic delivery and MHC I upregulation is more desirable for presentation to CD8+ T cells, APCs loaded with antigen in endo-lysosomes are directed to MHC II for presentation to CD4+ T cells (Szeto et al., 2015). Therefore, the upregulation of the MHC II antigen presentation pathways by DCs after treatment was also investigated. To test this, DCs were stained with anti-mouse I-Ab antibody 24 and 48 hours post-treatment to measure MHC II surface levels. Based on the previous results (Figure 5-5), showing co-localisation of FITC-ova30 with endo-lysosomes, it was hypothesised that DCs treated with ova30 alone would upregulate the MHC II pathway. Although not expected, the upregulation of MHC II by CP1/ova30, CP1, CP2/ova30 or CP2 would potentially suggest the internalisation of either polymer or ova30 into the endosomes after treatment.

Figure 5-7 shows that after 24 hours, treatment of JAWSII cells with ova30 alone did not cause a distinct upregulation in MHC II. However, after 48 hours post-delivery, there was a marked upregulation. CP1 and CP1/ova caused a noticeable increase in MHC II surface presentation 24 and 48 hours after delivery (Figure 5-7A). As previously mentioned, this could suggest that the endocytic pathway is utilised by CP1 for internalisation. As CP1 alone caused an upregulation in MHC II, it may be that the DCs recognised the polymer as a foreign antigen. Similar results were observed for CP2 and CP2/ova (Figure 5-7B), although less pronounced than CP1 and CP1/ova. Whilst CP1 alone caused a higher MHC II upregulation than CP1/ova, treatment with CP2/ova caused a slightly higher MHC II upregulation than CP2 alone. Interestingly, CP2 alone did not cause a significant increase in MHC I 24 and 48 hours post-treatment (Figure 5-6B), but an increase in MHC II presentation was observed (Figure 5-7B). This implies that potentially more than one intracellular delivery mechanism is utilised by CP2 for entry, as both cytoplasmic delivery (indicated by an increase in MHC I) and endo-lysosomal delivery (indicated by an increase in MHC II) was achieved. The stimulants LPS and IFN-γ also caused an apparent increase in MHC II upregulation (Figure 5-7C).

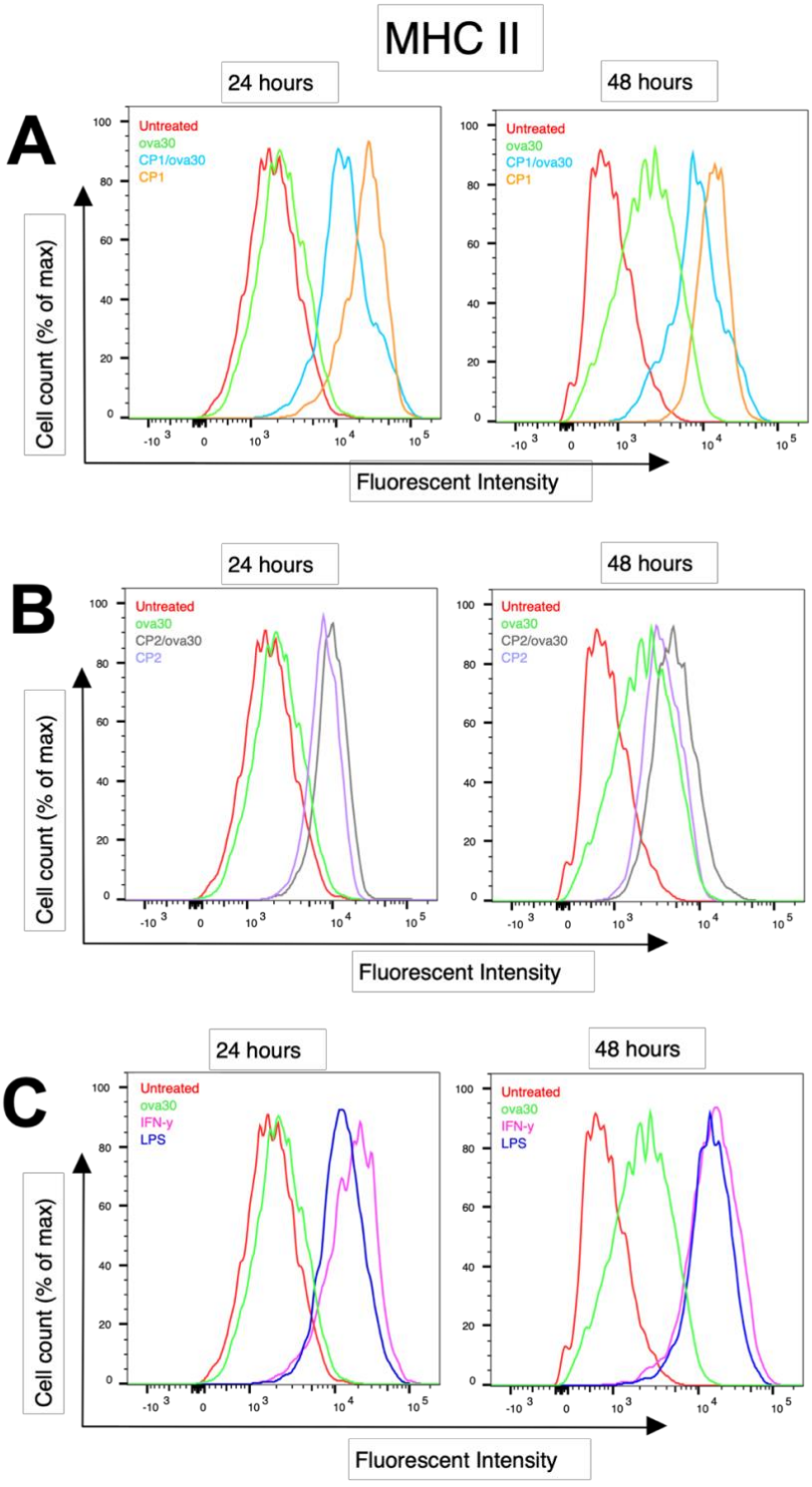

Figure 5-7. Surface presentation of MHC II by JAWSII cells after incubation with various formulations. DCs were treated for 1 hour at pHe 6.5 with ova30 alone and A) CP1/ova30 and CP1 or B) CP2/ova30 and CP2. Ova30 concentration was 100 µM. CP1 and CP2 concentrations were 1 mg/mL. MHC II levels were assessed after 24 or 48 hours of further incubation and compared to untreated DCs. C) Positive controls LPS (2 µg/mL) or IFN-γ (10 ng/mL) were incubated with DCs for 24 or 48 hours before staining.

5.2.5 Upregulation of co-stimulatory molecules

In addition to MHC upregulation (signal 1), to be effective DCs, the expression of co-stimulatory molecules (signal 2) is also essential for optimal T cell stimulation. To further understand the potential of DCs to activate T cells, the expression of the co-stimulatory markers CD40 and CD80 were measured after DCs treatment. Resting JAWSII cells (without activation) have been reported to have low expression of CD40 and high expression of CD80 (Zapala et al., 2011). Figure 5-8 shows the increased expression of CD40 in DCs treated with all formulations indicating DC maturation and activation. However, only LPS showed an increased expression of CD80 after treatment which suggests that LPS is superior at inducing DC maturation and T cell stimulation.

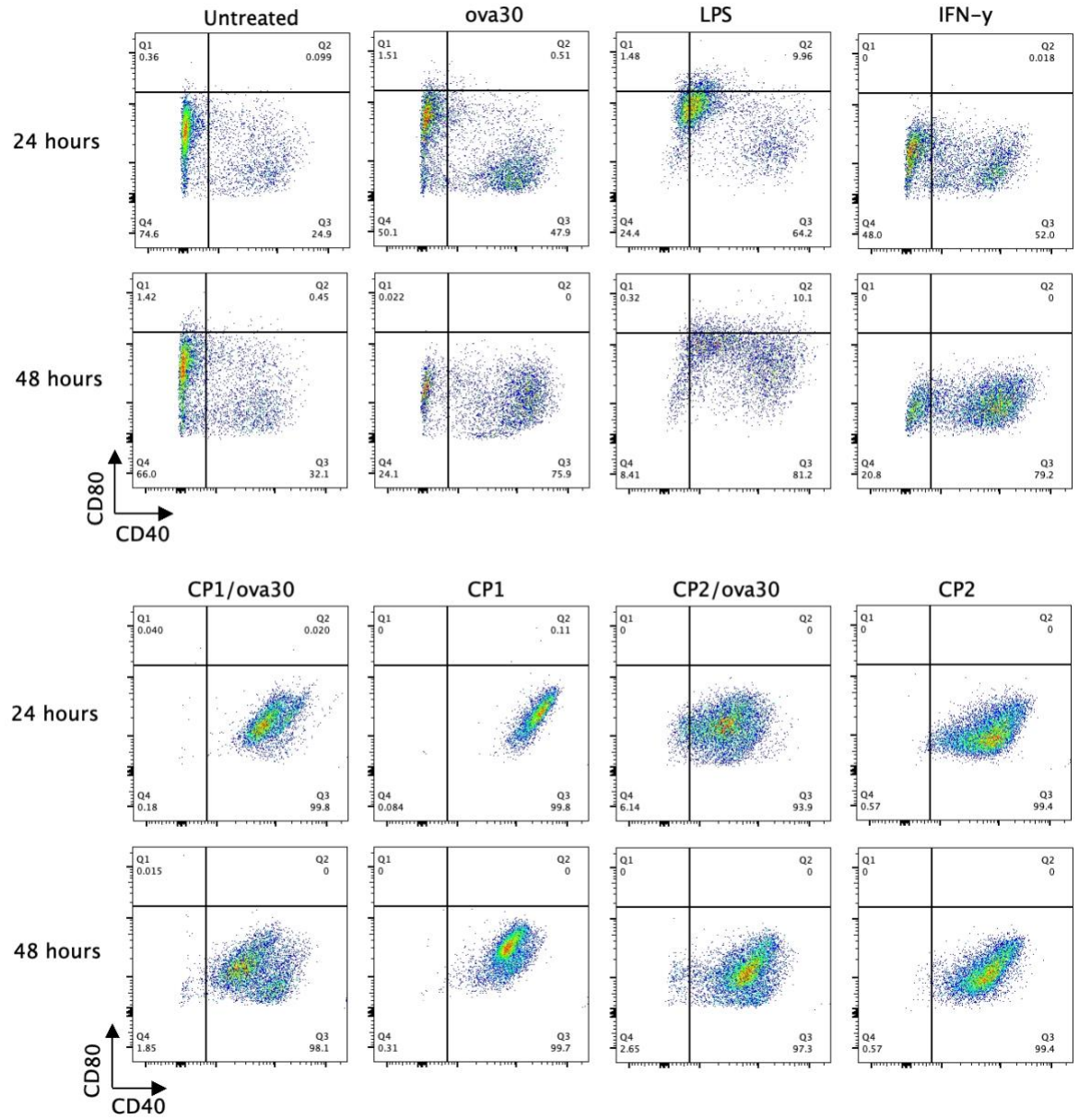

Figure 5-8. Expression of maturation markers CD40 vs CD80 by JAWSII cells after incubation with various formulations. DCs were treated with ova30 alone (100 µM), CP1 (1 mg/mL), CP2 (1 mg/mL), CP1/ova30 or CP2/ova30 for 1 hour at pHe 6.5. Surface levels of CD80 and CD40 were measured 24 or 48 hours of further incubation after treatment and compared to untreated DCs. LPS (2 µg/mL) and IFN-γ (10 ng/mL) were incubated with DCs for 24 or 48 hours before staining.

5.2.6 Cytokine secretion

An additional measure of DC activation and maturation is the secretion of pro-inflammatory cytokines (signal 3). Zapala *et al*. (2011) measured a dramatic increase in the production of IL-

6 and TNF-α in the culture media of JAWSII cells exposed to LPS but not IFN-γ. Here, ELISA measurements of IL-6 and TNF-α in the culture media 24 and 48 hours post-treatment also confirmed that LPS could dramatically increase the secretion of cytokines (Figure 5-9). Contrary to Zapala *et al.* (2011), it was found that IFN-γ stimulation also induced secretion of IL-6 and TNF-α, but the effects were not as pronounced as stimulation with LPS. Modest IL-6 and TNF-α secretion levels were observed in DCs treated with ova30 only.

No IL-6 and TNF-α were produced after treatment with CP1 or CP2, suggesting that the polymers are not highly immunogenic. Unexpectedly, CP1/ova30 and CP2/ova30 did not increase the secretion of cytokines. Most surprisingly, for the treatment of CP2/ova30, which previously showed higher MHC I upregulation than ova30 and the controls LPS and IFN-γ.

For the transformation of immature DCs (such as JAWSII cells) into mature DCs for functional T cell activation, several distinct signals are required: (I) the loading of antigen peptide onto MHC, (II) expression of co-stimulatory molecules and (III) secretion of cytokines (Hubo et al., 2013). The inability to activate one or more of these signals may hinder the DC's ability to produce an efficient T cell response.

Table 5-1 summarises the ability of each CP to upregulate these signals compared to the controls. As the main interest of DC manipulation is to activate CD8+ T cells, only MHC I activation is summarised. A tick mark was used if the CP polymers were able to upregulate MHC I, CD40, CD80, IL-6 or TNF-α levels compared to untreated DCs 24 or 48 hours post-treatment (significant or not) as it is unknown what levels of each signal are required for T cell stimulation. The summary results in this table highlight a potential limitation in using the novel cationic polymers for the *ex vivo* manipulation of DCs. Whilst treatment with CP1/ova30 and CP2/ova30 increased the upregulation of MHC I and expression of CD40 (compared to untreated DCs), the expression of CD80 and production of cytokines IL-6 and TNF-α were not elevated after treatment. The reason for this is not well understood and further experiments will be required in the future to explore this.

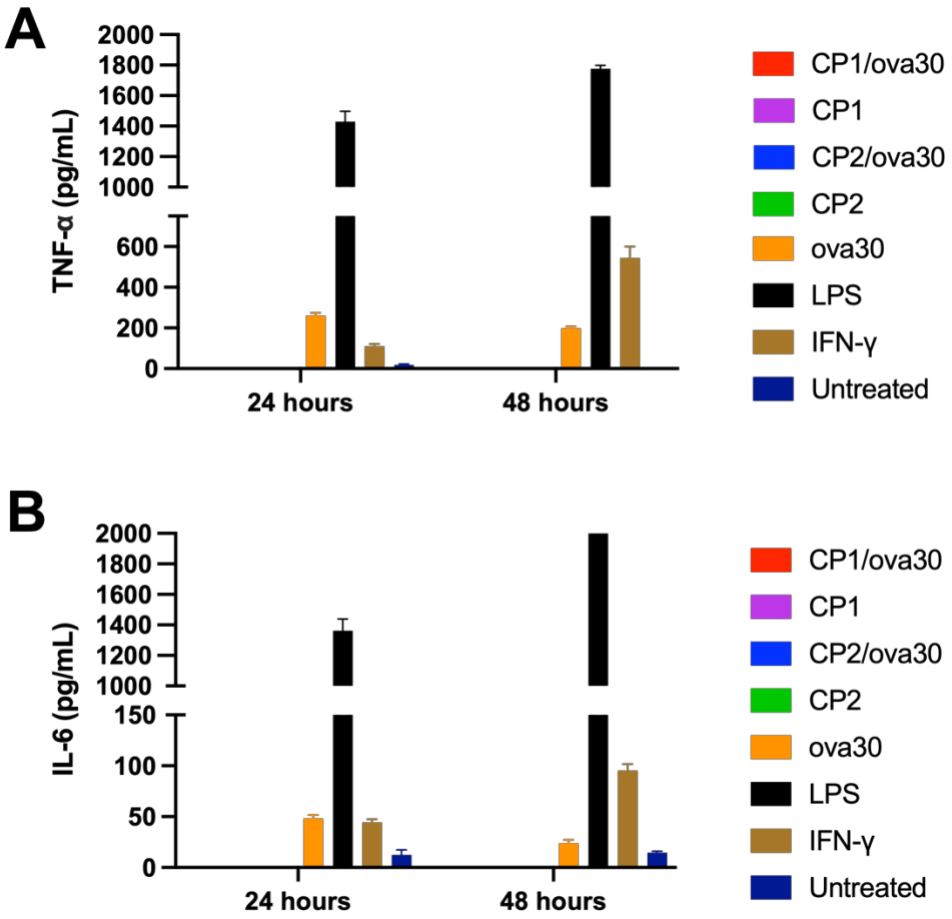

Figure 5-9. Secretion of A) TNF-α and B) IL-6 by JAWSII cells after incubation with various formulations. DCs were treated with ova30 alone (100 µM), CP1 (1 mg/mL), CP2 (1 mg/mL), CP1/ova30 or CP2/ova30 for 1 hour at pHe 6.5. Cytokine levels were determined by ELISA 24 and 48 post-treatment and compared to untreated DCs. LPS (2 µg/mL) and IFN-γ (10 ng/mL) were incubated with DCs for 24 or 48 hours before analysis. Mean ± SD, n=3.

Table 5-1. Summary of the signals required for T cell activation.

	Signal 1: MHC	Signal 2: Co-stimulatory molecules		Signal 3: Cytokine production	
	MHC I	CD40	CD80	TNF-α	IL-6
ova30	✓	✓	x	✓	✓
CP1/ova30	✓	✓	x	x	x
CP2/ova30	✓	✓	x	x	x
LPS	✓	✓	✓	✓	✓
IFN-γ	✓	✓	x	✓	✓

5.2.7 IL-2 secretion from RF33.70 cells

Considering all of the data, preliminary experiments were conducted to determine whether the upregulation of MHC I, co-stimulatory molecules and cytokines by DCs were sufficient to stimulate T cells. The T-cell hybridomas RF33.70 recognises the ova-derived SIINFEKL peptide in the context of H-2^b. Production of IL-2 from CD8+ T cells is a key hallmark indicating efficient antigen presentation and recognition (Abbas et al., 2018). Thus, the measurement of IL-2 production from RF33.70 cells after co-culturing with DCs was used as an indicator of successful MHC I upregulation and T cell stimulation. RF33.70 were generously provided as a gift by Professor K. L. Rock (University of Massachusetts Medical Centre).

After 24 hours post-treatment, DCs were co-cultured with RF33.70 cells at a ratio of 1:10 for 24 hours and the levels of IL-2 in the culture supernatant were determined by ELISA. The most promising CP formulation (CP2/ova30) was used in the following experiment as previous data revealed a higher MHC I upregulation when treated with CP2/ova30 than with CP1/ova30. Treatment with CP2/ova30 was compared with CP2 alone and ova30 alone and the controls LPS and IFN-γ. As an additional control, RF33.70 cells were cultured with αCD3/CD28 beads, which activate and expand mouse T -cells (ThermoFisher, 2022). Untreated DCs cultured with RF33.70 cells and RF33.70 cells cultured alone with no stimulus acted as negative controls.

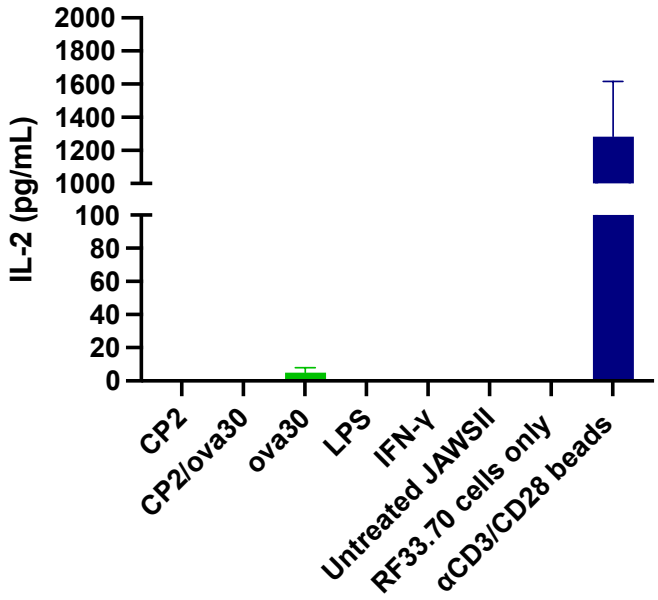

Figure 5-10. Secretion of IL-2 by RF33.70 after co-culturing with JAWSII cells. DCs were treated with ova30 alone (100 µM), CP2 (1 mg/mL) or CP2/ova30 for 1 hour at pHe 6.5. 24 hours post-treatment, DCs were harvested and co-cultured with RF33.70 (1:10) for 24 hours. IL-2 cytokine levels in the culture supernatant were determined by ELISA compared to untreated JAWSII cells co-cultured with RF33.70 cells. LPS (2 µg/mL) and IFN-γ (10 ng/mL) were incubated with DCs for 24 hours before co-culturing with RF33.70 cells. RF33.70 cells only were cultured without any stimulus. αCD3/CD28 beads were cultured with RF33.70 cells at 1 bead/RF33.70 cell. Mean ± SD, n=3.

As shown in Figure 5-10, RF33.70 incubation with αCD3/CD28 beads resulted in a substantial increase in IL-2 production (1284.5 ± 333.1 pg/mL). DC treatment with ova30 and subsequent co-culturing with RF33.70 cells caused a slight increase in IL-2 production (5.0 ± 2.9 pg/mL). However, there was no detectable increase in IL-2 secretion when RF33.70 cells were co-cultured with DCs treated with LPS, IFN-γ or CP2/ova30. This was most surprising for DCs stimulated with LPS, as previous experiments had shown an increase in MHC I, CD40, CD80, TNF-α and IL-6 after stimulation (Table 5-1). The reason for this is unknown and requires further investigation. For CP2/ova30 treated DCs, the absence of IL-2 production by RF33.70 cells may be due to the lack of co-stimulatory molecules CD80 and production of cytokines TNF-α and IL-6 by DCs, thereby generating an inefficient RF33.70 response. This highlights a major challenge to overcome for the use of the cationic pH-responsive polymers for cell

engineering applications. Further studies and optimisation will be required to address these limitations.

Whilst the upregulation of MHC, co-stimulatory molecules and secretion of cytokines has been reported in JAWSII cells stimulated with LPS and IFN-γ (Zapala et al., 2011), to the best of our knowledge, no data exists explicitly regarding the stimulation of JAWSII by LPS and IFN-γ for the stimulation of RF33.70 cells. At 24 hours post-treatment of DCs, when DCs were co-cultured with RF33.70 cells, the MHC I levels by DCs, were higher in DCs treated with ova30 than LPS or IFN-γ (Figure 5-6). It could be speculated that the MHC I upregulation in DCs stimulated with LPS or IFN-γ was not sufficient for T cell stimulation. This could also be true for DCs treated with ova30 only as RF33.70 cells only showed a slight upregulation in IL-2 production after co-culturing.

5.3 Conclusions

In this work, two anionic polymers, PP50 and PLP-NDA18, were initially tested for their ability to engineer DCs by facilitating the cytoplasmic delivery of the negatively charged model antigen ova30 and upregulate MHC I presentation. Neither PP50 nor PLP-NDA18, by co-incubation with ova30, were able to successfully enhance delivery or upregulate antigen presentation. These results encouraged the exploration of two novel cationic polymers, CP1 and CP2, to investigate whether they would show enhanced delivery and expression of ova30.

CP1 showed superior haemolytic activity than CP2 at pHe 6.5. However, DCs displayed higher MHC I surface levels when CP2 was co-incubated with ova30 (CP2/ova30) compared to CP1 co-incubated with ova30 (CP1/ova30), ova30 alone or stimulation with LPS and IFN-γ. More studies are needed to elucidate the mechanism of CP1 or CP2 entry and understand any potential interactions of polymers with ova30.

All treatments were found to enhance the expression of the co-stimulatory molecule CD40, but only DC stimulation with LPS showed a slight increase in CD80 expression. The inability of CP1/ova30 or CP2/ova to increase the production of cytokines TNF-α and IL-6 highlights a key concern, as the upregulation of MHC, co-stimulatory molecules and expression of cytokines are all required for optimal T cell stimulation.

Finally, co-culturing of DCs with RF33.70 T cells revealed that only treatment of DCs with ova30 alone was able to produce any measurable IL-2 release from RF33.70 cells. This suggests that the MHC I upregulation, co-stimulation or cytokine production was insufficient in DCs treated with CP1/ova, LPS or IFN-γ for T cell stimulation.

Overall, this chapter provides novel and preliminary findings on which to base further investigations on using cationic polymers for cell engineering applications. Whilst these studies provide evidence of the potential of cationic polymers for the *ex vivo* manipulation of DCs, additional studies (including optimisation of treatment time, polymer concentration, and polymer structure) are required to address the limitations found to obtain the best results for the stimulation of T cells.

Chapter 6

Conclusions and Future Work

6.1 Conclusions

This thesis aimed to explore the use of pH-responsive polymers for the intracellular delivery of macromolecules. In addition, to determine the suitability of pH-responsive polymers for therapeutic applications such as cell engineering.

Previously published work on PP50, demonstrating successful delivery of different sized fluorescent payloads, the apoptotic peptide Bim (Kopytynski et al., 2020), and the cryopreservent trehalose (Chen et al., 2020; Lynch et al., 2011, 2010) lay the groundwork for the thesis. The goal of this work was to greatly extend the knowledge surrounding PP50 as an intracellular delivery system and demonstrate the capabilities of PP50 to deliver macromolecules for a range of applications.

Further, based on previous studies revealing successful PLP-NDA18 mediated delivery of trehalose and different sized fluorescent payloads (Chen et al., 2020, 2017) the ability of PLP-NDA18 to deliver macromolecules was briefly investigated.

For cell engineering applications, PP50 and PLP-NDA18, were tested for their ability to manipulate DCs *ex vivo*. However, the results of these studies prompted the exploration of two cationic polymers (newly synthesised in the Chen group) to assess their capabilities as intracellular delivery agents for cell engineering applications.

A research summary and the major achievements of this project are summarised below.

1. PP50 is an efficient pH-responsive *in vitro* intracellular delivery platform

The pH-dependent membrane lytic abilities of PP50 was confirmed using FITC-dextran (150 kDa) as a model payload. Enhanced delivery of FITC-dextran was shown at the mildly acidic

pHe 6.5 compared to neutral pHe using a simple delivery method of co-incubation of payload and PP50.

Here, the mechanisms underlying PP50 mediated delivery of FITC-dextran was investigated for the first time using endocytosis inhibitors and fluorescently labelled PP50. Whilst a decrease in Cy5-PP50 was found in cells pre-treated with cytochalasin D (a macropinocytosis and actin polymerisation inhibitor) and chlorpromazine (a CME inhibitor), this was not correlated with a decrease in FITC-dextran. Altogether this suggests that lower concentrations of PP50 can still aid high levels of payloads into cells.

2. PP50 can deliver a range of macromolecules to different intracellular sites

The ability of PP50 to deliver anti-NPC and anti-β-tubulin antibodies to specific intracellular sites demonstrates the capabilities of PP50 to deliver large macromolecules intracellularly and to their specific desired target site. Further, fluorescently labelled PP50 was shown to co-localise with the mitochondria, suggesting an additional application of Cy5-PP50 as a mitochondria targeting agent.

Slightly anionic peptides FITC-p53 and FITC-ova (323-339) were successfully delivered by co-incubation of PP50 and peptide. However, optimal delivery of cationic peptides Histone-FAM and KLAK were discovered using a sequential delivery method rather than co-incubation of PP50 and payload at the same time. The work presented herein is the first to report the sequential delivery of PP50 and cationic peptides to increase delivery efficiency.

3. PP50 enhances the cytotoxicity of saporin through multiple death pathways

Novel *in vitro* applications of PP50 was explored by examining the delivery of the functional cell membrane-impermeable protein saporin to A549 cells. By co-incubation, PP50 successfully enhanced the cytotoxicity of saporin, as measured by a decrease in cell viability compared to delivery to saporin alone. The PP50 delivery platform itself, however, was shown to be non-toxic. PP50 mediated saporin uptake was found to be primarily reliant on macropinocytosis and actin polymerisation for internalisation but also secondarily dependent on lipid raft mediated endocytosis for entry. Successful saporin entry was accompanied by a

decrease in protein synthesis and activation of caspases 8, 9 and 3/7 before the onset of apoptosis and cell death.

Furthermore, this is the first report of PP50 mediated delivery of functional proteins to 3D spheroids, which mimics solid tumours *in vitro*. Co-incubation of PP50 with saporin significantly reduced the cell viability of A549 multicellular spheroids over 3 days. PP50 mediated delivery of saporin was also shown to be more potent than the delivery with the parent polymer, PLP. This highlights the potential expansion of PP50 to *in vivo* cancer therapy applications.

4. PLP-NDA18 can greatly enhance the cytotoxicity of saporin

Likewise, the co-incubation of PLP-NDA18 greatly enhanced the cytotoxicity of saporin *in vitro*. PLP-NDA18 mediated saporin delivery was fast, showing the internalisation of saporin within 10 minutes. In addition, the ability of PLP-NDA18 to enhance the cytotoxicity of saporin and reduce the cell viability at very low concentrations (0.003125 mg/mL) suggests that PLP-NDA18's membrane destabilising ability is effective at low concentrations. The work presented here is the first reported study on the functional delivery of proteins by co-incubation of PLP-NDA18 and saporin for therapeutic applications.

5. Cationic pH-responsive polymers are promising candidates for cell engineering applications

This project is the first to investigate the use of PP50 and PLP-NDA18 for ex vivo cell engineering applications using the model antigen ova30. The unsuccessful delivery of ova30 by PP50 and PLP-NDA18 to upregulate MHC I on JAWSII DCs was theorised to be due to repulsion between the anionic polymers, cell membrane and negatively charged antigen.

The exploration of cationic polymers CP1 and CP2 is the first reported use of these polymers as intracellular delivery agents. CP2 was deemed the most promising cationic polymer, demonstrating enhanced cytoplasmic delivery of ova30 and a significant increase in surface presentation of MHC I. In addition, delivery was correlated with an increase in co-stimulatory molecule CD40, showing CP2 to a promising intracellular platform for the *ex vivo* modification of DCs. CP2 mediated ova30 delivery was not correlated with an increase in CD80 or the

production of cytokines IL-6 and TNF-α or IL-2 when co-cultured with RF33.70 T cells. Together, this result suggests that cationic polymers are promising candidates for cell engineering applications, but further optimisation and work need to be conducted to reach their full potential as intracellular delivery agents.

6.1 Future work

The following future work is recommended to expand the work on the pH-responsive biomimetic polymers used within this thesis and fully explore their potential for therapeutic applications.

6.1.1 Saporin delivery mediated by virus-mimicking liposomes for *in vivo* applications

Efficient *in vivo* intracellular delivery has enormous potential, especially in cancer therapy. In this thesis, PP50 and PLP-NDA18 were shown to enhance the cytotoxicity of saporin, an immunotoxin that has been widely studied for its use in cancer therapy (Polito et al., 2013). Furthermore, PP50 was shown to deliver saporin to 3D spheroids, an *in vitro* model for solid tumours. The simple mixing, i.e. co-incubation of polymer and therapeutic cargo, is predominantly suitable for *in vitro* and *ex vivo* applications, which was the main focus of this thesis. However, for *in vivo* settings, this is not advantageous due to the potential separation of polymer and payload in the bloodstream leading to off-site targeting.

Previous work in the Chen group showed that liposomes decorated with PP75 enabled efficient membrane destabilisation for the encapsulation of calcein and doxorubicin for drug delivery (Chen and Chen, 2016). Here, to extend the work on saporin for *in vivo* applications, liposomes decorated with either PP75, PP50 or PLP-NDA18 could be tested for their ability to encapsulate saporin and aid efficient intracellular delivery and release of saporin to enhance its cytotoxic effect. Furthermore, this work can be extended to the testing of other endosomolytic polymers established in the Chen group.

6.1.2 Investigation of the mechanism of polymer-mediated intracellular delivery

Polymer-mediated intracellular delivery can be due to (I) direct membrane penetration, (II) endocytosis and endosomal escape, or (III) a combination of both. In this study, the PP50-

mediated intracellular delivery mechanism was investigated using FITC-dextran and saporin. However, the mechanism of intracellular delivery by the polymers PLP-NDA18, CP1 and CP2 are not well understood and is worth exploring in the future. Similar to the work conducted in this thesis, a range of endocytosis inhibitors, including cytochalasin D, MβCD, nystatin, chlorpromazine and amiloride, could be used to block specific endocytosis pathways and determine if one or more of these pathways are utilised for polymer-mediated payload delivery. In addition, the LDH assay could be employed to measure plasma membrane damage (Kumar et al., 2018).

6.1.3 Intracellular delivery of ova30

6.1.3.1 Conjugation of anionic polymers with ova30

Delivery of ova30 using anionic polymers should be further investigated. In the current study, the cytoplasmic delivery of ova30 by PP50 and PLP-NDA18 and upregulation of MHC I was not successful. This could have been to repulsion between the negatively charged cell membrane, negatively charged peptide and negatively charged polymer. Khormaee *et al.* (2013) showed that PP75-siRNA conjugates delivered *in vitro* and *in vivo* effectively knocked down the expression of targeted proteins. Using the same principle of conjugating payload to polymer, a commercially made ova30 amide, where the C terminus of ova30 is amidated, could be conjugated to PP50 or PLP-NDA18. The upregulation of MHC I would be tested to see if the delivery efficiency is improved by conjugation as opposed to co-incubation.

6.1.3.2 Cationic-mediated ova30 delivery

It will be of great importance to further investigate the antigen presentation, upregulation of co-stimulatory molecules and secretion of cytokines by DCs treated with cationic polymers and ova30. In particular, the co-incubation of CP1 or CP2 with ova30 did not produce any measurable IL-6 and TNF-α by DCs or IL-2 when co-cultured with RF33.70 T cells.

Optimisation of delivery parameters, e.g., treatment time and polymer concentration, could be investigated. Understanding how the positively charged cationic polymers interact with the negatively charged ova30 may help refine and optimise the delivery process. Transmission Electron Microscopy and Dynamic Light Scattering could be employed to visualise whether

the cationic polymers form micelles in solution and if the size of the micelles increases when co-incubated with ova30. This could either suggest that the ova30 is encapsulated into the core of the CP micelles or that they are decorated on the surface of the micelles. By fluorescently labelling the polymer, confocal microscopy can be used to see any co-localisation between the polymer and FITC-ova30 inside the cell.

6.2 Closing remarks

The research presented in this PhD thesis expands the current knowledge surrounding pH-responsive polymers as intracellular delivery platforms. The work on PLP-NDA18 and PP50 demonstrates their use as intracellular delivery systems for macromolecules and opens new avenues for their use *in vivo* for cancer therapies. The reported work on cationic polymers (CP1 and CP2) provides a solid foundation for further work exploring their full potential as intracellular delivery agents for *ex vivo* applications.

Bibliography

Abbas, A.K., Trotta, E., R. Simeonov, D., Marson, A., Bluestone, J.A., 2018. Revisiting IL-2: Biology and therapeutic prospects. Sci. Immunol. 3, eaat1482. https://doi.org/10.1126/sciimmunol.aat1482

Abdellatif, A.A., Younis, M.A., Alsharidah, M., Al Rugaie, O., Tawfeek, H.M., 2022. Biomedical Applications of Quantum Dots: Overview, Challenges, and Clinical Potential. Int. J. Nanomedicine Volume 17, 1951–1970. https://doi.org/10.2147/IJN.S357980

Abdellatif, A.A.H., 2019. Fluorescent Nanoparticles Conjugated Long-acting Somatostatin Analog for Potent Suppression and Bioimaging Breast Cancer (Clinical trial registration No. NCT04138342). clinicaltrials.gov.

Abdellatif, A.A.H., Ibrahim, M.A., Amin, M.A., Maswadeh, H., Alwehaibi, M.N., Al-Harbi, S.N., Alharbi, Z.A., Mohammed, H.A., Mehany, A.B.M., Saleem, I., 2020. Cetuximab Conjugated with Octreotide and Entrapped Calcium Alginate-beads for Targeting Somatostatin Receptors. Sci. Rep. 10, 4736. https://doi.org/10.1038/s41598-020-61605-y

Albarran, B., Hoffman, A.S., Stayton, P.S., 2011. Efficient Intracellular Delivery of a Pro-Apoptotic Peptide With A pH-Responsive Carrier. React. Funct. Polym. 71, 261–265. https://doi.org/10.1016/j.reactfunctpolym.2010.09.008

Anassi, E., Ndefo, U.A., 2011. Sipuleucel-T (Provenge) Injection. Pharm. Ther. 36, 197–202.

Andrian, T., Riera, R., Pujals, S., Albertazzi, L., 2021. Nanoscopy for endosomal escape quantification. Nanoscale Adv. 3, 10–23. https://doi.org/10.1039/D0NA00454E

Auriac, A., Willemetz, A., Canonne-Hergaux, F., 2010. Lipid raft-dependent endocytosis: a new route for hepcidin-mediated regulation of ferroportin in macrophages | Haematologica. Haematologica 95.

Azevedo, C., Macedo, M.H., Sarmento, B., 2018. Strategies for the enhanced intracellular delivery of nanomaterials. Drug Discov. Today 23, 944–959. https://doi.org/10.1016/j.drudis.2017.08.011

Bagga, S., Hosur, M.V., Batra, J.K., 2003a. Cytotoxicity of ribosome-inactivating protein saporin is not mediated through α2-macroglobulin receptor. FEBS Lett. 541, 16–20. https://doi.org/10.1016/S0014-5793(03)00280-1

Bagga, S., Seth, D., Batra, J.K., 2003b. The Cytotoxic Activity of Ribosome-inactivating Protein Saporin-6 Is Attributed to Its rRNA N-Glycosidase and Internucleosomal DNA Fragmentation Activities*. J. Biol. Chem. 278, 4813–4820. https://doi.org/10.1074/jbc.M207389200

Ballabio, A., 2016. The awesome lysosome. EMBO Mol. Med. 8, 73–76. https://doi.org/10.15252/emmm.201505966

Bazban-Shotorbani, S., Hasani-Sadrabadi, M.M., Karkhaneh, A., Serpooshan, V., Jacob, K.I., Moshaverinia, A., Mahmoudi, M., 2017. Revisiting structure-property relationship of pH-responsive polymers for drug delivery applications. J. Controlled Release 253, 46–63. https://doi.org/10.1016/j.jconrel.2017.02.021

Beltrán-Gracia, E., López-Camacho, A., Higuera-Ciapara, I., Velázquez-Fernández, J.B., Vallejo-Cardona, A.A., 2019. Nanomedicine review: clinical developments in liposomal applications. Cancer Nanotechnol. 10, 11. https://doi.org/10.1186/s12645-019-0055-y

Benjaminsen, R.V., Mattebjerg, M.A., Henriksen, J.R., Moghimi, S.M., Andresen, T.L., 2013. The Possible "Proton Sponge " Effect of Polyethylenimine (PEI) Does Not Include Change in Lysosomal pH. Mol. Ther. 21, 149–157. https://doi.org/10.1038/mt.2012.185

Bhargava, A., Mishra, D., Banerjee, S., Mishra, P.K., 2012. Dendritic cell engineering for tumor immunotherapy: from biology to clinical translation. Immunotherapy 4, 703–718. https://doi.org/10.2217/imt.12.40

Bishop, C.J., Kozielski, K.L., Green, J.J., 2015. Exploring the role of polymer structure on intracellular nucleic acid delivery via polymeric nanoparticles. J. Control. Release Off. J. Control. Release Soc. 219, 488–499. https://doi.org/10.1016/j.jconrel.2015.09.046

Biswas, S., Torchilin, V.P., 2014. Nanopreparations for organelle-specific delivery in cancer. Adv. Drug Deliv. Rev., Cancer nanotechnology 66, 26–41. https://doi.org/10.1016/j.addr.2013.11.004

Björklund, M., 2019. Cell size homeostasis: Metabolic control of growth and cell division. Biochim. Biophys. Acta BBA - Mol. Cell Res. 1866, 409–417. https://doi.org/10.1016/j.bbamcr.2018.10.002

Boatright, K.M., Salvesen, G.S., 2003. Mechanisms of caspase activation. Curr. Opin. Cell Biol. 15, 725–731. https://doi.org/10.1016/j.ceb.2003.10.009

Bolognesi, A., Polito, L., Scicchitano, V., Orrico, C., Pasquinelli, G., Musiani, S., Santi, S., Riccio, M., Bortolotti, M., Battelli, M.G., 2012. Endocytosis and intracellular localisation of type 1 ribosome-inactivating protein saporin-s6. J. Biol. Regul. Homeost. Agents 26, 97–109.

Bolshakov, A.P., Stepanichev, M.Yu., Dobryakova, Y.V., Spivak, Y.S., Markevich, V.A., 2020. Saporin from Saponaria officinalis as a Tool for Experimental Research, Modeling, and Therapy in Neuroscience. Toxins 12, 546. https://doi.org/10.3390/toxins12090546

Bonardi, M.A., French, R.R., Amlot, P., Gromo, G., Modena, D., Glennie, M.J., 1993. Delivery of Saporin to Human B-Cell Lymphoma Using Bispecific Antibody: 8.

Bratek-Skicki, A., 2021. Towards a new class of stimuli-responsive polymer-based materials – Recent advances and challenges. Appl. Surf. Sci. Adv. 4, 100068. https://doi.org/10.1016/j.apsadv.2021.100068

Brighenti, R., Li, Y., Vernerey, F.J., 2020. Smart Polymers for Advanced Applications: A Mechanical Perspective Review. Front. Mater. 7, 196. https://doi.org/10.3389/fmats.2020.00196

Brock, D.J., Kustigian, L., Jiang, M., Graham, K., Wang, T.-Y., Erazo-Oliveras, A., Najjar, K., Zhang, J., Rye, H., Pellois, J.-P., 2018. Efficient cell delivery mediated by lipid-specific endosomal escape of supercharged branched peptides. Traffic 19, 421–435. https://doi.org/10.1111/tra.12566

Brooks, J., Minnick, G., Mukherjee, P., Jaberi, A., Chang, L., Espinosa, H.D., Yang, R., 2020. High Throughput and Highly Controllable Methods for In Vitro Intracellular Delivery. Small 16, 2004917. https://doi.org/10.1002/smll.202004917

Bruun, K., Hille, C., 2019. Study on intracellular delivery of liposome encapsulated quantum dots using advanced fluorescence microscopy. Sci. Rep. 9, 10504. https://doi.org/10.1038/s41598-019-46732-5

Caliendo, F., Dukhinova, M., Siciliano, V., 2019. Engineered Cell-Based Therapeutics: Synthetic Biology Meets Immunology. Front. Bioeng. Biotechnol. 7, 43. https://doi.org/10.3389/fbioe.2019.00043

Cameron, D.C., Tong, I.-T., 1993. Cellular and metabolic engineering: An overview. Appl. Biochem. Biotechnol. 38, 105–140. https://doi.org/10.1007/BF02916416

Canton, I., Battaglia, G., 2012. Endocytosis at the nanoscale. Chem. Soc. Rev. 41, 2718. https://doi.org/10.1039/c2cs15309b

Casey, J.R., Grinstein, S., Orlowski, J., 2010. Sensors and regulators of intracellular pH. Nat. Rev. Mol. Cell Biol. 11, 50–61. https://doi.org/10.1038/nrm2820

Cavallaro, U., Soria, M.R., 1995. Targeting plant toxins to the urokinase and α2-macroglobulin receptors. Semin. Cancer Biol. 6, 269–278. https://doi.org/10.1006/scbi.1995.0035

Cavazzana, M., Bushman, F.D., Miccio, A., André-Schmutz, I., Six, E., 2019. Gene therapy targeting haematopoietic stem cells for inherited diseases: progress and challenges. Nat. Rev. Drug Discov. 18, 447–462. https://doi.org/10.1038/s41573-019-0020-9

Cebrian, I., Cristina Croce, Guerrero, N.A., Blanchard, N., Mayorga, L.S., 2016. Rab22a controls MHC-I intracellular trafficking and antigen cross-presentation by dendritic cells. EMBO Rep. 17, 1753–1765. https://doi.org/10.15252/embr.201642358

Cerea, A., Caprettini, V., Bruno, G., Lovato, L., Melle, G., Tantussi, F., Capozza, R., Moia, F., Dipalo, M., Angelis, F.D., 2018. Selective intracellular delivery and intracellular recordings combined in MEA biosensors. Lab. Chip 18, 3492–3500. https://doi.org/10.1039/C8LC00435H

Chatin, B., Mével, M., Devallière, J., Dallet, L., Haudebourg, T., Peuziat, P., Colombani, T., Berchel, M., Lambert, O., Edelman, A., Pitard, B., 2015. Liposome-based Formulation for Intracellular Delivery of Functional Proteins. Mol. Ther. - Nucleic Acids 4. https://doi.org/10.1038/mtna.2015.17

Cheever, M.A., Higano, C.S., 2011. PROVENGE (Sipuleucel-T) in Prostate Cancer: The First FDA-Approved Therapeutic Cancer Vaccine. Clin. Cancer Res. 17, 3520–3526. https://doi.org/10.1158/1078-0432.CCR-10-3126

Chen, R., Eccleston, M.E., Yue, Z., Slater, N.K.H., 2009a. Synthesis and pH-responsive properties of pseudo-peptides containing hydrophobic amino acid grafts. https://doi.org/10.1039/b902822f

Chen, R., Khormaee, S., Eccleston, M.E., Slater, N.K.H., 2009b. The role of hydrophobic amino acid grafts in the enhancement of membrane- disruptive activity of pH-responsive pseudo-peptides. Biomaterials 30, 1954–1961. https://doi.org/10.1016/j.biomaterials.2008.12.036

Chen, R., Yue, Z., Eccleston, M.E., Slater, N.K.H., 2008. Aqueous solution behaviour and membrane disruptive activity of pH-responsive PEGylated pseudo-peptides and their intracellular distribution. https://doi.org/10.1016/j.biomaterials.2008.07.040

Chen, R., Yue, Z., Eccleston, M.E., Williams, S., Slater, N.K.H., 2005. Modulation of cell membrane disruption by pH-responsive pseudo-peptides through grafting with hydrophilic side chains. https://doi.org/10.1016/j.jconrel.2005.07.011

Chen, S., Chen, R., 2016. A Virus-Mimicking, Endosomolytic Liposomal System for Efficient, pH-Triggered Intracellular Drug Delivery. ACS Appl. Mater. Interfaces 8, 22457–22467. https://doi.org/10.1021/acsami.6b05041

Chen, S., Wang, S., Kopytynski, M., Bachelet, M., Chen, R., 2017. Membrane-Anchoring, Comb-Like Pseudopeptides for Efficient, pH- Mediated Membrane Destabilization and Intracellular Delivery. Appl. Mater. Interfaces 9, 8021–8029. https://doi.org/10.1021/acsami.7b00498

Chen, S., Wu, L., Ren, J., Bemmer, V., Zajicek, R., Chen, R., 2020. Comb-like Pseudopeptides Enable Very Rapid and Efficient Intracellular Trehalose Delivery for Enhanced

Cryopreservation of Erythrocytes. ACS Appl. Mater. Interfaces acsami.0c03260. https://doi.org/10.1021/acsami.0c03260

Chen, Y.H., Keiser, M.S., Davidson, B.L., 2018. Viral Vectors for Gene Transfer. Curr. Protoc. Mouse Biol. 8, e58. https://doi.org/10.1002/cpmo.58

Chou, L.Y.T., Ming, K., Chan, W.C.W., 2011. Strategies for the intracellular delivery of nanoparticles. Chem Soc Rev 40, 233–245. https://doi.org/10.1039/C0CS00003E

ClinicalTrials.gov [WWW Document], 2022. URL https://www.clinicaltrials.gov/ct2/results?cond=&term=liposome&cntry=&state=&city=&dist=

Costa, E.C., Moreira, A.F., de Melo-Diogo, D., Gaspar, V.M., Carvalho, M.P., Correia, I.J., 2016. 3D tumor spheroids: an overview on the tools and techniques used for their analysis. Biotechnol. Adv. 34, 1427–1441. https://doi.org/10.1016/j.biotechadv.2016.11.002

Creemers, J.H.A., Pawlitzky, I., Grosios, K., Gileadi, U., Middleton, M.R., Gerritsen, W.R., Mehra, N., Rivoltini, L., Walters, I., Figdor, C.G., Ottevanger, P.B., de Vries, I.J.M., 2021. Assessing the safety, tolerability and efficacy of PLGA-based immunomodulatory nanoparticles in patients with advanced NY-ESO-1-positive cancers: a first-in-human phase I open-label dose-escalation study protocol. BMJ Open 11, e050725. https://doi.org/10.1136/bmjopen-2021-050725

Crommelin, D.J.A., van Hoogevest, P., Storm, G., 2020. The role of liposomes in clinical nanomedicine development. What now? Now what? J. Controlled Release 318, 256–263. https://doi.org/10.1016/j.jconrel.2019.12.023

Crowley, L.C., Marfell, B.J., Scott, A.P., Waterhouse, N.J., 2016. Quantitation of Apoptosis and Necrosis by Annexin V Binding, Propidium Iodide Uptake, and Flow Cytometry. Cold Spring Harb. Protoc. 2016, pdb.prot087288. https://doi.org/10.1101/pdb.prot087288

Cui, X., Hartanto, Y., Zhang, H., 2017. Advances in multicellular spheroids formation. J. R. Soc. Interface 14, 20160877. https://doi.org/10.1098/rsif.2016.0877

Dai, S., Ravi, P., Chiu Tam, K., 2008. pH-Responsive polymers : synthesis, properties and applications. Soft Matter 4, 435–449. https://doi.org/10.1039/B714741D

Dai, Y., Xu, C., Sun, X., Chen, X., 2017. Nanoparticle design strategies for enhanced anticancer therapy by exploiting the tumour microenvironment. Chem. Soc. Rev. 46, 3830–3852. https://doi.org/10.1039/C6CS00592F

David, R.M., Doherty, A.T., 2017. Viral Vectors: The Road to Reducing Genotoxicity. Toxicol. Sci. Off. J. Soc. Toxicol. 155, 315–325. https://doi.org/10.1093/toxsci/kfw220

De Charette, M., Marabelle, A., Houot, R., 2016. Turning tumour cells into antigen presenting cells: The next step to improve cancer immunotherapy? https://doi.org/10.1016/j.ejca.2016.09.010

de Duve, C., 2005. The lysosome turns fifty. Nat. Cell Biol. 7, 847–849. https://doi.org/10.1038/ncb0905-847

Deirram, N., Zhang, C., Kermaniyan, S.S., Johnston, A.P.R., Such, G.K., 2019. pH-Responsive Polymer Nanoparticles for Drug Delivery. Macromol. Rapid Commun. 40, 1800917. https://doi.org/10.1002/marc.201800917

Dell'Angelica, E.C., Mullins, C., Caplan, S., Bonifacino, J.S., 2000. Lysosome-related organelles. FASEB J. 14, 1265–1278. https://doi.org/10.1096/fasebj.14.10.1265

Diebold, S.S., Cotten, M., Koch, N., Zenke, M., 2001. MHC class II presentation of endogenously expressed antigens by transfected dendritic cells. Gene Ther. 8, 487–493. https://doi.org/10.1038/sj.gt.3301433

Dinca, A., Chien, W.-M., Chin, M.T., 2016. Intracellular Delivery of Proteins with Cell-Penetrating Peptides for Therapeutic Uses in Human Disease. Int. J. Mol. Sci. 17, 263. https://doi.org/10.3390/ijms17020263

Doherty, G.J., McMahon, H.T., 2009. Mechanisms of Endocytosis. Annu. Rev. Biochem. 78, 857–902. https://doi.org/10.1146/annurev.biochem.78.081307.110540

Dovgan, B., Barlič, A., Knežević, M., Miklavčič, D., 2017. Cryopreservation of Human Adipose-Derived Stem Cells in Combination with Trehalose and Reversible Electroporation. J. Membr. Biol. 250, 1–9. https://doi.org/10.1007/s00232-016-9916-z

Ducheyne, Paul., 2011. Comprehensive biomaterials. Elsevier.

Duncan, R., Richardson, S.C.W., 2012. Endocytosis and Intracellular Trafficking as Gateways for Nanomedicine Delivery: Opportunities and Challenges. Mol. Pharm. 9, 2380–2402. https://doi.org/10.1021/mp300293n

Dyer, P.D.R., Kotha, A.K., Pettit, M.W., Richardson, S.C.W., 2013. Imaging Select Mammalian Organelles Using Fluorescent Microscopy: Application to Drug Delivery, in: Weissig, V., Elbayoumi, T., Olsen, M. (Eds.), Cellular and Subcellular Nanotechnology: Methods and Protocols, Methods in Molecular Biology. Humana Press, Totowa, NJ, pp. 195–209. https://doi.org/10.1007/978-1-62703-336-7_19

Eccleston, M.E., Kuiper, M., Gilchrist, F.M., Slater, N.K.H., 2000. pH-responsive pseudo-peptides for cell membrane disruption. J. Controlled Release 69, 297–307. https://doi.org/10.1016/S0168-3659(00)00316-3

Eccleston, M.E., Slater, N.K.H., Tighe, B.J., 1999. Synthetic routes to responsive polymers; co-polycondensation of tri-functional amino acids with diacylchlorides. React. Funct. Polym. 42, 147–161.

Eccleston, M.E., Williams, S.L., Yue, Z., Chen, R., Lee, C.K., Anikina, E., Pawlyn, C., Barrand, M.A., Slater, N.K.H., 2005. Design and In-vitro Testing of Effective Poly(l-Lysine Iso-Phthalamide) Based Drug Targeting Systems for Solid Tumours. Food Bioprod. Process., 7th World Congress of Chemical Engineering 83, 141–146. https://doi.org/10.1205/fbp.04401

Edidin, M., 2003. Lipids on the frontier: a century of cell-membrane bilayers. Nat. Rev. Mol. Cell Biol. 4, 414–418. https://doi.org/10.1038/nrm1102

Elahi, R., Khosh, E., Tahmasebi, S., Esmaeilzadeh, A., 2018. Immune Cell Hacking: Challenges and Clinical Approaches to Create Smarter Generations of Chimeric Antigen Receptor T Cells. Front. Immunol. 9, 1717. https://doi.org/10.3389/fimmu.2018.01717

Evans, B.C., Fletcher, R.B., Kilchrist, K.V., Dailing, E.A., Mukalel, A.J., Colazo, J.M., Oliver, M., Cheung-Flynn, J., Brophy, C.M., Tierney, J.W., Isenberg, J.S., Hankenson, K.D., Ghimire, K., Lander, C., Gersbach, C.A., Duvall, C.L., 2019. An anionic, endosome-escaping polymer to potentiate intracellular delivery of cationic peptides, biomacromolecules, and nanoparticles. Nat. Commun. 10, 5012. https://doi.org/10.1038/s41467-019-12906-y

Fabbri, M., Smart, C., Pardi, R., 2003. T lymphocytes. Int. J. Biochem. Cell Biol. 35, 1004–1008. https://doi.org/10.1016/S1357-2725(03)00037-2

Fan, Y., Marioli, M., Zhang, K., 2021. Analytical characterization of liposomes and other lipid nanoparticles for drug delivery. J. Pharm. Biomed. Anal. 192, 113642. https://doi.org/10.1016/j.jpba.2020.113642

Farhood, B., Najafi, M., Mortezaee, K., 2019. CD8+ cytotoxic T lymphocytes in cancer immunotherapy: A review. J. Cell. Physiol. 234, 8509–8521. https://doi.org/10.1002/jcp.27782

Farshbaf, M., Davaran, S., Zarebkohan, A., Annabi, N., Akbarzadeh, A., Salehi, R., 2018. Significant role of cationic polymers in drug delivery systems. Artif. Cells Nanomedicine Biotechnol. 46, 1872–1891. https://doi.org/10.1080/21691401.2017.1395344

Fischbach, M.A., Bluestone, J.A., Lim, W.A., 2013. Cell-Based Therapeutics: The Next Pillar of Medicine 5, 179–7.

Fischer, D., Li, Y., Ahlemeyer, B., Krieglstein, J., Kissel, T., 2003. In vitro cytotoxicity testing of polycations: influence of polymer structure on cell viability and hemolysis. Biomaterials 24, 1121–1131. https://doi.org/10.1016/S0142-9612(02)00445-3

Fodor, W.L., 2003. Tissue engineering and cell based therapies, from the bench to the clinic: the potential to replace, repair and regenerate. Reprod. Biol. Endocrinol. RBE 1, 102. https://doi.org/10.1186/1477-7827-1-102

Foroozandeh, P., Aziz, A.A., 2018. Insight into Cellular Uptake and Intracellular Trafficking of Nanoparticles. Nanoscale Res. Lett. 13, 339. https://doi.org/10.1186/s11671-018-2728-6

Fouad, Y.A., Aanei, C., 2017. Revisiting the hallmarks of cancer. Am. J. Cancer Res. 7, 1016–1036.

Francia, V., Reker-Smit, C., Boel, G., Salvati, A., 2019. Limits and challenges in using transport inhibitors to characterize how nano-sized drug carriers enter cells. Nanomed. 14, 1533–1549. https://doi.org/10.2217/nnm-2018-0446

Freund, G., Sibler, A.-P., Desplancq, D., Oulad-Abdelghani, M., Vigneron, M., Gannon, J., Van Regenmortel, M.H., Weiss, E., 2013. Targeting endogenous nuclear antigens by electrotransfer of monoclonal antibodies in living cells. mAbs 5, 518–522. https://doi.org/10.4161/mabs.25084

Fu, A., Tang, R., Hardie, J., Farkas, M.E., Rotello, V.M., 2014. Promises and Pitfalls of Intracellular Delivery of Proteins. Bioconjug. Chem. 25, 1602–1608. https://doi.org/10.1021/bc500320j

Fu, H., Ding, J., Flutter, B., Gao, B., 2008. Investigation of endogenous antigen processing by delivery of an intact protein into cells. J. Immunol. Methods 335, 90–97. https://doi.org/10.1016/j.jim.2008.02.017

Gaston, J., Maestrali, N., Lalle, G., Gagnaire, M., Masiero, A., Dumas, B., Dabdoubi, T., Radošević, K., Berne, P.-F., 2019. Intracellular delivery of therapeutic antibodies into specific cells using antibody-peptide fusions. Sci. Rep. 9, 18688. https://doi.org/10.1038/s41598-019-55091-0

Goldberg, M.S., 2015. Immunoengineering: How Nanotechnology Can Enhance Cancer Immunotherapy. Cell 161, 201–204. https://doi.org/10.1016/j.cell.2015.03.037

Gong, N., Zhang, Y., Teng, X., Wang, Yongchao, Huo, S., Qing, G., Ni, Q., Li, X., Wang, J., Ye, X., Zhang, T., Chen, S., Wang, Yongji, Yu, J., Wang, P.C., Gan, Y., Zhang, J., Mitchell, M.J., Li, J., Liang, X.-J., 2020. Proton-driven transformable nanovaccine for cancer immunotherapy. Nat. Nanotechnol. 15, 1053–1064. https://doi.org/10.1038/s41565-020-00782-3

Gordon, S., 2016. Phagocytosis: An Immunobiologic Process. Immunity 44, 463–475. https://doi.org/10.1016/j.immuni.2016.02.026

Gruenberg, J., Griffiths, G., Howell, K.E., 1989. Characterization of the early endosome and putative endocytic carrier vesicles in vivo and with an assay of vesicle fusion in vitro. J. Cell Biol. 108, 1301–1316. https://doi.org/10.1083/jcb.108.4.1301

Gupta, B., Levchenko, T.S., Torchilin, V.P., 2005. Intracellular delivery of large molecules and small particles by cell-penetrating proteins and peptides. Adv. Drug Deliv. Rev., Protein- and Peptide-Mediated Transduction: Mechanisms and Implications for Drug Delivery 57, 637–651. https://doi.org/10.1016/j.addr.2004.10.007

Hao, G., Ping Xu, Z., Li, L., 2018. Manipulating extracellular tumour pH: an effective target for cancer therapy. RSC Adv. 8, 22182–22192. https://doi.org/10.1039/C8RA02095G

He, L., Sayers, E.J., Watson, P., Jones, A.T., 2018. Contrasting roles for actin in the cellular uptake of cell penetrating peptide conjugates. Sci. Rep. 8, 7318. https://doi.org/10.1038/s41598-018-25600-8

He, M., Huang, L., Hou, X., Zhong, C., Bachir, Z.A., Lan, M., Chen, R., Gao, F., 2019. Efficient ovalbumin delivery using a novel multifunctional micellar platform for targeted melanoma immunotherapy. Int. J. Pharm. 560, 1–10. https://doi.org/10.1016/j.ijpharm.2019.01.027

Heathman, T.R., Nienow, A.W., McCall, M.J., Coopman, K., Kara, B., Hewitt, C.J., 2015. The translation of cell-based therapies: clinical landscape and manufacturing challenges. Regen. Med. https://doi.org/10.2217/rme.14.73

Hendel, A., Bak, R.O., Clark, J.T., Kennedy, A.B., Ryan, D.E., Roy, S., Steinfeld, I., Lunstad, B.D., Kaiser, R.J., Wilkens, A.B., Bacchetta, R., Tsalenko, A., Dellinger, D., Bruhn, L., Porteus, M.H., 2015. Chemically modified guide RNAs enhance CRISPR-Cas genome editing in human primary cells. Nat. Biotechnol. 33, 985–989. https://doi.org/10.1038/nbt.3290

Hermanson, G.T., 2013. Chapter 10 - Fluorescent Probes, in: Hermanson, G.T. (Ed.), Bioconjugate Techniques (Third Edition). Academic Press, Boston, pp. 395–463. https://doi.org/10.1016/B978-0-12-382239-0.00010-8

Ho, V.H.B., Slater, N.K.H., Chen, R., 2011. pH-responsive endosomolytic pseudo-peptides for drug delivery to multicellular spheroids tumour models. Biomaterials 32, 2953–2958. https://doi.org/10.1016/j.biomaterials.2011.01.010

Hoffmann, K., Milech, N., Juraja, S.M., Cunningham, P.T., Stone, S.R., Francis, R.W., Anastasas, M., Hall, C.M., Heinrich, T., Bogdawa, H.M., Winslow, S., Scobie, M.N., Dewhurst, R.E., Florez, L., Ong, F., Kerfoot, M., Champain, D., Adams, A.M., Fletcher, S., Viola, H.M., Hool, L.C., Connor, T., Longville, B.A.C., Tan, Y.-F., Kroeger, K., Morath, V., Weiss, G.A., Skerra, A., Hopkins, R.M., Watt, P.M., 2018. A platform for discovery of functional cell-penetrating peptides for efficient multi-cargo intracellular delivery. Sci. Rep. 8, 12538. https://doi.org/10.1038/s41598-018-30790-2

Hou, A.J., Chen, L.C., Chen, Y.Y., 2021. Navigating CAR-T cells through the solid-tumour microenvironment. Nat. Rev. Drug Discov. 20, 531–550. https://doi.org/10.1038/s41573-021-00189-2

Huang, J.G., Leshuk, T., Gu, F.X., 2011. Emerging nanomaterials for targeting subcellular organelles. Nano Today 6, 478–492. https://doi.org/10.1016/j.nantod.2011.08.002

Huang, R., Li, X., He, Y., Zhu, W., Gao, Lei, Liu, Y., Gao, Li, Wen, Q., Zhong, J.F., Zhang, C., Zhang, X., 2020. Recent advances in CAR-T cell engineering. J. Hematol. Oncol.J Hematol Oncol 13, 86. https://doi.org/10.1186/s13045-020-00910-5

Hubbell, J.A., Thomas, S.N., Swartz, M.A., 2009. Materials engineering for immunomodulation. Nature 462, 449–460. https://doi.org/10.1038/nature08604

Hubo, M., Trinschek, B., Kryczanowsky, F., Tüttenberg, A., Steinbrink, K., Jonuleit, H., 2013. Costimulatory Molecules on Immunogenic Versus Tolerogenic Human Dendritic Cells. Front. Immunol. 4.

Hui, S.W., Li, L.H., 2000. In Vitro and Ex Vivo Gene Delivery to Cells by Electroporation, in: Jaroszeski, M.J., Heller, R., Gilbert, R. (Eds.), Electrochemotherapy, Electrogenetherapy, and Transdermal Drug Delivery: Electrically Mediated Delivery of Molecules to Cells, Methods in Molecular Medicine. Humana Press, Totowa, NJ, pp. 157–171. https://doi.org/10.1385/1-59259-080-2:157

Huntington, J.A., Stein, P.E., 2001. Structure and properties of ovalbumin. J. Chromatogr. B. Biomed. Sci. App., Elucidation of Allergens in Food 756, 189–198. https://doi.org/10.1016/S0378-4347(01)00108-6

Hur, J., Chung, A.J., 2021. Microfluidic and Nanofluidic Intracellular Delivery. Adv. Sci. 8, 2004595. https://doi.org/10.1002/advs.202004595

Ito, M., Hayashi, K., Adachi, E., Minamisawa, T., Homma, S., Koido, S., Shiba, K., 2014. Combinatorial Contextualization of Peptidic Epitopes for Enhanced Cellular Immunity. PLoS ONE 9, e110425. https://doi.org/10.1371/journal.pone.0110425

Jhaveri, A., Torchilin, V., 2016. Intracellular delivery of nanocarriers and targeting to subcellular organelles. Expert Opin. Drug Deliv. 13, 49–70. https://doi.org/10.1517/17425247.2015.1086745

Jiang, Z., Liu, H., He, H., Yadava, N., Chambers, J.J., Thayumanavan, S., 2020. Anionic Polymers Promote Mitochondrial Targeting of Delocalized Lipophilic Cations. Bioconjug. Chem. 31, 1344–1353. https://doi.org/10.1021/acs.bioconjchem.0c00079

Jiangsu Simcere Pharmaceutical Co., Ltd., 2022. An Open, Multi-cohort, Phase II Clinical Study Evaluating the Efficacy and Safety of Docetaxel Polymer Micelles for Injection in Patients With Advanced Malignant Solid Tumors (Clinical trial registration No. NCT05254665). clinicaltrials.gov.

Jovic, M., Sharma, M., Rahajeng, J., Caplan, S., 2010. The early endosome: a busy sorting station for proteins at the crossroads. Histol. Histopathol. 25, 99–112.

Kabanov, A.V., Kabanov, V.A., 2002. DNA Complexes with Polycations for the Delivery of Genetic Material into Cells [WWW Document]. ACS Publ. https://doi.org/10.1021/bc00031a002

Kaladharan, K., Kumar, A., Gupta, P., Illath, K., Santra, T.S., Tseng, F.-G., 2021. Microfluidic Based Physical Approaches towards Single-Cell Intracellular Delivery and Analysis. Micromachines 12, 631. https://doi.org/10.3390/mi12060631

Khan, A.A., Allemailem, K.S., Almatroodi, S.A., Almatroudi, A., Rahmani, A.H., 2020. Recent strategies towards the surface modification of liposomes: an innovative approach for different clinical applications. 3 Biotech 10, 163. https://doi.org/10.1007/s13205-020-2144-3

Khormaee, S., Choi, Y., Shen, M.J., Xu, B., Wu, H., Griffiths, G.L., Chen, R., Slater, N.K.H., Park, J.K., 2013. Endosomolytic anionic polymer for the cytoplasmic delivery of siRNAs in localized in vivo applications. Adv. Funct. Mater. 23. https://doi.org/10.1002/adfm.201201945

Kim, H., Kitamatsu, M., Ohtsuki, T., 2018. Enhanced intracellular peptide delivery by multivalent cell-penetrating peptide with bioreducible linkage. Bioorg. Med. Chem. Lett. 28, 378–381. https://doi.org/10.1016/j.bmcl.2017.12.035

Kim, S.K., Foote, M.B., Huang, L., 2012. The targeted intracellular delivery of cytochrome C protein to tumors using lipid-apolipoprotein nanoparticles. Biomaterials 33, 3959–3966. https://doi.org/10.1016/j.biomaterials.2012.02.010

Knight, S., Collins, M., Takeuchi, Y., 2013. Insertional mutagenesis by retroviral vectors: current concepts and methods of analysis. Curr. Gene Ther. 13, 211–227. https://doi.org/10.2174/1566523211313030006

Kocak, G., Tuncer, C., Bütün, V., 2017. pH-Responsive polymers. Polym. Chem. 8, 144–176. https://doi.org/10.1039/C6PY01872F

Kopytynski, M., Chen, S., Legg, S., Minter, R., Chen, R., 2020. A Versatile Polymer-Based Platform for Intracellular Delivery of Macromolecules. Adv. Ther. 3, 1900169. https://doi.org/10.1002/adtp.201900169

Kumar, P., Nagarajan, A., Uchil, P.D., 2018. Analysis of Cell Viability by the Lactate Dehydrogenase Assay. Cold Spring Harb. Protoc. 2018. https://doi.org/10.1101/pdb.prot095497

Lai, P.-S., Pai, C.-L., Peng, C.-L., Shieh, M.-J., Berg, K., Lou, P.-J., 2008. Enhanced cytotoxicity of saporin by polyamidoamine dendrimer conjugation and photochemical internalization. J. Biomed. Mater. Res. A 87A, 147–155. https://doi.org/10.1002/jbm.a.31760

Lai, Y.-P., Jeng, C.-J., Chen, S.-C., 2011. The Roles of CD4+ T Cells in Tumor Immunity. ISRN Immunol. 2011, 1–6. https://doi.org/10.5402/2011/497397

Laidlaw, B.J., Craft, J.E., Kaech, S.M., 2016. The multifaceted role of CD4+ T cells in CD8+ T cell memory. Nat. Rev. Immunol. 16, 102–111. https://doi.org/10.1038/nri.2015.10

Lam, S.K., Tse, Y.C., Robinson, D.G., Jiang, L., 2007. Tracking down the elusive early endosome. Trends Plant Sci. 12, 497–505. https://doi.org/10.1016/j.tplants.2007.09.001

Lamaze, C., Schmid, S.L., 1995. The emergence of clathrin-independent pinocytic pathways. Curr. Opin. Cell Biol. 7, 573–580. https://doi.org/10.1016/0955-0674(95)80015-8

Lazzari, G., Couvreur, P., Mura, S., 2017. Multicellular tumor spheroids: a relevant 3D model for the in vitro preclinical investigation of polymer nanomedicines. Polym. Chem. 8, 4947–4969. https://doi.org/10.1039/C7PY00559H

Lee, H.-G., Cho, M.-Z., Choi, J.-M., 2020. Bystander CD4+ T cells: crossroads between innate and adaptive immunity. Exp. Mol. Med. 52, 1255–1263. https://doi.org/10.1038/s12276-020-00486-7

Liechty, W.B., Chen, R., Farzaneh, F., Tavassoli, M., Slater, N.K.H., 2009. Synthetic pH-Responsive Polymers for Protein Transduction. Adv. Mater. Deerfield Beach Fla 21, 3910–3914. https://doi.org/10.1002/adma.200901733

Liechty, W.B., Kryscio, D.R., Slaughter, B.V., Peppas, N.A., 2010. Polymers for Drug Delivery Systems. Annu. Rev. Chem. Biomol. Eng. 1, 149–173. https://doi.org/10.1146/annurev-chembioeng-073009-100847

Lim, W.A., June, C.H., 2017. The Principles of Engineering Immune Cells to Treat Cancer. Cell 168, 724–740. https://doi.org/10.1016/j.cell.2017.01.016

Lin, D.H., Hoelz, A., 2019. The Structure of the Nuclear Pore Complex (An Update). Annu. Rev. Biochem. 88, 725–783. https://doi.org/10.1146/annurev-biochem-062917-011901

Liras, A., 2010. Future research and therapeutic applications of human stem cells: general, regulatory, and bioethical aspects. J. Transl. Med. 8, 131. https://doi.org/10.1186/1479-5876-8-131

Lorenz, J.N., Gruenstein, E., 1999. A simple, nonradioactive method for evaluating single-nephron filtration rate using FITC-inulin. Am. J. Physiol.-Ren. Physiol. 276, F172–F177. https://doi.org/10.1152/ajprenal.1999.276.1.F172

Luo, D., Saltzman, W.M., 2000. Synthetic DNA delivery systems. Nat. Biotechnol. 18, 33–37. https://doi.org/10.1038/71889

Luzio, J.P., Rous, B.A., Bright, N.A., Pryor, P.R., Mullock, B.M., Piper, R.C., 2000. Lysosome-endosome fusion and lysosome biogenesis. J. Cell Sci. 113, 1515–1524. https://doi.org/10.1242/jcs.113.9.1515

Lynch, A.L., Chen, R., Dominowski, P.J., Shalaev, E.Y., Yancey, R.J., Slater, N.K.H., 2010. Biopolymer mediated trehalose uptake for enhanced erythrocyte cryosurvival. Biomaterials 31, 6096–6103. https://doi.org/10.1016/j.biomaterials.2010.04.020

Lynch, A.L., Chen, R., Slater, N.K.H., 2011. pH-responsive polymers for trehalose loading and desiccation protection of human red blood cells. Biomaterials 32, 4443–4449. https://doi.org/10.1016/j.biomaterials.2011.02.062

Martínez-Jothar, L., Beztsinna, N., van Nostrum, C.F., Hennink, W.E., Oliveira, S., 2019. Selective Cytotoxicity to HER2 Positive Breast Cancer Cells by Saporin-Loaded Nanobody-Targeted Polymeric Nanoparticles in Combination with Photochemical Internalization. Mol. Pharm. 16, 1633–1647. https://doi.org/10.1021/acs.molpharmaceut.8b01318

Mellman, I., 1996. Endocytosis and Molecular Sorting. Annu. Rev. Cell Dev. Biol. 12, 575–625. https://doi.org/10.1146/annurev.cellbio.12.1.575

Mercado, S.A., Orellana-Tavra, C., Chen, A., Slater, N.K.H., 2016. The intracellular fate of an amphipathic pH-responsive polymer: Key characteristics towards drug delivery. Mater. Sci. Eng. C 69, 1051–1057. https://doi.org/10.1016/j.msec.2016.08.004

Mercado, S.A., Slater, N.K.H., 2016a. Increased cryosurvival of osteosarcoma cells using an amphipathic pH-responsive polymer for trehalose uptake. Cryobiology 73, 175–180. https://doi.org/10.1016/j.cryobiol.2016.08.002

Mercado, S.A., Slater, N.K.H., 2016b. The functional and structural effects of an amphipathic pH responsive biopolymer: A comprehensive study in osteosarcoma cells. Eur. Polym. J. 74, 158–167. https://doi.org/10.1016/j.eurpolymj.2015.11.026

Meyer, M., Philipp, A., Oskuee, R., Schmidt, C., Wagner, E., 2008. Breathing Life into Polycations: Functionalization with pH-Responsive Endosomolytic Peptides and Polyethylene Glycol Enables siRNA Delivery. J. Am. Chem. Soc. 130, 3272–3273. https://doi.org/10.1021/ja710344v

Moktan, S., Raucher, D., 2012. Anticancer activity of proapoptotic peptides is highly improved by thermal targeting using elastin-like polypeptides. Int. J. Pept. Res. Ther. 18, 227–237. https://doi.org/10.1007/s10989-012-9295-y

Morales-Cruz, M., Figueroa, C.M., González-Robles, T., Delgado, Y., Molina, A., Méndez, J., Morales, M., Griebenow, K., 2014. Activation of caspase-dependent apoptosis by intracellular delivery of cytochrome c-based nanoparticles. J. Nanobiotechnology 12, 33. https://doi.org/10.1186/s12951-014-0033-9

Mukherjee, S., Ghosh, R.N., Maxfield, F.R., 1997. Endocytosis. Physiol. Rev. 77, 759–803. https://doi.org/10.1152/physrev.1997.77.3.759

Nakamura, H., DeRose, R., Inoue, T., 2019. Harnessing biomolecular condensates in living cells. J. Biochem. (Tokyo) 166, 13–27. https://doi.org/10.1093/jb/mvz028

Naldini, L., 2015. Gene therapy returns to centre stage. Nature 526, 351–360. https://doi.org/10.1038/nature15818

Naldini, L., 2011. Ex vivo gene transfer and correction for cell-based therapies. Nat. Rev. Genet. 12, 301–315. https://doi.org/10.1038/nrg2985

Narayanan, S., Surendranath, K., Bora, N., Surolia, A., Karande, A.A., 2005. Ribosome inactivating proteins and apoptosis. FEBS Lett. 579, 1324–1331. https://doi.org/10.1016/j.febslet.2005.01.038

Nelson, P.T., Alafuzoff, I., Bigio, E.H., Bouras, C., Braak, H., Cairns, N.J., Castellani, R.J., Crain, B.J., Davies, P., Tredici, K.D., Duyckaerts, C., Frosch, M.P., Haroutunian, V., Hof, P.R., Hulette, C.M., Hyman, B.T., Iwatsubo, T., Jellinger, K.A., Jicha, G.A., Kövari, E., Kukull, W.A., Leverenz, J.B., Love, S., Mackenzie, I.R., Mann, D.M., Masliah, E., McKee, A.C., Montine, T.J., Morris, J.C., Schneider, J.A., Sonnen, J.A., Thal, D.R., Trojanowski, J.Q., Troncoso, J.C., Wisniewski, T., Woltjer, R.L., Beach, T.G., 2012. Correlation of Alzheimer Disease Neuropathologic Changes With Cognitive Status: A Review of the Literature. J. Neuropathol. Exp. Neurol. 71, 362–381. https://doi.org/10.1097/NEN.0b013e31825018f7

Nerem, M., 1991. Cellular engineering 19, 529–545.

Nowakowska-Gołacka, J., Sominka, H., Sowa-Rogozińska, N., Słomińska-Wojewódzka, M., 2019. Toxins Utilize the Endoplasmic Reticulum-Associated Protein Degradation Pathway in Their Intoxication Process. Int. J. Mol. Sci. 20, 1307. https://doi.org/10.3390/ijms20061307

Obeagu, E., Ifeanyi, Ochei, K., Nwachukwu, B., 2015. Methaemoglobinaemia:A Review 3, 2262–2269.

Pack, D.W., Hoffman, A.S., Pun, S., Stayton, P.S., 2005. Design and development of polymers for gene delivery. Nat. Rev. Drug Discov. 4, 581–593. https://doi.org/10.1038/nrd1775

Pala, L., Senn, H.M., Caldwell, S.T., Prime, T.A., Warrington, S., Bright, T.P., Prag, H.A., Wilson, C., Murphy, M.P., Hartley, R.C., 2020. Enhancing the Mitochondrial Uptake of Phosphonium Cations by Carboxylic Acid Incorporation. Front. Chem. 8, 783. https://doi.org/10.3389/fchem.2020.00783

Park, S.E., Sajid, M.I., Parang, K., Tiwari, R.K., 2019. Cyclic Cell-Penetrating Peptides as Efficient Intracellular Drug Delivery Tools. Mol. Pharm. 16, 3727–3743. https://doi.org/10.1021/acs.molpharmaceut.9b00633

Peptide Property Calculator [WWW Document], 2022. URL https://www.novoprolabs.com/tools/calc_peptide_property (accessed 2.21.22).

Petrova, V., Annicchiarico-Petruzzelli, M., Melino, G., Amelio, I., 2018. The hypoxic tumour microenvironment. Oncogenesis 7, 1–13. https://doi.org/10.1038/s41389-017-0011-9

Plank, C., Oberhauser, B., Mechtler, K., Koch, C., Wagner, E., 1994. The influence of endosome-disruptive peptides on gene transfer using synthetic virus-like gene transfer systems. J. Biol. Chem. 269, 12918–12924. https://doi.org/10.1016/S0021-9258(18)99963-1

Plank, C., Zauner, W., Wagner, E., 1998. Application of membrane-active peptides for drug and gene delivery across cellular membranes. Adv. Drug Deliv. Rev., Transport of Macromolecules and Viruses 34, 21–35. https://doi.org/10.1016/S0169-409X(98)00005-2

Polito, L., Bortolotti, M., Farini, V., Battelli, M.G., Barbieri, L., Bolognesi, A., 2009. Saporin induces multiple death pathways in lymphoma cells with different intensity and timing as compared to ricin. Int. J. Biochem. Cell Biol. 41, 1055–1061. https://doi.org/10.1016/j.biocel.2008.09.021

Polito, L., Bortolotti, M., Mercatelli, D., Battelli, M.G., Bolognesi, A., 2013. Saporin-S6: A Useful Tool in Cancer Therapy. Toxins 5, 1698–1722. https://doi.org/10.3390/toxins5101698

Pontes, B., Ayala, Y., Fonseca, A.C.C., Romão, L.F., Amaral, R.F., Salgado, L.T., Lima, F.R., Farina, M., Viana, N.B., Moura-Neto, V., Nussenzveig, H.M., 2013. Membrane Elastic

Properties and Cell Function. PLoS ONE 8, e67708. https://doi.org/10.1371/journal.pone.0067708

Poteryaev, D., Datta, S., Ackema, K., Zerial, M., Spang, A., 2010. Identification of the Switch in Early-to-Late Endosome Transition. Cell 141, 497–508. https://doi.org/10.1016/j.cell.2010.03.011

Qiao, Z.-Y., Lai, W.-J., Lin, Y.-X., Li, D., Nan, X.-H., Wang, Y., Wang, H., Fang, Q.-J., 2017. Polymer–KLAK Peptide Conjugates Induce Cancer Cell Death through Synergistic Effects of Mitochondria Damage and Autophagy Blockage. Bioconjug. Chem. 28, 1709–1721. https://doi.org/10.1021/acs.bioconjchem.7b00176

Raes, L., Stremersch, S., Fraire, J.C., Brans, T., Goetgeluk, G., De Munter, S., Van Hoecke, L., Verbeke, R., Van Hoeck, J., Xiong, R., Saelens, X., Vandekerckhove, B., De Smedt, S., Raemdonck, K., Braeckmans, K., 2020. Intracellular Delivery of mRNA in Adherent and Suspension Cells by Vapor Nanobubble Photoporation. Nano-Micro Lett. 12, 185. https://doi.org/10.1007/s40820-020-00523-0

Rai, R., Alwani, S., Badea, I., 2019. Polymeric Nanoparticles in Gene Therapy: New Avenues of Design and Optimization for Delivery Applications. Polymers 11, 745. https://doi.org/10.3390/polym11040745

Raman, V., Van Dessel, N., Hall, C.L., Wetherby, V.E., Whitney, S.A., Kolewe, E.L., Bloom, S.M.K., Sharma, A., Hardy, J.A., Bollen, M., Van Eynde, A., Forbes, N.S., 2021. Intracellular delivery of protein drugs with an autonomously lysing bacterial system reduces tumor growth and metastases. Nat. Commun. 12, 6116. https://doi.org/10.1038/s41467-021-26367-9

Rennick, J.J., Johnston, A.P.R., Parton, R.G., 2021. Key principles and methods for studying the endocytosis of biological and nanoparticle therapeutics. Nat. Nanotechnol. 16, 266–276. https://doi.org/10.1038/s41565-021-00858-8

Richardson, S.C.W., Wallom, K.-L., Ferguson, E.L., Deacon, S.P.E., Davies, M.W., Powell, A.J., Piper, R.C., Duncan, R., 2008. The use of fluorescence microscopy to define polymer localisation to the late endocytic compartments in cells that are targets for drug delivery. J. Controlled Release 127, 1–11. https://doi.org/10.1016/j.jconrel.2007.12.015

R. Nödling, A., M. Mills, E., Li, X., Cardella, D., J. Sayers, E., Wu, S.-H., T. Jones, A., P. Luk, L.Y., Tsai, Y.-H., 2020. Cyanine dye mediated mitochondrial targeting enhances the anti-cancer activity of small-molecule cargoes. Chem. Commun. 56, 4672–4675. https://doi.org/10.1039/C9CC07931A

Roy, S.G., De, P., 2014. pH responsive polymers with amino acids in the side chains and their potential applications. J. Appl. Polym. Sci. 131. https://doi.org/10.1002/app.41084

Ruseska, I., Zimmer, A., 2020. Internalization mechanisms of cell-penetrating peptides. Beilstein J. Nanotechnol. 11, 101–123. https://doi.org/10.3762/bjnano.11.10

Russell, M.R.G., Nickerson, D.P., Odorizzi, G., 2006. Molecular mechanisms of late endosome morphology, identity and sorting. Curr. Opin. Cell Biol., Membranes and organelles 18, 422–428. https://doi.org/10.1016/j.ceb.2006.06.002

Sadelain, M., Rivière, I., Riddell, S., 2017. Therapeutic T cell engineering. Nature 545, 423–431. https://doi.org/10.1038/nature22395

Sahay, G., Alakhova, D.Y., Kabanov, A.V., 2010. Endocytosis of nanomedicines. J. Controlled Release 145, 182–195. https://doi.org/10.1016/j.jconrel.2010.01.036

Samal, K.S., Dash, M., Vlierberghe, S.V., L. Kaplan, D., Chiellini, E., Blitterswijk, C. van, Moroni, L., Dubruel, P., 2012. Cationic polymers and their therapeutic potential. Chem. Soc. Rev. 41, 7147–7194. https://doi.org/10.1039/C2CS35094G

Schmaljohann, D., 2006. Thermo- and pH-responsive polymers in drug delivery. Adv. Drug Deliv. Rev., 2006 Supplementary Non-Thematic Collection 58, 1655–1670. https://doi.org/10.1016/j.addr.2006.09.020

Schnorenberg, M.R., Bellairs, J.A., Samaeekia, R., Acar, H., Tirrell, M.V., LaBelle, J.L., 2019. Activating the Intrinsic Pathway of Apoptosis Using BIM BH3 Peptides Delivered by Peptide Amphiphiles with Endosomal Release. Materials 12, 2567. https://doi.org/10.3390/ma12162567

Shah, N., Perales, M.-A., Turtle, C.J., Cairo, M.S., Cowan, A.J., Saeed, H., Budde, L.E., Tan, A., Lee, Z., Kai, K., Marcondes, M.Q., Zalevsky, J., Tagliaferri, M.A., Patel, K.K., 2021. Phase I study protocol: NKTR-255 as monotherapy or combined with daratumumab or rituximab in hematologic malignancies. Future Oncol. 17, 3549–3560. https://doi.org/10.2217/fon-2021-0576

Sharei, A., Poceviciute, R., Jackson, E.L., Cho, N., Mao, S., Hartoularos, G.C., Jang, D.Y., Jhunjhunwala, S., Eyerman, A., Schoettle, T., Langer, R., Jensen, K.F., 2014. Plasma membrane recovery kinetics of a microfluidic intracellular delivery platform. Integr Biol 6, 470–475. https://doi.org/10.1039/C3IB40215K

Sharei, A., Trifonova, R., Jhunjhunwala, S., Hartoularos, G.C., Eyerman, A.T., Lytton-Jean, A., Angin, M., Sharma, S., Poceviciute, R., Mao, S., Heimann, M., Liu, S., Talkar, T., Khan, O.F., Addo, M., Andrian, U.H. von, Anderson, D.G., Langer, R., Lieberman, J., Jensen, K.F., 2015. Ex Vivo Cytosolic Delivery of Functional Macromolecules to Immune Cells. PLOS ONE 10, e0118803. https://doi.org/10.1371/journal.pone.0118803

Sharei, A., Zoldan, J., Adamo, A., Sim, W.Y., Cho, N., Jackson, E., Mao, S., Schneider, S., Han, M.-J., Lytton-Jean, A., Basto, P.A., Jhunjhunwala, S., Lee, J., Heller, D.A., Kang, J.W., Hartoularos, G.C., Kim, K.-S., Anderson, D.G., Langer, R., Jensen, K.F., 2013. A vector-free microfluidic platform for intracellular delivery. Proc. Natl. Acad. Sci. U. S. A. 110, 2082–7. https://doi.org/10.1073/pnas.1218705110

Shen, Q., Xu, L., Li, R., Wu, G., Li, S., Saw, P.E., Zhou, Y., Xu, X., 2021. A tumor microenvironment (TME)-responsive nanoplatform for systemic saporin delivery and effective breast cancer therapy. Chem. Commun. 57, 2563–2566. https://doi.org/10.1039/D0CC07808E

Shete, H.K., Prabhu, R.H., Patravale, V.B., 2014. Endosomal Escape: A Bottleneck in Intracellular Delivery. J. Nanosci. Nanotechnol. 14, 460–474. https://doi.org/10.1166/jnn.2014.9082

Shi, J., Ma, Y., Zhu, J., Chen, Y., Sun, Y., Yao, Y., Yang, Z., Xie, J., 2018. A Review on Electroporation-Based Intracellular Delivery. Molecules 23, 3044. https://doi.org/10.3390/molecules23113044

Sikriwal, D., Ghosh, P., Batra, J.K., 2008. Ribosome inactivating protein saporin induces apoptosis through mitochondrial cascade, independent of translation inhibition. Int. J. Biochem. Cell Biol. 40, 2880–2888. https://doi.org/10.1016/j.biocel.2008.06.004

Simões, S., Slepushkin, V., Düzgünes, N., Pedroso de Lima, M.C., 2001. On the mechanisms of internalization and intracellular delivery mediated by pH-sensitive liposomes. Biochim. Biophys. Acta BBA - Biomembr. 1515, 23–37. https://doi.org/10.1016/S0005-2736(01)00389-3

Smith, J.E., 1987. Erythrocyte Membrane: Structure, Function, and Pathophysiology. Vet. Pathol. 24, 471–476. https://doi.org/10.1177/030098588702400601

Sonawane, N.D., Szoka, F.C., Verkman, A.S., 2003. Chloride Accumulation and Swelling in Endosomes Enhances DNA Transfer by Polyamine-DNA Polyplexes*. J. Biol. Chem. 278, 44826–44831. https://doi.org/10.1074/jbc.M308643200

Stewart, M.P., Langer, R., Jensen, K.F., 2018. Intracellular Delivery by Membrane Disruption: Mechanisms, Strategies, and Concepts. Chem. Rev. 118, 7409–7531. https://doi.org/10.1021/acs.chemrev.7b00678

Stewart, M.P., Sharei, A., Ding, X., Sahay, G., Langer, R., Jensen, K.F., 2016. In vitro and ex vivo strategies for intracellular delivery. Nature 538, 183–192. https://doi.org/10.1038/nature19764

Stuart, M.A.C., Huck, W.T.S., Genzer, J., Müller, M., Ober, C., Stamm, M., Sukhorukov, G.B., Szleifer, I., Tsukruk, V.V., Urban, M., Winnik, F., Zauscher, S., Luzinov, I., Minko, S., 2010. Emerging applications of stimuli-responsive polymer materials. Nat. Mater. 9, 101–113. https://doi.org/10.1038/nmat2614

Subarsky, P., Hill, R.P., 2003. The hypoxic tumour microenvironment and metastatic progression. Clin. Exp. Metastasisbystander 20, 237–250.

Sun, M., Duan, X., 2020. Recent advances in micro/nanoscale intracellular delivery. Nanotechnol. Precis. Eng. 3, 18–31. https://doi.org/10.1016/j.npe.2019.12.003

Szeto, G.L., Van Egeren, D., Worku, H., Sharei, A., Alejandro, B., Park, C., Frew, K., Brefo, M., Mao, S., Heimann, M., Langer, R., Jensen, K., Irvine, D.J., 2015. Microfluidic squeezing for intracellular antigen loading in polyclonal B-cells as cellular vaccines. Sci. Rep. 5, 10276. https://doi.org/10.1038/srep10276

Takemoto, H., Nishiyama, N., 2021. Construction of nanomaterials based on pH-responsive polymers for effective tumor delivery. Polym. J. 53, 1353–1360. https://doi.org/10.1038/s41428-021-00542-7

Tamošiūnas, M., Mir, L.M., Chen, W.-S., Lihachev, A., Venslauskas, M., Šatkauskas, S., 2016. Intracellular Delivery of Bleomycin by Combined Application of Electroporation and Sonoporation in Vitro. J. Membr. Biol. 249, 677–689. https://doi.org/10.1007/s00232-016-9911-4

Tarragó-Trani, M.T., Storrie, B., 2007. Alternate routes for drug delivery to the cell interior: Pathways to the Golgi apparatus and endoplasmic reticulum. Adv. Drug Deliv. Rev., Organelle-Specific Targeting in Drug Delivery and Design 59, 782–797. https://doi.org/10.1016/j.addr.2007.06.006

Teo, S.L.Y., Rennick, J.J., Yuen, D., Al-Wassiti, H., Johnston, A.P.R., Pouton, C.W., 2021. Unravelling cytosolic delivery of cell penetrating peptides with a quantitative endosomal escape assay. Nat. Commun. 12, 3721. https://doi.org/10.1038/s41467-021-23997-x

ThermoFisher, 2022. Dynabeads™ Mouse T-Activator CD3/CD28 for T-Cell Expansion and Activation [WWW Document]. URL https://www.thermofisher.com/order/catalog/product/11456D (accessed 3.6.22).

Tiefenboeck, P., Kim, J.A., Trunk, F., Eicher, T., Russo, E., Teijeira, A., Halin, C., Leroux, J.-C., 2017. Microinjection for the *ex Vivo* Modification of Cells with Artificial Organelles. ACS Nano 11, 7758–7769. https://doi.org/10.1021/acsnano.7b01404

Torchilin, V.P., 2006. Recent Approaches to Intracellular Delivery of Drugs and Dna and Organelle Targeting. Annu. Rev. Biomed. Eng. 8, 343–375. https://doi.org/10.1146/annurev.bioeng.8.061505.095735

Torchilin, V.P., 2005. Recent advances with liposomes as pharmaceutical carriers. Nat. Rev. Drug Discov. 4, 145–160. https://doi.org/10.1038/nrd1632

Trif, M., Craciunescu, O., 2015. Liposome as efficient system for intracellular delivery of bioactive molecules, in: Nanotechnology and Functional Foods. John Wiley & Sons, Ltd, pp. 191–213. https://doi.org/10.1002/9781118462157.ch12

Trombetta, E.S., Mellman, I., 2005. Cell Biology of Antigen Processing in Vitro and in Vivo. Annu. Rev. Immunol. 23, 975–1028. https://doi.org/10.1146/annurev.immunol.22.012703.104538

University of Washington, 2022. A Phase 1/2 Study of ABI-009 (Nab-Rapamycin) With Pazopanib (VOTRIENT®) in Patients With Advanced Nonadipocytic Soft-Tissue Sarcomas (Clinical trial registration No. NCT03660930). clinicaltrials.gov.

Uribe-Querol, E., Rosales, C., 2020. Phagocytosis: Our Current Understanding of a Universal Biological Process. Front. Immunol. 11, 1066. https://doi.org/10.3389/fimmu.2020.01066

Varkouhi, A.K., Scholte, M., Storm, G., Haisma, H.J., 2011. Endosomal escape pathways for delivery of biologicals. J. Controlled Release 151, 220–228. https://doi.org/10.1016/j.jconrel.2010.11.004

Vergara, M.N., Gutierrez, C., O'Brien, D.R., Canto-Soler, M.V., 2013. Ex vivo electroporation of retinal cells: A novel, high efficiency method for functional studies in primary retinal cultures. Exp. Eye Res. 109, 40–50. https://doi.org/10.1016/j.exer.2013.01.010

Vermeulen, L.M.P., De Smedt, S.C., Remaut, K., Braeckmans, K., 2018. The proton sponge hypothesis: Fable or fact? Eur. J. Pharm. Biopharm. 129, 184–190. https://doi.org/10.1016/j.ejpb.2018.05.034

Walsh, M.J., Dodd, J.E., Hautbergue, G.M., 2013. Ribosome-inactivating proteins. Virulence 4, 774–784. https://doi.org/10.4161/viru.26399

Walther, W., Stein, U., 2000. Viral Vectors for Gene Transfer 23.

Wan, J., Sun, L., Wu, P., Wang, F., Guo, J., Cheng, J., Wang, C., 2018. Synthesis of indocyanine green functionalized comblike poly(aspartic acid) derivatives for enhanced cancer cell ablation by targeting the endoplasmic reticulum. Polym. Chem. 9, 1206–1215. https://doi.org/10.1039/C7PY01994G

Wang, D., Green, M.D., Chen, K., Daengngam, C., Kotsuchibashi, Y., 2016. Stimuli-Responsive Polymers: Design, Synthesis, Characterization, and Applications. Int. J. Polym. Sci. 2016, 1–2. https://doi.org/10.1155/2016/6480259

Wang, F., Ogasawara, M.A., Huang, P., 2010. Small mitochondria-targeting molecules as anti-cancer agents. Mol. Aspects Med., Mitochondria, Apoptosis and Cancer 31, 75–92. https://doi.org/10.1016/j.mam.2009.12.003

Wang, Q., Cheng, H., Peng, H., Zhou, H., Li, P.Y., Langer, R., 2015. Non-genetic engineering of cells for drug delivery and cell-based therapy. Adv. Drug Deliv. Rev., Editor's Collection 2015 91, 125–140. https://doi.org/10.1016/j.addr.2014.12.003

Wang, Q., Yu, J., Kadungure, T., Beyene, J., Zhang, H., Lu, Q., 2018. ARMMs as a versatile platform for intracellular delivery of macromolecules. Nat. Commun. 9, 960. https://doi.org/10.1038/s41467-018-03390-x

Wang, R., Chow, Y.T., Chen, S., Ma, D., Luo, T., Tan, Y., Sun, D., 2018. Magnetic Force-driven in Situ Selective Intracellular Delivery. Sci. Rep. 8, 14205. https://doi.org/10.1038/s41598-018-32605-w

Wang, S., Li, Z., Li, S., Di, R., Ho, C.-T., Yang, G., 2016. Ribosome-inactivating proteins (RIPs) and their important health promoting property. RSC Adv. 6, 46794–46805. https://doi.org/10.1039/C6RA02946A

Wei, M., Gao, Y., Li, X., Serpe, M.J., 2016. Stimuli-responsive polymers and their applications. Polym. Chem. 8, 127–143. https://doi.org/10.1039/C6PY01585A

Woodsworth, D.J., Holt, R.A., 2017. Cell-Based Therapeutics: Making a Faustian Pact with Biology. Trends Mol. Med. 23, 104–115. https://doi.org/10.1016/j.molmed.2016.12.004

Wu, Y.-C., Wu, T.-H., Clemens, D.L., Lee, B.-Y., Wen, X., Horwitz, M.A., Teitell, M.A., Chiou, P.-Y., 2015. Massively parallel delivery of large cargo into mammalian cells with light pulses. Nat. Methods 12, 439–444. https://doi.org/10.1038/nmeth.3357

Xu, X., Li, T., Shen, S., Wang, J., Abdou, P., Gu, Z., Mo, R., 2019. Advances in Engineering Cells for Cancer Immunotherapy. Theranostics 9, 7889–7905. https://doi.org/10.7150/thno.38583

Yang, N.J., Hinner, M.J., 2015. Getting across the cell membrane: an overview for small molecules, peptides, and proteins. Methods Mol. Biol. Clifton NJ 1266, 29–53. https://doi.org/10.1007/978-1-4939-2272-7_3

Yèagle, P.L., 1989. Lipid regulation of cell membrane structure and function. FASEB J. 3, 1833–1842. https://doi.org/10.1096/fasebj.3.7.2469614

Yesylevskyy, S., Marrink, S.-J., Mark, A.E., 2009. Alternative Mechanisms for the Interaction of the Cell-Penetrating Peptides Penetratin and the TAT Peptide with Lipid Bilayers. Biophys. J. 97, 40–49. https://doi.org/10.1016/j.bpj.2009.03.059

Yi Kang, J., Kim, S., Kim, J., Kang, N.-G., Yang, C.-S., Min, S.-J., Woong Kim, J., 2021. Cell-penetrating peptide-conjugated lipid/polymer hybrid nanovesicles for endoplasmic reticulum-targeting intracellular delivery. J. Mater. Chem. B 9, 464–470. https://doi.org/10.1039/D0TB01940B

Yoshikawa, T., Sugita, T., Mukai, Y., Yamanada, N., Nagano, K., Nabeshi, H., Yoshioka, Y., Nakagawa, S., Abe, Y., Kamada, H., Tsunoda, S., Tsutsumi, Y., 2008. Organelle-Targeted Delivery of Biological Macromolecules Using the Protein Transduction Domain: Potential Applications for Peptide Aptamer Delivery into the Nucleus. J. Mol. Biol. 380, 777–782. https://doi.org/10.1016/j.jmb.2008.05.047

Yuan, P., Mao, X., Wu, X., Liew, S.S., Li, L., Yao, S.Q., 2019. Mitochondria-Targeting, Intracellular Delivery of Native Proteins Using Biodegradable Silica Nanoparticles. Angew. Chem. Int. Ed. 58, 7657–7661. https://doi.org/10.1002/anie.201901699

Zakeri, A., Kouhbanani, M.A.J., Beheshtkhoo, N., Beigi, V., Mousavi, S.M., Hashemi, S.A.R., Karimi Zade, A., Amani, A.M., Savardashtaki, A., Mirzaei, E., Jahandideh, S., Movahedpour, A., 2018. Polyethylenimine-based nanocarriers in co-delivery of drug and gene: a developing horizon. Nano Rev. Exp. 9, 1488497. https://doi.org/10.1080/20022727.2018.1488497

Zalba, S., ten Hagen, T.L.M., 2017. Cell membrane modulation as adjuvant in cancer therapy. Cancer Treat. Rev. 52, 48–57. https://doi.org/10.1016/j.ctrv.2016.10.008

Zapala, L., Drela, N., Bil, J., Nowis, D., Basak, G.W., Lasek, W., 2011. Optimization of activation requirements of immature mouse dendritic JAWSII cells for in vivo application. Oncol. Rep. 25, 831–840. https://doi.org/10.3892/or.2010.1128

Zhang, G.-N., Gupta, P., Wang, M., Barbuti, A.M., Ashby, C.R., Zhang, Y.-K., Zeng, L., Xu, Q., Fan, Y.-F., Chen, Z.-S., 2020. Lipid-Saporin Nanoparticles for the Intracellular Delivery

of Cytotoxic Protein to Overcome ABC Transporter-Mediated Multidrug Resistance In Vitro and In Vivo. Cancers 12. https://doi.org/10.3390/cancers12020498

Zhong, J., Li, L., Zhu, X., Guan, S., Yang, Q., Zhou, Z., Zhang, Z., Huang, Y., 2015. A smart polymeric platform for multistage nucleus-targeted anticancer drug delivery. Biomaterials 65, 43–55. https://doi.org/10.1016/j.biomaterials.2015.06.042

Appendix A

Proton Nuclear magnetic resonance (^{1}H-NMR) was utilised to confirm the structure of PLP. Briefly, PLP in its acidic form (5 mg) was dissolved in d_6-DMSO (0.8 mL) before being transferred to an NMR tube and analysed via ^{1}H-NMR at room temperature. The spectrum was obtained using a 400 MHz spectrometer (Bruker, Germany).

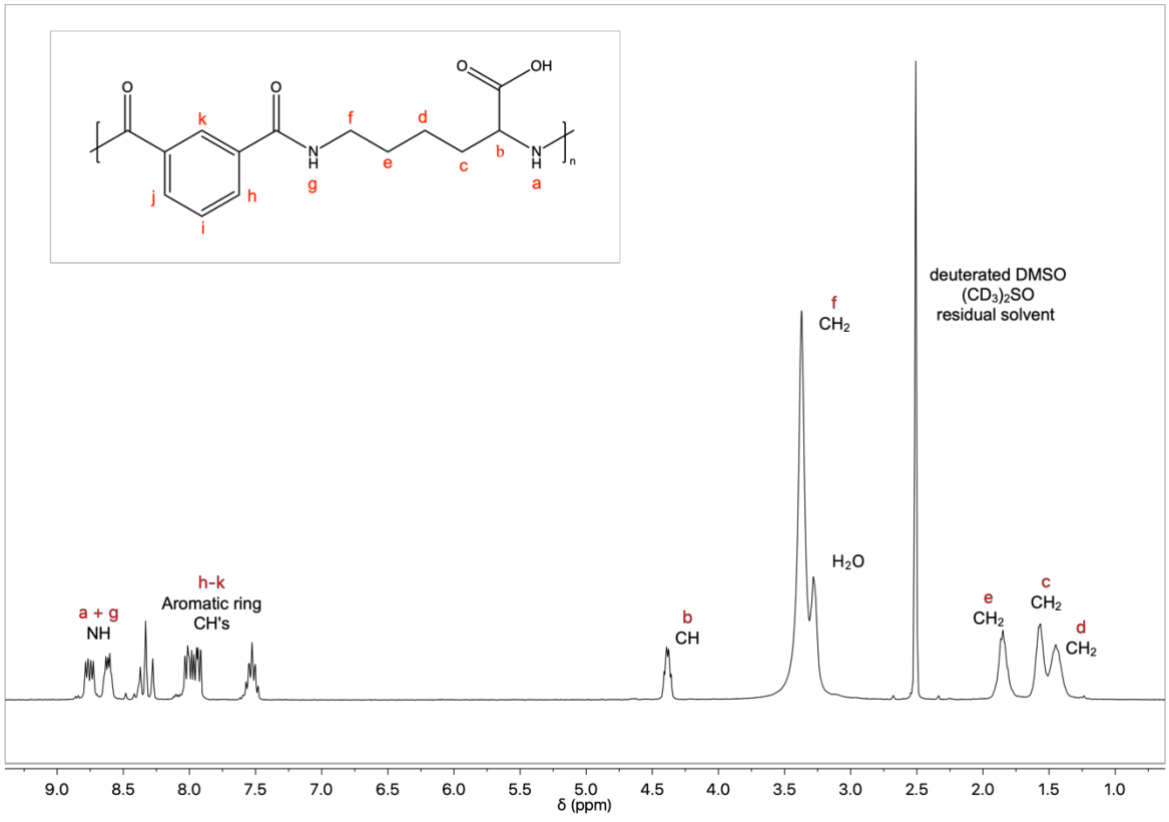

Figure A-1. ^{1}H-NMR spectrum of PLP methyl ester in DMSO-d6 at room temperature.

Appendix B

Proton Nuclear magnetic resonance (^{1}H-NMR) was utilised to confirm the structure of PP50. Briefly, PP50 in its acidic form (5 mg) was dissolved in d_6-DMSO (0.8 mL) before being transferred to an NMR tube and analysed via ^{1}H-NMR at room temperature. The spectrum was obtained using a 400 MHz spectrometer (Bruker, Germany). The degree of substitution with L-phenylalanine was determined by the ratio of the integral of 7.13-7.33 ppm to the integral of 7.45-7.64. The degree grafting with L-phenylalanine used herein was equal to 49%.

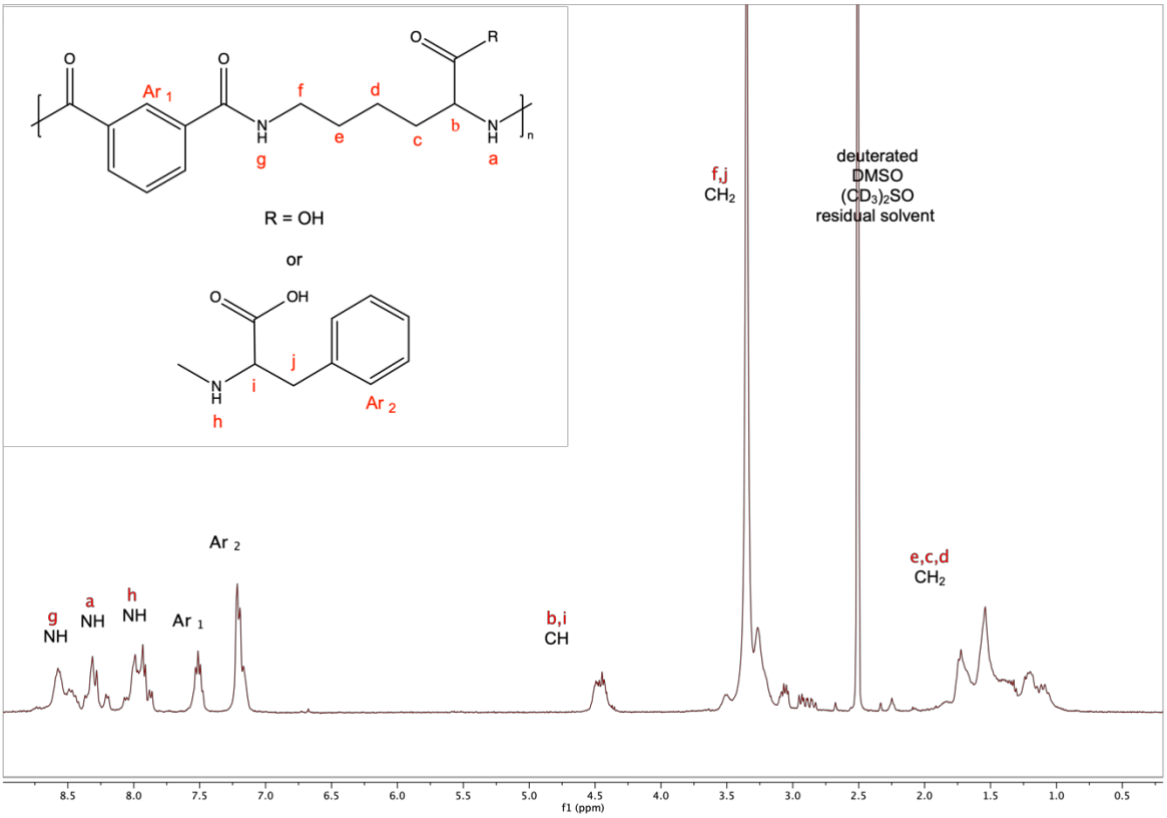

Figure B-1. ^{1}H-NMR spectrum of PP50 in DMSO-d6 at room temperature.

Appendix C

Proton Nuclear magnetic resonance (^{1}H-NMR) was utilised to confirm the structure of PLP-NDA18. Briefly, PLP-NDA18 in its acidic form (5 mg) was dissolved in d_6-DMSO (0.8 mL) before being transferred to an NMR tube and analysed via ^{1}H-NMR at room temperature. The spectrum was obtained using a 400 MHz spectrometer (Bruker, Germany). The degree of substitution with decylamine was determined by the ratio of the integral of 0.77-0.91 ppm to the integral of 7.45-7.64. The degree grafting with decylamine used herein was equal to 23%.

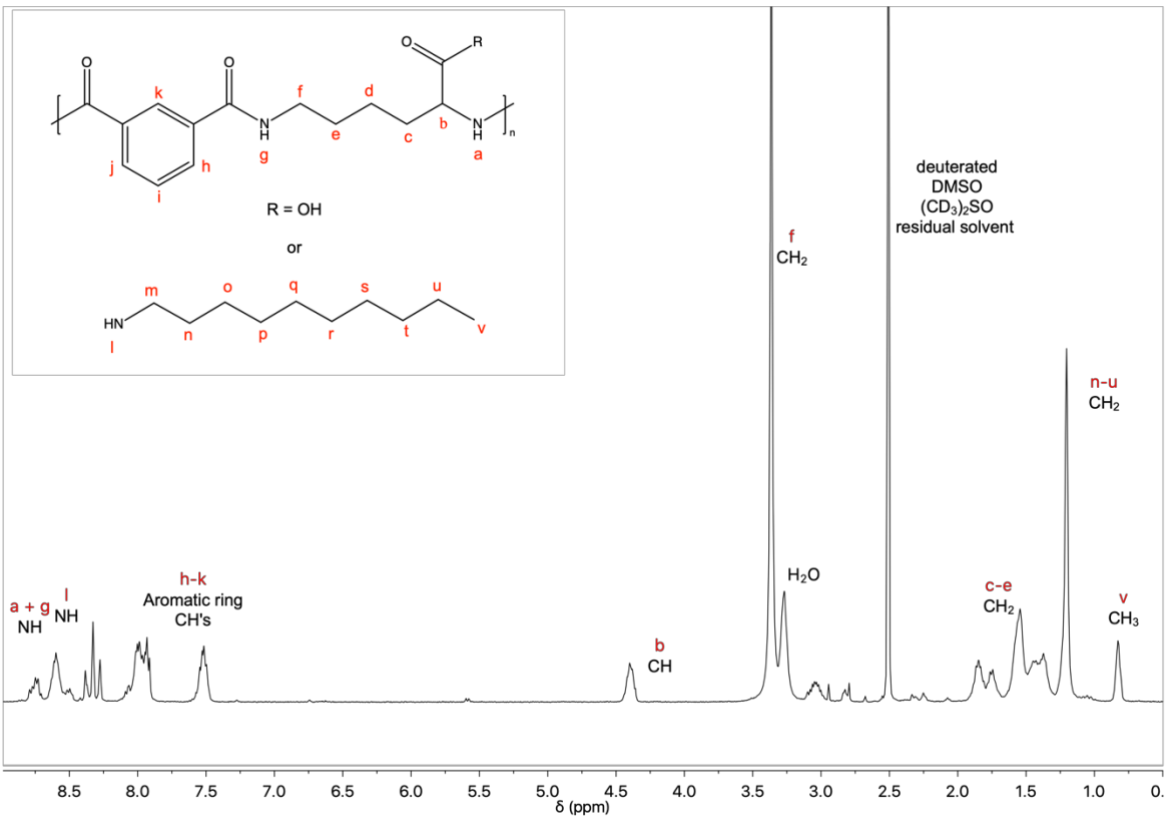

Figure C-1. ^{1}H-NMR spectrum of PLP-NDA18 in DMSO-d6 at room temperature.

Appendix D

Permissions summary table for third party copyright works

Name in this work	Source of work	Copyright holder	Permission requested date	Permission granted	Permission note
Figure 1-2	Strategies for the intracellular delivery of nanoparticles Chou, L. Y., Ming, K., & Chan, W. C. (2011). *Chemical Society reviews*, *40*(1), 233–245. https://doi.org/10.1039/c0cs00003e	© ROYAL SOCIETY OF CHEMISTRY	14/12/21	Yes	Rightslink® by Copyright Clearance Centre Marketplace Order License ID 1168400-2
Figure 1-3	Nanoscopy for endosomal escape quantification Andrian, T., Riera, R., Pujals, S., Albertazzi, L. (2021) *Nanoscale Adv*., (3) 10-23 https://doi.org/10.1039/D0NA00454E	© ROYAL SOCIETY OF CHEMISTRY	29/03/22	Yes	Rightslink® by Copyright Clearance Centre Marketplace Order License ID 1204892-1
Figure 1-4	Strategies for the enhanced intracellular delivery of nanomaterials. Azevedo, C.,	© Elsevier Ltd	14/12/21	Yes	Rightslink® by Copyright Clearance Centre Marketplace

	Macedo, M. H., & Sarmento, B. (2018). *Drug Discovery Today, 944-959, 23(5)* https://doi.org/10.1016/j.drudis.2017.08.011				Order License ID 1168400-1
Figure 1-9	Bystander $CD4^+$ T cells: crossroads between innate and adaptive immunity Lee, HG., Cho, MZ. & Choi, JM. *Exp Mol Med* **52,** 1255–1263 (2020) https://doi.org/10.1038/s12276-020-00486-7	© Korean Society of Medical Biochemistry and Molecular Biology	06/01/22	N/A	Open access under Creative Commons Attribution 4.0 International License
Table 1-2	In vitro and ex vivo strategies for intracellular delivery. Stewart, M., Sharei, A., Ding, X. *et al. Nature* **538,** 183–192 (2016). https://doi.org/10.1038/nature19764	© Nature Research	14/12/21	Yes	Rightslink® by Copyright Clearance Centre Marketplace Order License ID 1168407-1

Figures were Created with BioRender.com